PB89-224943

Sensitivity of a Regional Oxidant Model to Variations in Climate Parameters. Volume 1 and 2

Systems Applications, Inc., San Rafael, CA

Prepared for:

Environmental Protection Agency, Research Triangle Park, NC

Jul 89

U.S. Department of Commerce
National Technical Information Service
NTIS

PB89-224943

EPA/600/3-89/068
July 1989

SENSITIVITY OF A REGIONAL OXIDANT MODEL TO VARIATIONS IN CLIMATE PARAMETERS, VOLUME I AND II

by

R. E. Morris, M. W. Gery, M. K. Liu,
G. E. Moore, C. Daley, and S. M. Greenfield

Systems Applications Inc.
101 Lucas Valley Road
San Rafael, California 94903

Project Officer

J. Bufalini
Atmospheric Research & Exposure Assessment Lab
Research Triangle Park, North Carolina 27711

U. S. ENVIRONMENTAL PROTECTION AGENCY
ATMOSPHERIC RESEARCH & EXPOSURE ASSESSMENT LAB
OFFICE OF RESEARCH AND DEVELOPMENT
RESEARCH TRIANGLE PARK, NORTH CAROLINA @&&!!

REPRODUCED BY
U.S. DEPARTMENT OF COMMERCE
NATIONAL TECHNICAL INFORMATION SERVICE
SPRINGFIELD, VA. 22161

TECHNICAL REPORT DATA

(Please read Instructions on the reverse before completing)

1. REPORT NO.

2.

3. RECIPIENT'S ACCESSION NO.
PB89 224943/AS

4. TITLE AND SUBTITLE
SENSITIVITY OF A REGIONAL OXIDANT MODEL TO VARIATIONS IN CIMATE PARAMETERS, VOLUME I AND II

5. REPORT DATE
July 1989

6. PERFORMING ORGANIZATION CODE

7. AUTHOR(S)
R. E. Morris, M. W. Gery, M. K. Liu,
G. E. Moore, C. Daley, and S. M. Greenfield

8. PERFORMING ORGANIZATION REPORT NO.

9. PERFORMING ORGANIZATION NAME AND ADDRESS
Systems Applications Inc.
101 Lucas Valley Road
San Rafael, California 94903

10. PROGRAM ELEMENT NO.
A101T/G/98/01-6204

11. CONTRACT/GRANT NO.
IAG-DW 14931805

12. SPONSORING AGENCY NAME AND ADDRESS
Atmospheric Research & Exposure Assessment Lab
Office of Research and Development
U.S. Environmental Protection Agency
Research Triangle Park, North Carolina 27711

13. TYPE OF REPORT AND PERIOD COVERED
Final Report

14. SPONSORING AGENCY CODE
EPA/600/09

15. SUPPLEMENTARY NOTES

16. ABSTRACT

In order to investigate the sensitivity of ozone concentrations to future climate variations, a regional oxidant model was applied for future climate scenarios to two regions: one covering central California (San Joaquin Valley, Sierra Nevada mountains and the San Francisco Bay Area) and the other covering the midwestern and southeastern United States. Based on model calculations, the effects of increased temperature on ambient ozone concentrations results in an increase of the area of exceedances of the ozone air quality standard, a movement of the peak ozone concentration closer to the urban areas, and the resultant increase in the exposure of people to harmful levels of ozone concentrations. The calculations for California indicate that the maximum daily ozone concentrations may increase from 2 to 20 percent and the number of people exposed to hourly ozone concentrations in excess of the air quality standard may triple as a result of a temperature increase. Similar, although less dramatic, results were seen for the midwestern and southeastern applications.

17. KEY WORDS AND DOCUMENT ANALYSIS

a. DESCRIPTORS	b. IDENTIFIERS/OPEN ENDED TERMS	c. COSATI Field/Group

18. DISTRIBUTION STATEMENT
RELEASE TO PUBLIC

19. SECURITY CLASS *(This Report)*
UNCLASSIFIED

20. SECURITY CLASS *(This page)*
UNCLASSIFIED

21. NO. OF PAGES
149 145

22. PRICE

EPA Form 2220-1 (9-73)

NOTICE

This document has been reviewed in accordance with U.S. Environmental Protection Agency policy and approved for publication. Mention of trade names or commercial products does not constitute endorsement or recommendation for use.

Contents

Volume I

1 INTRODUCTION 1

Background 1

Methodology 2

Uncertainties 3

2 REGIONAL MODELING OF OZONE FORMATION UNDER FUTURE CHANGES IN CLIMATE 4

Definition of Temperature Increase 6

Effects of Temperature Change on Other Meteorological Variables 8

Definition of Stratospheric Ozone Reduction 14

Definition of Modeling Scenarios 15

Uncertainties 15

Results of the Simulations--Climate Change Scenario #1 17

Results of the Simulations--Climate Change Scenario #2 26

Implications of the Analysis for Air Quality Controls 28

3 THE SENSITIVITY OF OZONE CONCENTRATIONS TO CLIMATE VARIABILITY 98

Methodology 99

The Data Base 102

Selection of Variables for the Analysis 108

The Sensitivity of Maximum Daily Ozone Concentration to the Meteorological Variables 119

The Feasibility of Using Meteorological Classification Schemes for Predicting Ozone Concentrations 133

4 RECOMMENDATIONS 135

References 139

Volume II

Appendix A: Description of the RTM-III Model

Appendix B: Modeling Domains, Episodes, and Inputs

Appendix C: Hourly Mixed-Layer Ozone Concentrations (pphm) at 3-Hour Intervals for the Central California Episode (August 5-10, 1981) and the Base Case

Appendix D: Hourly Mixed-Layer Ozone Concentrations (pphm) at 3-Hour Intervals for the Central California Episode (August 5-10, 1981) and the First Climate Sensitivity Scenario (4°C Temperature Increase with Attendant Water Vapor Concentrations Increase)

Appendix E: Hourly Mixed-Layer Ozone Concentrations (pphm) at 3-Hour Intervals for the Midwestern/Southwestern Episode (July 14-21, 1980) and the Base Case

Appendix F: Hourly Mixed-Layer Ozone Concentrations (pphm) at 3-Hour Intervals for the Midwestern/Southwestern Episode (July 14-21, 1980) and the First Climate Sensitivity Scenario (4°C Temperature Increase with Attendant Water Vapor Concentrations Increase)

1 INTRODUCTION

BACKGROUND

Global atmospheric changes are expected to occur within the next several decades because of increases in levels of pollutants in the atmosphere. These changes are associated with (1) warming of the atmosphere due to the greenhouse effect of trace gases, (2) depletion of the stratospheric ozone layer, and (3) modification of tropospheric chemistry. The emitted materials responsible for those changes are carbon dioxide, carbon monoxide, methane, chlorofluoro-hydrocarbons, nitrous oxide, and other trace gases.

As atmospheric concentrations of the so-called "greenhouse gases" continue to increase, the potential climate change and consequent environmental impacts have become issues of great concern worldwide. Such climate changes could significantly affect the chemistry and dynamics of the troposphere and ultimately endanger human health and sensitive ecological systems. Of particular concern to many parties, including the Environmental Protection Agency (EPA) and National Park service (NPS), is the possibility that increased temperature and depletion of stratospheric ozone may result in increases in tropospheric concentrations of ozone. The resulting increased reactivity of the troposphere would also result in increased concentrations of other photochemically active species, such as hydrogen peroxide and peroxyacetyl nitrate. Hydrogen peroxide is believed to be one of the principal chemicals in the formation of sulfate and consequently acid deposition, by acting as an oxidizer of sulfur dioxide, while increased concentrations of ozone and peroxyacetyl nitrate may result in significant damage to forest ecosystems.

To provide an initial estimate of the possible effects of future climate changes on tropospheric oxidant concentrations, the EPA, through an interagency agreement with the NPS, funded a preliminary study that examined the effects of future climate changes on urban air quality at several U.S. cities (Gery, Edmond, and Whitten, 1987). Specifically, this study used a computer simulation model, OZIPM3, a simple photochemical trajectory box model, to study the effects of increased temperature and decreased stratospheric ozone on ozone formation. The results indicated that, if anticipated climate changes do occur, most of the cities studied will not be able to meet the current National Ambient Air Quality Standard (NAAQS) for ozone (0.12 ppm) without more emission controls than are currently envisioned.

This preliminary study, however, did not estimate the effects of future climate changes on ozone concentrations in the rural atmosphere. The simulation model used in the study, OZIPM3, does not completely simulate the complex interaction between the processes of transport, diffusion, chemistry, and deposition nor does it include any feedback mechanisms between these processes. In addition, because the model does not divide the atmosphere into more than one vertical layer, it does not properly account for emission, meteorological, and chemistry variations with height, which may be important in both urban and rural environments. Therefore, the purpose of the study reported here was to examine the ability of another model to assess the effects of future climate change on tropospheric air quality. This model, the RTM-III, is an Eulerian three-dimensional regional oxidant model that has been developed over several years (Liu, Morris, and Killus, 1984; Morris et al., 1987).

METHODOLOGY

This study involved two tasks. The first task was to examine past RTM-III calculations of regional ozone concentrations in order to estimate the sensitivity of the model to changes in climate. Ozone concentrations predicted by the model were related to meteorological input parameters in order to gain insight into how potential future perturbations of these meteorological parameters will affect ozone concentrations. The second task was to determine the sensitivity of the RTM-III to changes in climate by simulating a base case of current climate conditions and potential future climate sensitivity scenarios. (The results of the second task are reported in Section 2, and those of the first task in Section 3.)

To estimate the sensitivity of RTM-III calculations of ozone to climatic change, past model simulations were re-analyzed and the meteorological conditions used as input were classified into sets of variables. The predicted ozone concentrations associated with these sets of meteorological conditions were then examined to determine their sensitivity to variations in climatic conditions.

We then applied an updated version of the RTM-III to two modeling domains: one covering central California and the other covering the midwestern and southeastern United States. For each modeling domain the model was exercised for a base case of current temperature and ultraviolet light conditions, and for a future climate scenario reflecting the effects of global warming. The model's ozone concentration predictions were then analyzed to determine the sensitivity of the model's predictions of tropospheric air quality to climate changes.

This study provides a preliminary estimate of the sensitivity of calculations of air quality to climate changes, and should help identify those climate parameters to which the calculations are most sensitive. These results will help focus future research on the effects of possible changes in climate on air quality.

UNCERTAINTIES

The use of air quality simulation models (AQSM) to estimate changes in air quality due to changes in climate conditions is beset with limitations because of the quantitative uncertainty associated with assumptions about global climate change. Current climate models can only provide general indications of the direction of future climate changes; AQSMs, however, require specific meteorological inputs. Thus, for this preliminary estimate of the sensitivity of AQSM calculations of ozone concentrations to potential climate modifications, we used an AQSM (the RTM-III) to simulate current climate meteorological conditions and a simple modification of these conditions that reflects the general direction of potential climate changes. In no way do we claim that the future climate scenarios described here represent actual future climate conditions, only that they include some of the basic features predicted by climate models, namely, increased temperature and UV radiation.

2 REGIONAL MODELING OF OZONE FORMATION UNDER FUTURE CHANGES IN CLIMATE

The continued release of emissions of carbon dioxide (CO_2) and other trace gases has in recent years led to the concern that these trace gases will result in a global warming of the atmosphere by blocking the escape of thermal infrared radiation. This phenomenon is commonly referred to as the greenhouse effect (Dickinson and Cicerone, 1986; Ramanathan et al., 1985; Wang et al., 1986). To quantify the amount of global warming expected in the future, global circulation models (GCMs) and other climate models have been exercised with various estimates of future loadings of trace gases in the upper atmosphere. We analyzed the predictions of climate change from four GCMs to obtain two representative future climate scenarios: a 4°C temperature increase and a combination of a 4°C temperature increase with a 10 percent reduction in stratospheric ozone.

In this section we report the results of simulations of current climate conditions and two future climate scenarios using a regional air quality model, the RTM-III. The maximum daily ozone concentrations calculated by the model are presented along with an interpretation of the impact of possible climate changes on air quality management.

Our future climate scenarios were based on results from the following four GCMs:

National Center for Atmospheric Research (NCAR) Community Climate Model (CCM) model

National Aeronautics and Space Administration (NASA) Goddard Institute of Space Studies (GISS) model

National Oceanic and Atmospheric Administration (NOAA) General Fluid Dynamics Laboratory (GFDL) model

Oregon State University (OSU) model

Current estimates of the emission and retention of man-made CO_2 in the atmosphere indicate a distinct possibility that atmospheric concentrations of CO_2 will double within the next century. Under these conditions, several GCMs predict an increase in the global average surface temperature at sea level of from 1 to 5°C. The above four GCMs models predict that the doubling of CO_2 concentrations would increase the global average temperature in the range of 2 to 5°C (Wuebbles and Penner, 1988). The presence of other trace gases, in addition to CO_2, would increase the global warming further. Although the four GCMs generally agree on the level of increase of global average temperature, they do not agree in their predictions of temperature increases in specific regions, such as California. Studies conducted by Lawrence Livermore National Laboratory (LLNL) and others indicate that current GCMs cannot, as yet, provide meaningful results for specific regions of interest.

Because of these limitations, translating the output of GCMs to hourly average temperature increases for a specific region of interest, as required by a regional air quality model such as the RTM-III, is problematic. The temporal and spatial scales of a GCM (decades and thousands of kilometers) are not compatible with those of a model like RTM-III (hours and 10 to 50 km). Because of difficulties in adapting the GCM output to a regional model and the discrepancies in the predictions of the GCMs for many climate variables, we have assumed simply that the temperature increases by 4°C throughout the modeling region. A temperature increase of 4°C is in the higher range of increases in global average temperature predicted by the four GCMs (2°C to 5°C) yet is well within the range of those predictions. In fact, temperature increases in central California and the midwestern/southeastern U.S. could be substantially larger than 4°C since the GCM simulations we analyzed considered the effects of doubling CO_2 concentrations on temperature increases. The effects of increases of other trace gases, or a more than doubling of the CO_2 concentrations, would result in a higher temperature increase. Of course it is also possible that the GCMs may be overpredicting increases in temperature due to uncertainties in the GCM calculations. Nevertheless, the fact remains that atmospheric concentrations of CO_2 are rising and all of the results of climate models we studied agree that this will result in an increase in global average temperature.

DEFINITION OF TEMPERATURE INCREASE

The 4°C temperature increase predicted by the climate models is a global, sea-level, annual average value. In general, the increases predicted by the GCMs are relatively higher in polar regions and lower at the equator. The modeling regions in the study reported here lie in the mid latitudes, thus the temperature increases should be between those at the equator and at the polar regions. Although the four GCMs are in general agreement when predicting the global average temperature effects of a doubling of CO_2 concentrations, they are less in agreement when examining changes in temperature for specific regions. For example, the four models predict that, under a doubling of the CO_2 concentrations, the summer average temperature for the eight westernmost states would increase in the range of 2.5 to 5°C, while in the eastern United States the temperature increase would range from 2.5 to 5.5°C. These results support the assumption of a 4°C temperature increase for the central California and midwestern/southeastern regions.

A consideration in defining this increased temperature scenario is how to relate this 4°C average increase to the temperature fields used as input to the RTM-III, which vary diurnally and by vertical layer. For the present study it was decided to add 4°C to each grid cell in each layer for each hour of the episode. While this approach may be viewed as an oversimplification of the actual phenomena, it is not unrealistic, as is discussed below.

None of the output from the GCMs is reported to sufficient temporal and spatial resolution to resolve the temperature increases as hourly variations for a specific region. There is some speculation that the increase in global average temperature would have a greater impact on the nighttime low temperature than on the daytime maximum. However, in the absence of better information, it will be assumed that the 4°C increase in surface temperature occurs uniformly throughout the diurnal cycle.

The next consideration in the definition of the increased temperature climate scenario is how to relate the temperature increase to the vertical layers of the RTM-III. The RTM-III contains three vertical layers. The first layer corresponds to the mixed layer. For daytime hours the top of this first layer is defined by an inversion below which rapid convective mixing occurs. It would appear that, because of rapid vertical mixing within this layer, an increase in surface temperature would result in a uniform temperature increase throughout the layer. For nighttime hours this first layer in RTM-III is defined as a shallow layer, usually approximately 50 to 150 meters thick. Since the top of this layer is usually defined by the magnitude of the wind speed and represents a mechanically well-mixed layer from the friction velocity and Coriolis parameter (Yu, 1978), any increase in the surface temperature would occur throughout the mixed-layer of the RTM-III.

The second layer in the RTM-III is a very thin layer (200 to 650 meters thick) that represents a transition between the mixed-layer and an inversion layer (the third layer aloft). This transition layer has a special function in the application of the RTM-III to central California. During the day the wind fields in the San Joaquin Valley are dominated by upslope flows near the surface, which are compensated by return flows aloft. Between the upslope winds at the surface and downsope return flow aloft is a shallow transition layer in which the slope flows counteract each other, resulting in a dead air space. Because of such convergence zones, there is significant transport between this transition layer and the mixed-layer. At night a similiar situation exists, except that the direction of the flow regimes is reversed, with the mixed layer containing the downslope (drainage) flows. Again there is some interaction between the mixed-layer and the transition layer in the convergence zones, especially in the valley, where the pooling of the drainage flows causes an uplifting of the air. It appears that the second layer is tied to the mixed layer quite strongly; this is borne out by the RTM-III simulations, in which the ozone predictions in the second layer are closer to those in the mixed-layer than the third-layer (Morris et al., 1987). Thus one could logically assume that any temperature increase in the mixed-layer would also be reflected by an increase in the second-layer.

Other climate effects researchers are assuming that the sea-level average temperature increase occurs throughout the troposphere (Wuebbles, 1988). Thus, to be consistent with other research and in the absence of any better information, we are assuming that the 4°C temperature increase also occurs in the third layer.

EFFECTS OF TEMPERATURE CHANGE ON OTHER METEOROLOGICAL VARIABLES

The atmosphere is a complicated system in which many variables, such as pressure, temperature, and winds, are in dynamic balance with each other. This linkage is described mathematically by the primitive equations (Pielke, 1984). Thus any modification of the temperature may also affect other meteorological variables. These other variables may include, but are not limited to the following:

Boundary (mixing) layer heights
Frequency and patterns of cloud cover and cloudiness
Water vapor concentrations
Wind fields, e.g. thermal winds
Stability
Emissions rates, both anthropogenic and biogenic
Frequency and intensity of climate variations

The procedures used to generate these inputs to the RTM-III for modeling the central California and midwestern/southeastern regions are given in Appendix B.

Boundary Layer Heights

One would expect that an increase in surface temperature would result in an increase in convective activity and a resultant increase in the convective mixing height. For the central California modeling domain the mixing heights were defined as the base of an inversion from temperature soundings. Since we have assumed that the 4°C temperature increase occurs uniformly throughout the vertical temperature sounding, the height of the inversion base and mixing height would remain unchanged. The mixing heights for the midwestern/southeastern modeling domain were created by the Meteorological Processor for Diffusion Analysis mixing height algorithm (Paumier et al., 1986), which estimates the convective mixing height as the base of the inversion but also contains some algorithms that may be sensitive to changes in temperature. However, changes in the mixing heights input into the RTM-III would also involve adjusting the layer-average wind, temperature, and water vapor fields. Quite a bit of uncertainity is associated with the location of the mixing height because of the spatial and temporal interpolation of the twice-daily mixing heights at radiosonde sites located 200 to 300 km. Therefore, the mixing heights for the climate change scenarios are the same ones used in the base case. As a result, the effects of temperature increases on ozone formation should be overstated by the model since the emissions are trapped in a smaller volume of air.

Cloudiness

There were clear skies throughout the period California episode studied here (5-10 August 1981). Thus it appears that we should assume continued clear skies for the climate change scenarios since the appearance of clouds would be unjustified and unreasonably confuse and complicate the analysis.

The episode selected for the midwestern/southeastern modeling domain (14 to 21 July 1980) includes periods of clouds and some precipitation. Increased cloudiness would increase precipitation, decrease ultraviolet light, and possibly increase vertical transport of pollutants, while a decrease in cloudiness would have the opposite effect. Thus increased cloudiness would most likely result in lower ozone concentrations due to reductions in UV radiation and possible increases in the occurrence of aqueous-phase chemistry. Since the specification of the increase, or decrease, of cloudiness associated with a 4°C temperature increase would be arbitrary, we have assumed that cloudiness remains unchanged. However, cloudiness should be considered as a climate change variable in future studies.

Water Vapor Concentrations

The relationship between temperature and water vapor concentrations can be determined via the Clausius-Clapeyron equation. The change in water vapor concentration in the atmosphere, as the temperature increases, depends on the supply of water at the surface. If the surface is dry, the water vapor concentration will not change. If there is a plentiful supply of water, the surface water flux would increase but the relative humidity would stay nearly constant. GCM results suggest that relative humidity would stay constant with increased temperature (Ramanathan, 1988). Thus, when atmospheric temperature T increases, the ratio of the vapor pressure to the saturation vapor pressure (i.e., relative humidity) would remain constant, i.e.:

$$r = \frac{e(T_D)}{e_s(T)} = \frac{e(T_D')}{e_s(T + \Delta T)}$$

$$e(T_D') = e(T_D)\,\frac{e_s(T + \Delta T)}{e_s\ (T)}$$

where T_D is the dew point and $e(T_D')$ is the vapor pressure when the temperature has been increased by ΔT. From the above equations water vapor concentrations for increased temperature conditions can be calculated from the original water vapor concentrations by multiplying by the factor $e_s(T + \Delta T)/e_s(T)$, which can be estimated from the Clausius-Clapeyron equation as follows:

$$\lambda = \frac{\exp\,[21.548 - 5388/(T + \Delta t)]}{\exp\,[21.548 - 5388/T]}$$

Assuming a temperature increase of 4°C and ambient temperatures of 250, 275, and 300 K, we get values for λ of 1.40, 1.32, and 1.26 respectively. Thus a 4°C temperature increase will be expected to increase the water vapor concentrations by 26 to 40 percent.

Increases in water vapor would result in a higher rate of production of the hydroxy radical and thus higher ozone concentrations. In general, however, maximum ozone concentrations are not that sensitive to changes in water vapor concentrations at normal levels of relative humidity.

Wind Fields

It is difficult to quantify the effects of increased temperature on the wind fields. For the central California episode it appears the increased temperature could result in significant alterations of the flow fields. Because of stagnant synoptic conditions during the California episode, the flow fields in the San Joaquin Valley are dominated by thermal upslope and downslope flows. Increased surface temperature could result in stronger slope flows. In addition, the increased temperature could also alter the temperature differential between the San Joaquin Valley and air over the Pacific Ocean, resulting in modifications of the strength of the land-sea breezes.

The wind fields for the central California application were generated by the Diagnostic Wind Model, which relies on observations and parameterizations of processes to obtain its wind fields (Kessler and Douglas, 1988; Morris et al., 1987). The Diagnostic Wind Model requires hourly values of a domain-mean surface temperature and lapse rate. The surface temperature and lapse rate are used in the denominator of the expression for calculating the Froude number, which describes the blocking and deflection of the synoptic wind flows by complex terrain. The lapse rate is also used to determine the strength of the thermally generated slope flows. The assumption of a uniform increase in temperature for the future climate scenario would not affect the lapse rate but may affect the Froude number calculations. An increase of 4°C in the temperature would change the Froude number by approximately 1 percent. This change is very small and would not significantly alter the flow fields, especially since the wind fields in the California episode (5-10 August 1981) are dominated by stagnant conditions without large amounts of blocking and deflection effects. Thus we are assuming no changes in the wind fields for the climate change scenarios for the California modeling domain.

The wind fields for the July 1980 midwestern/southeastern episode were generated by the Limited Fine Mesh (LFM) prognostic meteorological model. In principle it could be possible to alter the radiation parameterization and initial temperature fields of a prognostic model, such as the LFM, to create new wind fields under conditions of increased temperature. However, these fields were obtained from archived LFM output and rerunning the model to obtain new wind fields is a difficult task; the effort involved would have exceeded the resources and time constraints for this study. Thus the same wind fields were used for both the base case and climate change scenarios.

It appears reasonable that a change in the thermal structure of the atmosphere due to a temperature increase would modify wind patterns. However, it is hard to quantify at this time how those patterns would change, and what effect they would have on the model calculations of changes in air quality for the climate change scenarios.

Stability

It appears reasonable that increased surface temperature would result in an increase in convective activity and a corresponding increase in the frequency of unstable atmospheric conditions. In most air quality simulation models, such as the RTM-III, changes in stability affect plume rise and dispersion processes. In the RTM-III stabilty is calculated using a method proposed by Turner (1970) that relates stability class to surface wind speed and solar insolation. Since this stabilty classification scheme does not explicitly use temperature, we have no choice but to assume that stability does not change in the climate change scenarios.

Higher plume rise for point sources may result in local increases in ozone (due to the lack of NO titration) and possibly lower ground-level ozone values downwind. The occurrence of unstable conditions earlier in the day would bring emissions of hydrocarbons and nitrogen oxides (NO_x) together earlier in the day, resulting in a longer period of photochemical activity. Thus the lack of stability changes in the climate change scenarios may understate changes in ozone concentrations.

Emissions

It is well known that increased temperature results in increase evaporation and hence increased emission of volatile organic compounds (VOC). Temperature is also a key factor in emissions from automobiles. Since automobiles are the main class of reactive hydrocarbon emitters, and a major source for NO_x emissions, these emission changes could be significant. Automobiles tend to emit more reactive hydrocarbons and less NO_x and CO at higher ambient temperatures. Higher temperatures during the summer months, as is assumed in the California and midwestern/southeastern applications of the RTM-III, would also result in increased use of air conditioning systems and corresponding increases in emissions from power plants supplying the electricity.

Biogenic emissions are also known to increase with temperature as plant respiration increases. However, at extreme temperatures some plants will close their stomata openings to reduce moisture loss, resulting in decreased respiration and a lower rate of biogenic emissions. The net effect of increased temperature on anthropogenic and biogenic emissions is a definite increase in reactive hydrocarbons and possibly a decrease in low-level (area source) NO_x and increase in elevated (point source) NO_x, resulting in a more reactive atmosphere.

It is difficult to estimate emission rates and distribution 50 to 100 years in the future. Reactive hydrocarbon and NO_x emissions are currently controlled to meet air quality standards. In addition, automobiles that far in the future would be significantly more efficient than the current automobile fleet, and the widespread use of electric cars is a distinct possibility. On the other hand, population growth will increase emissions as more people use electricity, industrial products, and automobiles.

Given the uncertainities associated with estimating emissions so far in the future, we elected to use the base case 1980 NAPAP anthropogenic and biogenic emissions for the climate change scenarios. Future research should include efforts to estimate future emissions under increased temperature conditions.

DEFINITION OF STRATOSPHERIC OZONE REDUCTION

Several climatic and atmospheric modeling studies have indicated that the stratospheric ozone layer is decreasing due to chemical reactions with halocarbons (Cicerone et al., 1983; Prather, McElroy, and Wofsy, 1984), methane (Craig and Chou, 1982), and nitrous oxide (Weiss, 1981). Since stratospheric ozone is the principal attenuator of ultraviolet radiation, the reduction in the stratospheric ozone layer would result in increased penetration of UV-B to the troposphere. This phenomena would not only likely result in an increase in skin cancer, but also in increased photochemical reaction rates for specific atmospheric pollutants. These increased photochemical rates may, in turn, result in increased production of photochemical oxidants in the troposphere.

In fact, according to a recent study, the depletion of stratospheric ozone may be a more important factor than temperature increases in the formation of ozone in the urban environment (Gery, Edmond, and Whitten, 1987). That study assumed a reduction in the stratospheric ozone column of from 16.5 to 33 percent and calculated the effects of the stratospheric ozone reduction on air quality in several urban areas. However, since the study an international agreement to control emissions of chlorocarbons has been signed. Based on the implementation of emission reductions specified in the so-called Montreal protocol, new estimates of the stratospheric ozone reduction range from 0 to 20 percent, with the latest predictions being a few percent. However, it remains to be seen whether the proposed controls will be effective in the future.

Thus for the climate change scenario that includes depletion of stratospheric ozone concentrations we are assuming a 10 percent decrease. For the base case simulations we assume an ozone column of 0.300 cm-atm. This represents approximately the monthly average ozone column at North American latitudes during the months of July and August. Thus a 10 percent reduction in stratospheric ozone would result in an ozone column of 0.270 cm-atm. Photolysis rates were calculated by the method discussed by Gery, Edmond, and Whitten (1987).

DEFINITION OF MODELING SCENARIOS

Three modeling scenarios were defined to estimate the effect of future climate changes on tropospheric ozone concentrations. These scenarios consist of a base case and two future climate cases:

Base case--current meteorological and ozone column conditions

Scenario #1--4°C temperature increase and attendant increase in water vapor concentrations.

Scenario #2--4°C temperature and water vapor increases and a 10 percent reduction in stratospheric ozone concentrations.

The RTM-III was exercised for ozone episodes of approximately one-week duration for the central California and the midwestern/southeastern modeling domains for the base case and scenario #1. Due to limitations on time and resources for this work, scenario #2 was modeled only for four days from the midwestern/southeastern modeling episode.

UNCERTAINTIES

Before presenting the modeling results it is useful to review the uncertainities associated with assumptions in the modeling. These uncertainites can be roughly divided into three categories: (1) uncertainity in the assumptions used to define the climate change scenarios, (2) uncertainities in the model inputs, and (3) model limitations.

Definitions of the Climate Change Scenarios

Foremost among the uncertainties in the climate change scenarios is that the 4°C temperature increase is assumed to occur uniformly throughout the modeling domain and over the diurnal cycle. If most of the increase in temperature occurs at night, rather than in the day when photochemical activity occurs, then the assumption of uniform temperature change across the diurnal cycle may overstate the ozone concentrations, since ozone formation occurs during the day. If the temperature increase above the ground is less than 4°C, the assumption of a 4°C increase aloft may also overstate the ozone concentrations.

The assumption that mixing heights will not change with the increase in temperature will overstate ozone concentrations. By not including changes in cloudiness in the climate change scenarios, the effects of increased temperature will be either over- or underestimated, depending on whether cloudiness actually increases or decreases. The fact that stability is also not adjusted for the climate change scenarios may also result in an understatement of ozone concentrations.

The uncertainities associated with the water vapor concentrations stem from the assumption that the temperature increase is uniform and that relative humidity will remain constant as the temperature increases. As for the temperature, if daytime temperature and temperatures aloft do not increase 4°C, then the assumed water vapor concentrations will be too high and the resulting effects of increased temperature on ozone concentrations will be overstated.

Finally, the effects of holding emissions constant for the climate change scenarios will, most likely, result in an understatment of ozone concentrations. A significant increase in hydrocarbon emissions can be expected with a 4°C temperature increase and the population growth expected in the next 50 to 100 years. However, no one can predict the emission reductions that will occur in the future, or the possibility of more efficient emission controls. However, higher temperatures do result in an increase in emission rates, so that neglecting this change in emissions would result in an understatement of the changes in ozone concentrations.

Model Inputs

Quite a bit of uncertainty is associated with the meteorological and emissions inputs used in the applications of the RTM-III, as is true for all air quality models. Of particular note are the wind fields over complex terrain in the central California application. The ramifications of these uncertainties should, in general, be minimal since we are examining the sensitivity of a regional oxidant model to postulated changes in future climate conditions, and any possible deviations between model input and actual conditions would be the same for both the base case and climate change cases. However, since there is quite a bit of uncertainity in the temperature and water vapor concentration fields used as input, this uncertainity does transfer over to the calculations of ozone concentrations under increased temperature conditions. Depending on the base case temperature, an increase of 4°C will produce different effects in the photochemistry rates and resultant production of ozone.

Model Limitations

In any modeling study we cannot know with full certainty whether a model is capturing all of the effects of changes in meterological and emission input data. In this study we decided to change a minimal number of variables--temperature and water vapor--for the first climate change scenario. Thus the primary uncertainity will be in the chemical mechanism used. We have attempted to limit this uncertainity by incorporating into RTM-III the latest version of the Carbon Bond IV Mechanism, the CB-IV (Gery, Whitten, and Killus, 1988). For a brief description of the formulation of the RTM-III and the CB-IV mechanism, see Appendix A in this report.

RESULTS OF THE SIMULATIONS — CLIMATE CHANGE SCENARIO #1

The effects of increased temperature on tropospheric ozone concentations were studied in two separate simulations using RTM-II: a six-day ozone episode (5-10 August 1981) in California and an eight-day episode (14-21 July 1980) in the midwestern/southeastern United States. The RTM-III was run using current climate conditions (the base case) and an increased temperature scenario, which was characterized by a 4°C uniform temperature increase and attendant increase in water vapor concentration assuming constant specific humidity.

An Eulerian regional oxidant model, such as the RTM-III, will report multi-level gridded fields of hourly average concentration for each species (about 30) in the chemical mechanism. Clearly, not all of this data can or needs to be presented here. Of particular importance, in terms of air quality regulations and health effects, are the effects of climate changes on the maximum daily ozone concentrations. Thus in the following paragraphs we discuss the calculated changes in maximum daily ozone concentrations due to an increase in temperature for each day of the two episode simulations.

Central California

Maximum daily ozone concentrations were calculated at each grid point in the central California modeling domain for each day of the six-day episode. The results for the base case are displayed in isopleths for each day of the episode in Figure 2-1. The results for the climate change scenario are shown in Figure 2-2. The differences between the daily maximum ozone concentrations for the climate change scenario and the base case are shown in isopleths in Figure 2-3. (All figures for this chapter are collected at the end of the chapter.) The highest maximum daily ozone concentrations predicted by the RTM-III for each day are given in Table 2-1. Isopleths of the predicted hourly ozone concentrations at three-hour intervals for the base case and first climate change scenario are presented in Appendixes C and D.

August 5, 1981

On this day the main area of elevated ozone concentration is downwind of the San Francisco Bay Area for both the base case and climate change scenario (compare Figures 2-1a and 2-2a). The increase in temperature moves the location of the highest ozone concentration closer to the urban area. In fact, the increased temperature results in ozone concentrations that exceed the primary National Ambient Air Quality Standard (NAAQS) for ozone (12 pphm) whereas no exceedance is calculated in the base case. As predicted by the RTM-III, an increase in temperature of 4°C results in an area approximately 300 km exceeding the primary ozone standard on this day.

TABLE 2-1. Highest daily ozone concentrations predicted by the RTM-III for each day of the central California episode for the base case and the case of increased temperature.

	Maximum Daily Ozone Concentration (pphm)		
	Base Case	Increased Temperature	Percent Increase
5 August 1981	11.8	12.1	3
6 August 1981	15.0	18.0	20
7 August 1981	11.7	13.1	12
8 August 1981	13.5	13.7	2
9 August 1981	10.5	11.2	7
10 August 1981	9.1	9.8	8

In areas away from the San Francisco urban area the effects of the temperature increase are small (see Figure 2-3a). In many areas there is no change, but in some areas, such as downwind of Bakersfield, there is a slight increase in ozone. However, in Bakersfield itself there is a slight decrease of over 0.5 pphm. This decrease appears to be the result of increased mixed-layer NO concentrations from a point source whose plume rise was reduced because of bouyancy flux due to the increase in the ambient temperature. The increase of NO emissions in the mixed-layer results in the local suppression of ozone due to titration.

August 6, 1981

The highest ozone concentrations for the entire episode were calculated for both the base case and increased temperature case on this day (see Figures 2-1b, 2-2b, and 2-3b). The temperature increase results in increases in ozone throughout the modeling domain; the highest maximum daily ozone concentration increases from 15.0 pphm in the base case to 18.0 in the increased temperature scenario, a 20 percent increase (Table 2-1). The ozone peak is slightly further downwind in the increased temperature case. The region of predicted ozone concentration in excess of the NAAQS almost doubles from 3,700 km^2 (in the base case) to 6,600 km^2. Thus under the increased temperature scenario the model predicts exceedances of the NAAQS in the city of San Francisco.

In two of the main cities in the San Joaquin Valley, Fresno and Bakersfield, the temperature increase results in an increase of approximately 0.5 pphm (8 percent) in the maximum daily ozone concentration. In the rest of the valley ozone increases are on the order of 0.1 pphm. At regions distant from emission sources, such as the Sierra Nevada, there is little change in the ozone concentrations.

August 7, 1981

On August 7 the highest ozone concentrations for the base case and increased temperature scenario occur at the same site, approximately 80 km downwind of San Francisco (Figures 2-1c and 2-2c). However, ozone levels increase from 11.7 in the base case to 13.1 pphm under increased temperature. Again, under increased temperature the NAAQS is exceeded, where no exceedance occurred under current climate conditions. In the heart of the Oakland urban area ozone decreases by approximately 1 pphm (Figure 2-3c). This decrease may be due to the faster photochemical reactions caused by increased temperature, such that the more reactive hydrocarbons close to the urban areas are burned out before the time of peak photochemical production in the middle of the day. This is partially confirmed by the fact that the highest ozone concentration occurs earlier in the increased temperature scenario than in the base case.

In areas outside the San Francisco Bay Area urban plume the temperature increase has very little effect on ozone concentrations; the only significant effect is a slight increase (0.5 pphm) in the vicinity of Bakersfield.

August 8, 1981

On August 8 the highest ozone level in the increased temperature scenario (13.7 pphm) is only slightly higher than the highest value in the base case (13.5 pphm) (see Figures 2-1d and 2-2d). There is almost no difference between the two cases in the areal extent of the region in excess of the NAAQS. Again, the increased temperature scenario results in a slight (0.1 pphm) decrease in ozone at the San Francisco - Oakland urban center. In the remainder of the modeling domain there are slight increases in ozone, except for a small area around western Yosemite National Park, where there is a slight decrease in ozone (Figure 2-3d).

August 9, 1981

Ozone concentrations on August 9 are lower than the previous days in both the base case and the increased temperature scenario. Because of a shift in wind to the northwest, the highest daily ozone concentration is located southeast of the San Francisco Bay Area near Stockton. Over the northwestern portion of the modeling domain the temperature increase results in an increase in ozone (from 0.1 pphm in the base case to 2.0 pphm). Again the temperature increase has little effect on ozone concentrations in the remainder of the modeling domain, away from the influences of the San Francisco Bay Area urban plume (Figure 2-3e).

August 10, 1981

On August 10 an increase in wind speeds from the northwest results in a "tongue" of ozone spreading out from the San Francisco Bay Area down the San Joaquin Valley (Figures 2-1f and 2-2f). Although the highest ozone concentration on 10 August is the lowest for the six-day episode, for both the base case (9.1 pphm) and increased temperature scenario (9.8 pphm), ozone concentrations within the San Joaquin Valley are both higher and more widespread than on previous days. Throughout the entire modeling domain the ozone concentrations in the increased temperature scenario are higher than in the base case.

Midwestern/Southeastern Region

Maximum daily ozone concentrations were calculated at each grid point in the midwestern/southeastern U.S. for an eight-day ozone episode (July 14-21, 1980). The results for the base case are shown in isopleths in Figure 2-4. The results for the first climate change scenario are shown in Figure 2-5. The differences between the climate change scenario and the base case are shown in isopleths in Figure 2-6. The highest maximum daily ozone concentrations predicted by RTM-III for each day are given in Table 2-2.

July 14, 1980

On the first day of the episode the increased temperature has almost no effect on the ozone concentrations compared to the base case (Figures 2-4a and 2-5a). In fact,

TABLE 2-2. Highest maximum daily ozone concentrations predicted by the RTM-III for each day of the midwestern/southeastern episode for the base case and the case of increased temperature.

Date	Maximum Daily Ozone Concentration (pphm)		Percent Increase
	Base Case	Increased Temperature	
14 July 1980	11.3	11.3	0.0
15 July 1980	11.5	11.9	3.5
16 July 1980	12.5	13.0	4.0
17 July 1980	11.7	12.0	2.6
18 July 1980	11.2	12.1	8.0
19 July 1980	13.8	14.8	7.2
20 July 1980	11.1	11.2	0.9
21 July 1980	12.6	12.3	-2.4

the plot showing differences between the two cases (Figure 2-6a) reveals that there are about equal areas with increases and decreases in ozone and these differences rarely exceed 0.1 pphm in magnitude. The exception is in the vicinity of Pittsburg, where the increased temperature scenario results in a decrease in ozone of approximately 1 pphm. For a region of this size it would take over one day to minimize the effects of the initial conditions; thus, we cannot tell if this decrease is significant or just an artifact of the initial conditions. The highest ozone concentrations calculated for the base case and increased temperature case are the same (11.3 pphm).

July 15, 1980

On July 15 the highest ozone concentrations for the base case (11.5 pphm) and the increased temperature scenario (11.9 pphm) both occur in the urban plume downwind of Chicago. Except for an area stretching from Arkansas to Alabama, ozone concentrations are higher everywhere under the increased temperature scenario. The highest increase (approximately 1 pphm) occurs on the border between Minnesota and Iowa (Figure 2-6b).

July 16, 1980

The highest ozone concentration for the base case on July 16 (12.5 pphm) occurs in the urban plume downwind of Detroit. Under the increased temperature scenario the highest concentration (13.0 pphm) is still downwind of Detroit but the predicted area of exceedences of the ozone NAAQS increases by almost a factor of three from approximately 9,800 km^2 in the base case to 27,000 km^2. In the increased temperature scenario increases in ozone are mainly in the upper midwestern, southwestern, and southeastern portions of the modeling domain (Figure 2-6c). In three areas with elevated ozone (>10 pphm) in the base case--the Ohio River valley, New Orleans, and Iowa--the increases in ozone in the increased temperature scenario are less (<0.2 pphm) than is seen downwind of Detroit.

July 17, 1980

On July 17 ozone levels in the increased temperature scenario are higher than in the base case over almost the entire modeling domain (Figures 2-4d, 2-5d, and 2-6d). Significant increases, greater than 0.5 pphm, occur over an area connecting the cities of Chicago and Detroit. The highest calculated ozone concentration in the region is 12.0 pphm, compared to 11.7 pphm for the base case. There are slight increases in ozone (0.1 to 0.5 pphm) in other areas of base case predicted elevated ozone concentrations (> 10 pphm), i.e., Nashville, New Orleans, and Iowa. However, in the increased temperature scenario ozone levels over eastern Kansas are lower than in the base case (10.7 pphm compared to 11.7 pphm).

July 18, 1980

On July 18 ozone concentrations throughout the entire modeling domain increase significantly under the increased temperature scenario. Increases in excess of 1 pphm occur over Iowa, Wisconsin, and Pennsylvania; in most of the modeling domain increases are in excess of 0.5 pphm. The highest ozone concentration under the increased temperature scenario is 12.1 pphm, an exceedance of the NAAQS.

July 19, 1980

Urban plumes from St. Louis, Chicago, Detroit, and emissions from the Ohio River valley create a region of elevated ozone concentration covering Indiana, Illinois, Ohio, and Michigan. The highest calculated ozone concentrations of the episode occur on this day downwind of Detroit over Toronto (Figures 2-4f and 2-5f): 13.8 pphm in the base case and 14.8 pphm in the increased temperature case. In the latter case ozone levels are higher than in the base case over most of the region; the most significant increases (0.5 to 1 pphm) occur in Minnesota, Iowa, Wisconsin, and Michigan.

July 20, 1980

On July 20 the only significant increases in ozone under the increased temperature scenario occur in the upper northwestern portion of the region (Figures 2-4g, 2-5g, and 2-6g). The highest ozone concentration calculated for the base case on this day (11.1 pphm) occurs over Pittsburgh; for the increased temperature case it is 11.2 pphm, also over Pittsburgh. A more dramatic increase in ozone due to the increase in temperature occurs downwind of Chicago, from 10.7 pphm in the base case to 11.2 pphm.

July 21, 1980

On the last day of the episode the increased temperature results in significant ozone increases over a large portion of the region compared to the base case (Figure 2-6h). The main exception is near the center of the western boundary, where ozone under the increased temperature scenario is less than in the base case (12.3 pphm compared to 12.6 pphm). However, significant increases occur around Chicago, where the maximum daily ozone concentration in the Chicago plume increases from 11.1 in the base case to 12.3 pphm in the increased temperature scenario. Despite the fact that the highest ozone concentration on this day is lower in the increased temperature scenario than in the base case, the area of ozone concentrations in excess of the NAAQS increases from approximately 9,800 km^2 in the base case to 16,900 km^2 in the increased temperature scenario.

RESULTS OF THE SIMULATIONS — CLIMATE CHANGE SCENARIO #2

Because of limitations on the study, simulations of climate change scenario #2 were limited to four days of the midwestern/southeastern episode and the California episode was not simulated. Here we briefly examine the results of the simulation of the four days (July 14-17, 1980) in the midwestern/southeastern U.S. episode. In this second climate change scenario the temperature is assumed to increase by 4°C, as in scenario #1, and photolytic rates are assumed to increase due to a 10 percent reduction in the ozone column. Predicted maximum daily ozone concentrations for the second climate change scenario are shown in isopleths in Figure 2-7, and isopleths showing the differences between this case and the base case are shown in Figure 2-8.

As noted by Gery, Whitten, and Killus (1987), the effects of increased ultraviolet irradiance or temperature on tropospheric ozone concentrations depends on the oxidant-forming potential of the system. This in turn is generally a function of meteorological conditions and the efficiency of the atmospheric system in converting oxidant precursors to oxidants. For some atmospheric systems the increased energy results in increased reactivity in the morning hours, depleting enough oxidant precursors from the system to limit afternoon ozone production to levels lower than the base case.

For example, on July 14 of the modeled episode the patterns of increases and decreases in ozone for the two climate change scenarios are similar. This seems to indicate that the ozone formation potential for this day is precursor limited. Over most of the region the maximum daily ozone concentrations for the two scenarios differ by only 0.1 pphm; the biggest difference occurs in the northeastern portion of the modeling domain. The highest ozone concentration for all three scenarios on 14 July occurs over the Ohio River valley, where the value under increased UV and temperature conditions is 11.6 pphm compared to 11.3 pphm for both the base case and first climate change scenario. Thus for the Ohio River valley, the ozone formation potential may not be precursor limited. Differences in the two climate change scenarios occur on the Pennsylvania-Ohio border; under increased temperature alone (scenario #1) ozone is approximately 1 pphm lower than in the base case, whereas under scenario #2 (increased temperature and UV) ozone is only 0.1 pphm lower than in the base case.

On the other three days of the episode under the second climate change scenario, ozone levels are slightly lower (0 to 0.3 pphm) than under scenario #1. Both climate change scenarios produce a similiar pattern of increases and decreases in concentrations when compared to the base case for this episode. This is illustrated by the highest daily maximum ozone concentrations for July 15-17: the values under the second climate change scenario lie between the base case and first climate change case (see Table 2-2).

These results are consistent with those found by Gery, Whitten, and Killus, who showed that under conditions of increased temperature and UV radiation the highest ozone concentrations were frequently lower in cities with less oxidant precursors. This is because the increased energy, due to an increase in temperature and/or UV radiation, burns out the oxidant precursors earlier in the day, resulting in less oxidant precursors in the afternoon, the period of maximum ozone formation potential. The rather coarse grid spacing used in the midwestern/southeastern modeling domain (approximately 50 km on a side) reduces the peak precursor concentrations from the urban areas because of dilution in the large grid cells.

IMPLICATIONS OF THE ANALYSIS FOR AIR QUALITY CONTROLS

Although this preliminary model sensitivity analysis may be useful in anticipating the kinds of air quality controls that may be needed in responding to potential global climate changes, the uncertainties associated with predicting just how the climate may be modified preclude any definitive discussion here of regulatory controls. These preliminary modeling results can only indicate possible general trends in exceedances of the ozone standard and increases in the number of people exposed to unhealthy levels of ozone as a result of global climate change.

Our study indicates that under most conditions (i.e., immediately downwind of urban areas) increased temperature tends to (1) increase ozone concentrations, (2) move the location of the peak ozone concentration closer to urban areas, and (3) expand the area in which ozone concentrations exceed the primary ozone standard of 12 pphm. Thus the modeling study indicates that global warming will not only lead to more exceedences of the primary ozone standard over a larger area, but also to an increase in the number of people exposed to these elevated ozone concentrations. Maps of the ozone concentrations in the vicinity of the San Francisco Bay Area for the base case and first climate change scenario clearly show the increase in areas of exceedences of the NAAQS due to increases in temperature (Figure 2-9). Similar maps for the midwestern/southeastern modeling domain are given in Figure 2-10. A crucial question is whether future increases in global temperature will jeopardize the goal of attainment of the ozone standard in regions in the United States and increase the number of people exposed to unhealthy levels of ozone concentrations.

Census data from 1980 were mapped onto the two modeling regions (central California and midwestern/southeastern U.S.) to determine the number of people that may be exposed to higher levels of ozone concentrations as a result of increased ambient temperature. Table 2-3 presents estimates of the number of people-hours exposed to ozone concentrations in excess of 8, 12, and 16 pphm for the base case and the increased temperature case for the two modeling regions. These estimates were obtained by multiplying the population in a grid cell by the total number of hours that the predicted hourly ozone concentration in that grid cell exceeded 8, 12, or 16 pphm. Thus the figures in Table 2-3 are overstatements of the actual population exposure since people tend to spend 80 to 90 percent of their time indoors, and indoor ozone concentration levels are typically 10 to 70 percent of the outdoor level.

Table 2-3 indicates that approximately three times as many people in the central California modeling domain and 60 percent more people in the midwestern/southeastern modeling domain will be exposed to hourly ozone concentrations in excess of the NAAQS as a result of a 4°C temperature increase. In addition, the modeling results suggest that, with the increase in temperature, people in central California will be exposed to ozone concentrations in excess of 16 pphm whereas under current temperature conditions the modeled ozone concentrations do not exceed 16 pphm.

In air quality regulation, geographic areas are divided into air basins for purposes of classifying air quality, although air basins are sometimes further divided into local regions. A region is considered "nonattainment" of an air quality standard (NAAQS) if its estimated exceedance rate of the NAAQS is more than once per year over three years. Exceedances are counted in terms of days. The number of monitors recording an exceedance or the number of hours is not a factor in establishing an exceedance. Thus whether two monitors in a region measure an exceedance of the NAAQS or one monitor measures several hours of exceedance on the same day, that day counts as one exceedance of the NAAQS for that region.

In the RTM-III simulation of the six-day central California episode the number of exceedances of the NAAQS for the entire modeling domain doubles from 2 to 4 days due to increases in temperature (Table 2-1). For the eight-day episode in the midwestern/southeastern U.S the number of days in which predicted ozone concentrations exceed the NAAQS increased from 3 for the base case to 5 for the

TABLE 2-3. Number of people-hours of exposure to ozone concentrations in excess of 8, 12, and 16 pphm for the base case and the increased temperature case (climate change scenario #1).

	Exposure to $O_3 \geq 8$ pphm	Exposure to $O_3 \geq 12$ pphm	Exposure to $O_3 \geq 16$ pphm
Central California			
Base Case	70,509,216	660,876	0
Increased Temperature	102,012,064	2,052,143	92,220
Midwestern/Southeastern U.S.			
Base Case	1,722,590,208	29,805,348	0
Increased Temperature	1,956,205,568	47,528,944	0

increased temperature case. These exceedences occur in several different areas: Chicago, New Orleans, Iowa, Illinois, and downwind of Detroit.

To estimate the increases in exceedences and attainment status due to future increases in temperature we estimated the number of exceedences in each grid cell of the central California and midwestern/southeastern modeling domains. As discussed above, attainment or nonattainment is usually defined for entire air basins, although the definition of air basins is somewhat arbitrary and in some cases, at the discretion of the EPA, subregions within air basins are classified separately.

Table 2-4 gives the population exposed to exceedences of the NAAQS for ozone of 12 pphm. According the the RTM-III calculations for the California episode, a 4°C temperature increase will increase the number of exceedences of the NAAQS from 2 to 3 and increase the number of people exposed to an exceedence.

Out of a total of 5.5 million people living in the central California modeling domain in 1980, the percentage of people exposed to one exceedence of the NAAQS increases from 3 percent (175,080 people) for the base case to 8 percent (456,782 people) for the temperature increase case. Approximately 70,000 and 26,000 additional people would be exposed to, respectively, 2 and 3 exceedences of the ozone standard.

Increased temperature also expands the area of exceedences. Regions experiencing one, two, and three exceedences of the ozone NAAQS increase, respectively, from 5,200 to 7,100 km^2, 3,000 to 4,400 km^2, and 0 to 1,600 km^2.

Similiar results are seen for the midwestern/southeastern modeling domain. With an increase in temperature of 4°C, approximately 360,000 people would be exposed to two exceedances of the ozone standard. Out of approximately 35 million people in the midwestern/southeastern modeling domain, the percentage of people exposed to one exceedence of the NAAQS would increase from 25 percent (in the base case) to almost 30 percent.

These results must be viewed with caution. As discussed earlier, numerous simplifying assumptions were made in modeling the impacts of climate change on ozone, and

TABLE 2-4. Population exposed to exceedances of the National Ambient Air Quality Standard for ozone (12 pphm) for the base case and increased temperature case (climate change scenario #1). Population figures represent the total population in all model grid cells with a specified number of exceedances.

	Pop. in Grid Cells with 1 Exceed.	Pop. in Grid Cells with 2 Exceed.	Pop. in Grid Cells with 3 Exceed.
Central California			
Base Case	175,080	122,625	0
Increased Temperature	456,782	192,625	26,548
Midwestern/Southeastern U.S.			
Base Case	8,741,510	0	0
Increased Temperature	10,199,734	359,753	0

these assumptions add significantly to the quantitative uncertainty normally inherent in air quality modeling. Some of these assumptions, e.g., that the increase in temperature occurs everywhere, will tend to overstate the effects of increased temperature, while others, e.g., that hydrocarbon emissions do not increase under increased temperature conditions, tend to understate the impacts. The climate change scenarios presented here are simplistic and most likely do not completely describe the changes in climate associated with global warming.

The model's calculations of ozone under the simplified climate change scenarios discussed here should thus be viewed as possible trends rather than as conclusive impacts. The basic results of this modeling exercise are that increases in temperature will likely result in increases in maximum daily ozone concentrations, increases in the areas impacted by high ozone concentrations, and increases in the number of people exposed to unhealthy levels of ozone. Under these circumstances, currently planned emission control requirements to achieve attainment of the ozone standard may not be sufficient.

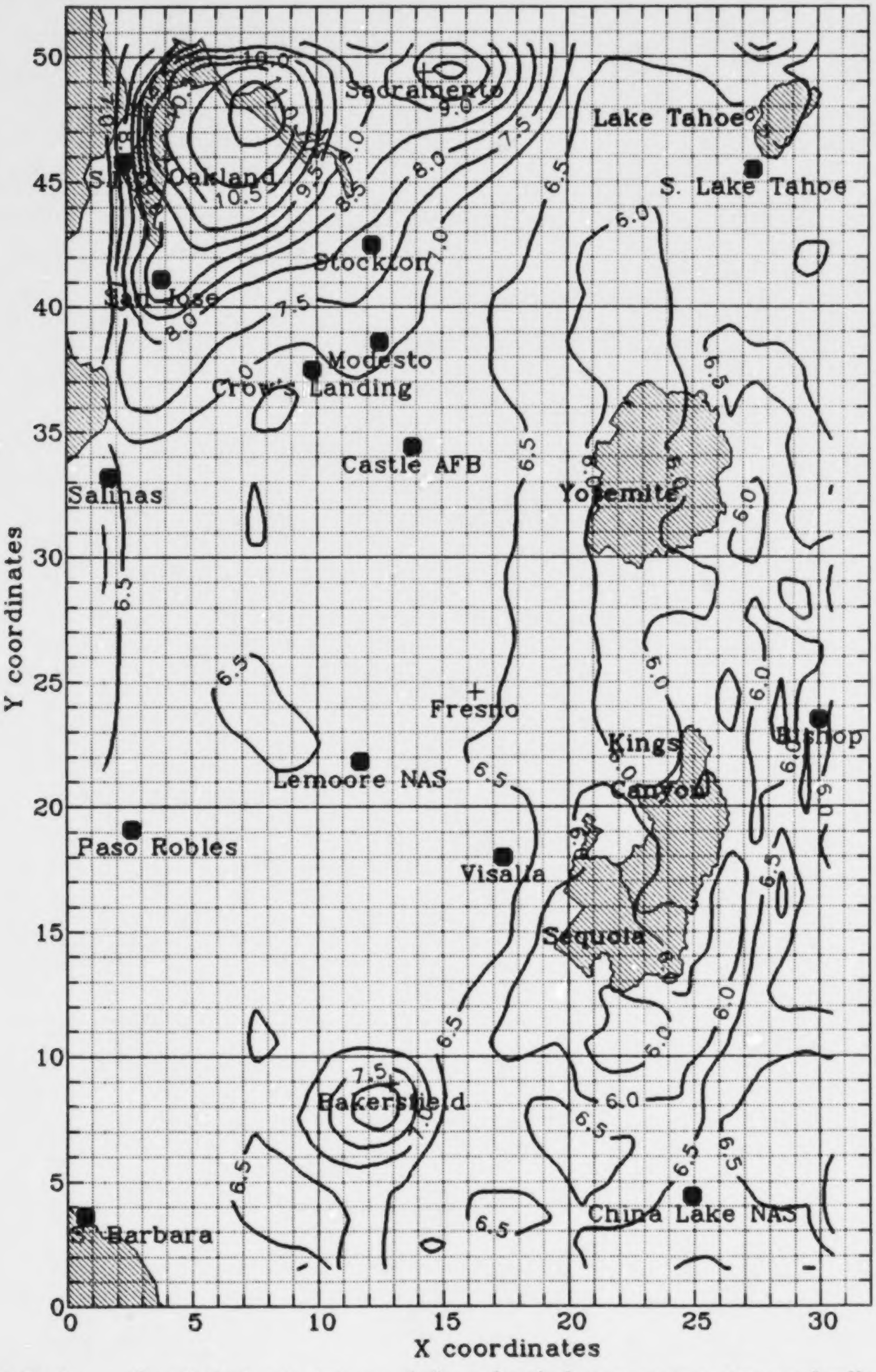
Sacramento
Lake Tahoe
S.F. Oakland
S. Lake Tahoe
Stockton
San Jose
Modesto
Crow's Landing
Castle AFB
Salinas
Yosemite
Fresno
Kings
Canyon
Bishop
Lemoore NAS
Paso Robles
Visalia
Sequoia
Bakersfield
China Lake NAS
S. Barbara
10.0
10.5
9.5
9.0
8.5
8.0
7.5
7.0
6.5
6.0
Y coordinates
X coordinates
0
5
10
15
20
25
30
35
40
45
50

Figure 2-1a. Predicted maximum daily mixed-layer ozone concentrations (pphm) for the base case scenario: August 5, 1981.

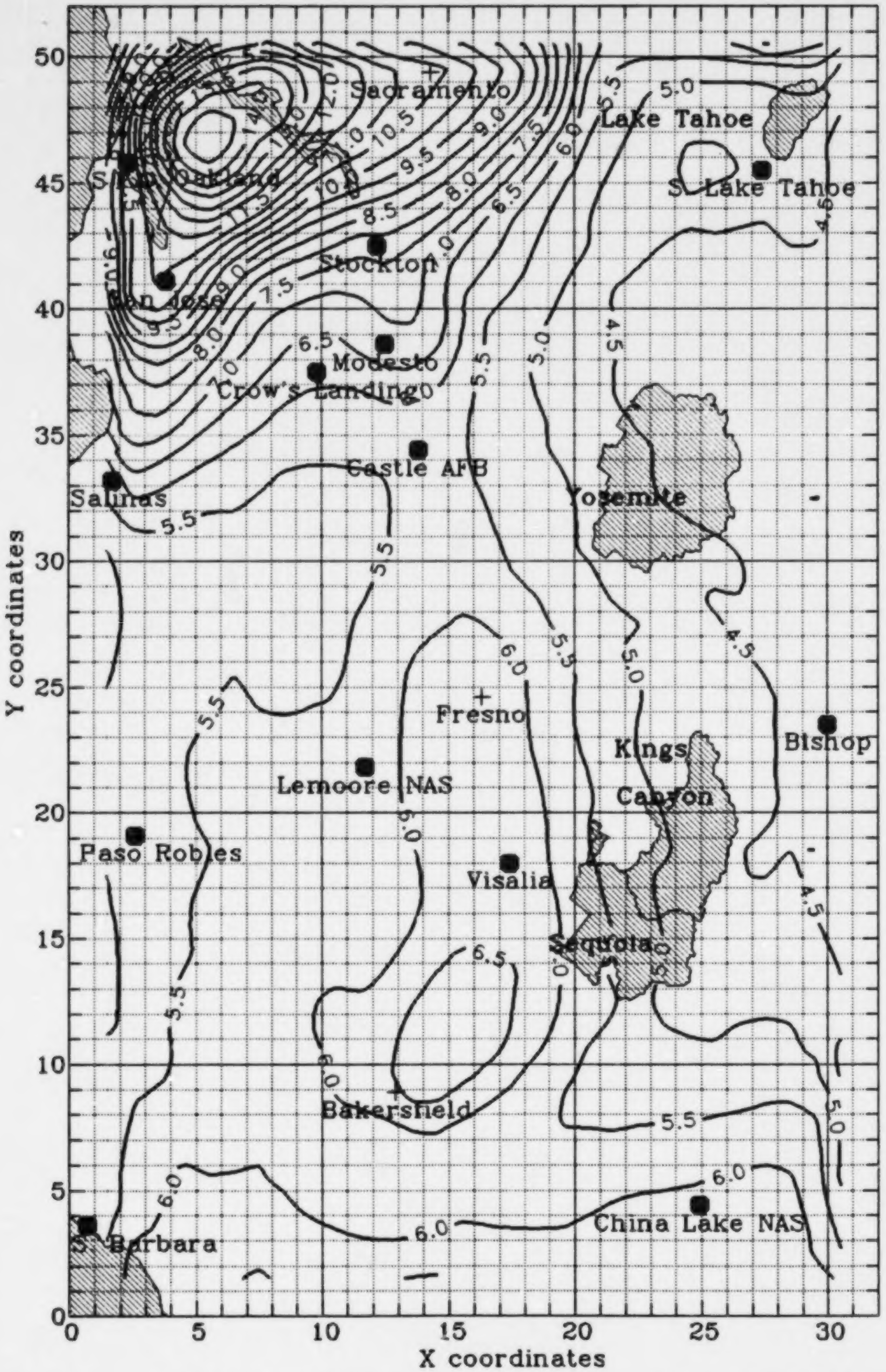

Y coordinates
X coordinates
0
5
10
15
20
25
30
35
40
45
50
Sacramento
Lake Tahoe
S. Lake Tahoe
S.F.
Oakland
San Jose
Stockton
Modesto
Crow's Landing
Castle AFB
Salinas
Yosemite
Fresno
Bishop
Kings
Canyon
Lemoore NAS
Paso Robles
Visalia
Sequoia
Bakersfield
China Lake NAS
S. Barbara
14.5
13.0
12.0
11.5
10.5
10.0
9.5
9.0
8.5
8.0
7.5
7.0
6.5
6.0
5.5
5.0
4.5

Figure 2-1b. Predicted maximum daily mixed-layer ozone concentrations (pphm) for the base case scenario: August 6, 1981.

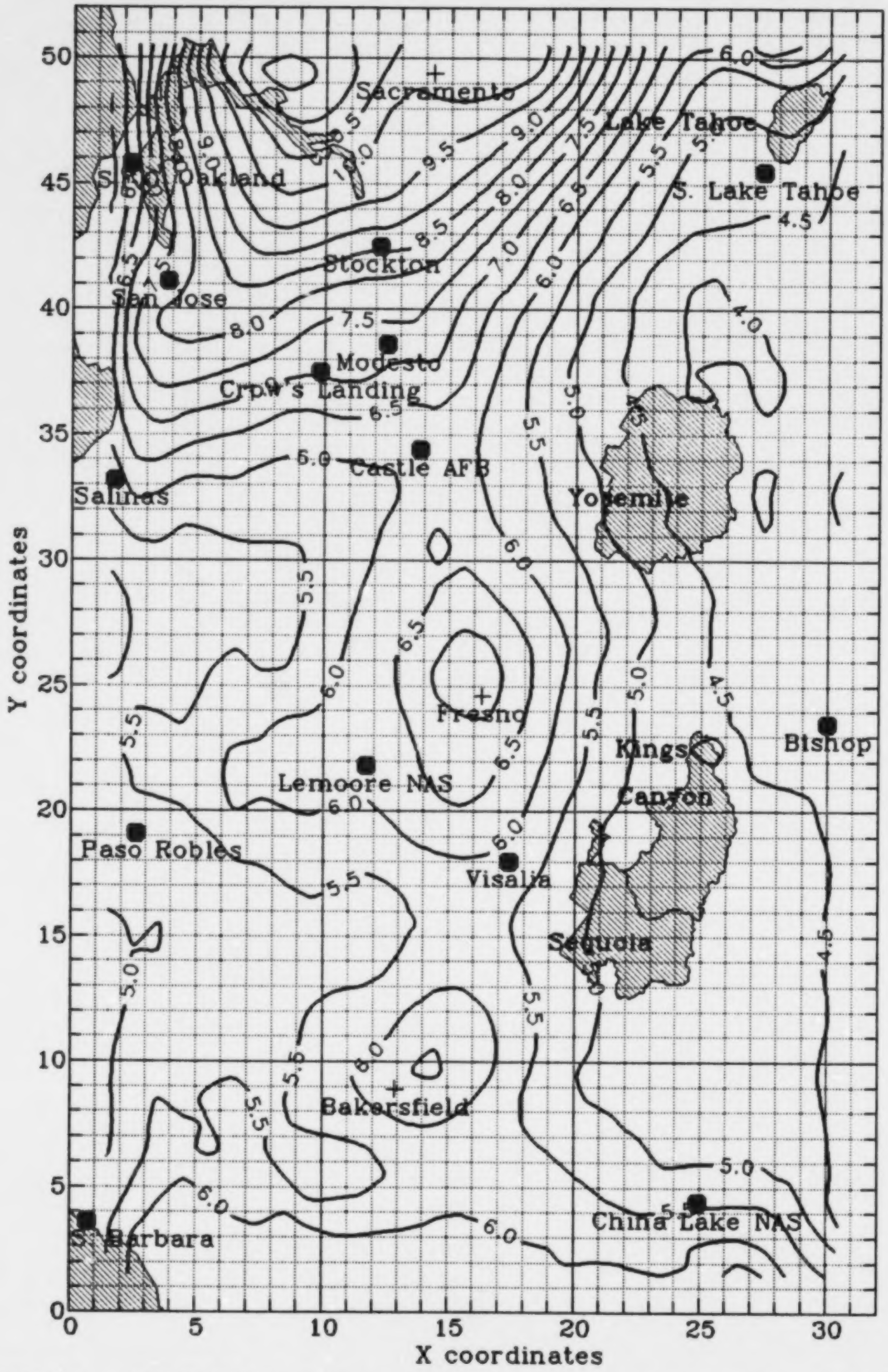
Sacramento
Lake Tahoe
S. Lake Tahoe
S.F.
Oakland
Stockton
San Jose
Modesto
Crow's Landing
Castle AFB
Salinas
Yosemite
Fresno
Kings
Canyon
Bishop
Lemoore NAS
Paso Robles
Visalia
Sequoia
Bakersfield
China Lake NAS
S. Barbara
Y coordinates
X coordinates
0
5
10
15
20
25
30
35
40
45
50
4.0
4.5
5.0
5.5
6.0
6.5
7.0
7.5
8.0
8.5
9.0
9.5
10.0

Figure 2-1c. Predicted maximum daily mixed-layer ozone concentrations (pphm) for the base case scenario: August 7, 1981.

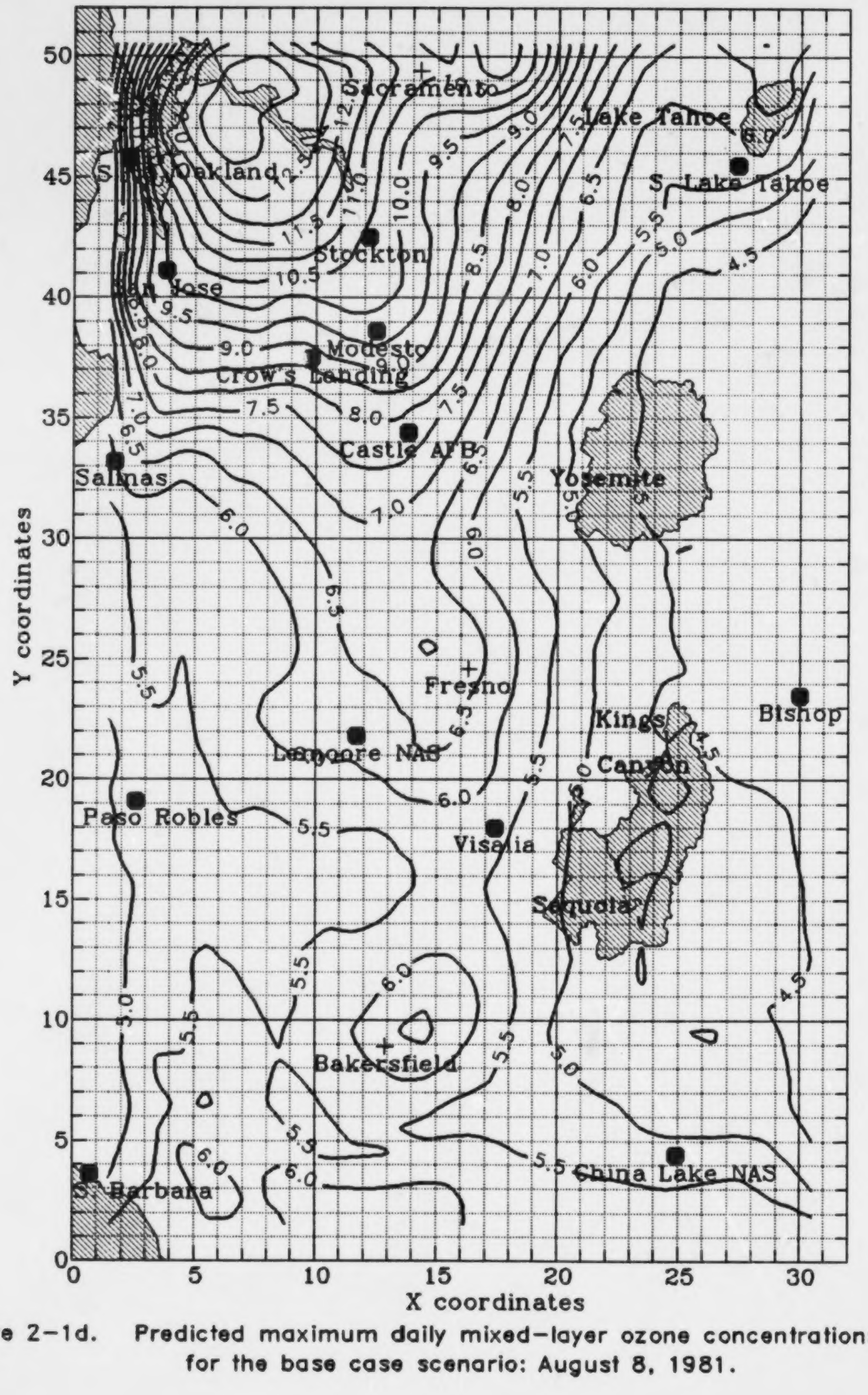
Sacramento
Lake Tahoe
S. Lake Tahoe
S.F.
Oakland
Stockton
San Jose
Modesto
Crow's Landing
Castle AFB
Salinas
Yosemite
Fresno
Kings
Canyon
Bishop
Lemoore NAS
Paso Robles
Visalia
Sequoia
Bakersfield
China Lake NAS
S. Barbara
Y coordinates
X coordinates
0
5
10
15
20
25
30
35
40
45
50
12.0
11.5
11.0
10.5
10.0
9.5
9.0
8.5
8.0
7.5
7.0
6.5
6.0
5.5
5.0
4.5

Figure 2-1d. Predicted maximum daily mixed-layer ozone concentrations (pphm) for the base case scenario: August 8, 1981.

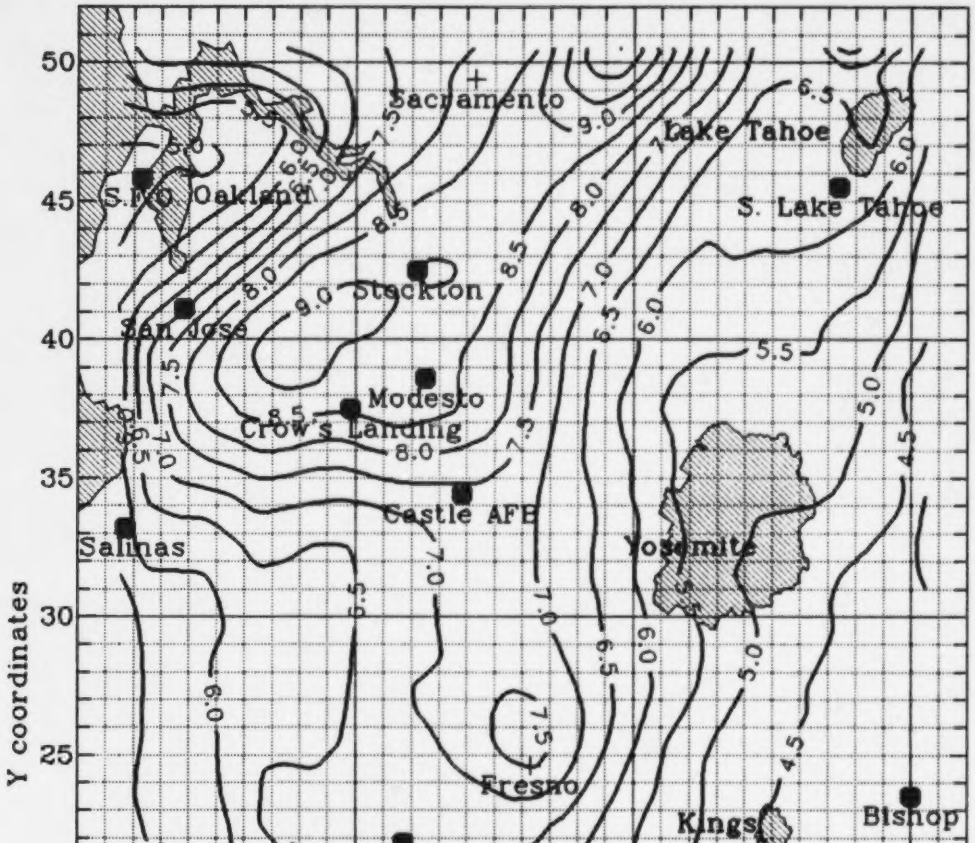
Sacramento
Lake Tahoe
S. Lake Tahoe
S.F.O. Oakland
Stockton
San Jose
Modesto
Crow's Landing
Castle AFB
Salinas
Yosemite
Fresno
Kings Canyon
Bishop
Lemoore NAS
Paso Robles
Visalia
Sequoia
Bakersfield
China Lake NAS
S. Barbara
Y coordinates
X coordinates
0
5
10
15
20
25
30
35
40
45
50

Figure 2-1e. Predicted maximum daily mixed-layer ozone concentrations (pphm) for the base case scenario: August 9, 1981.

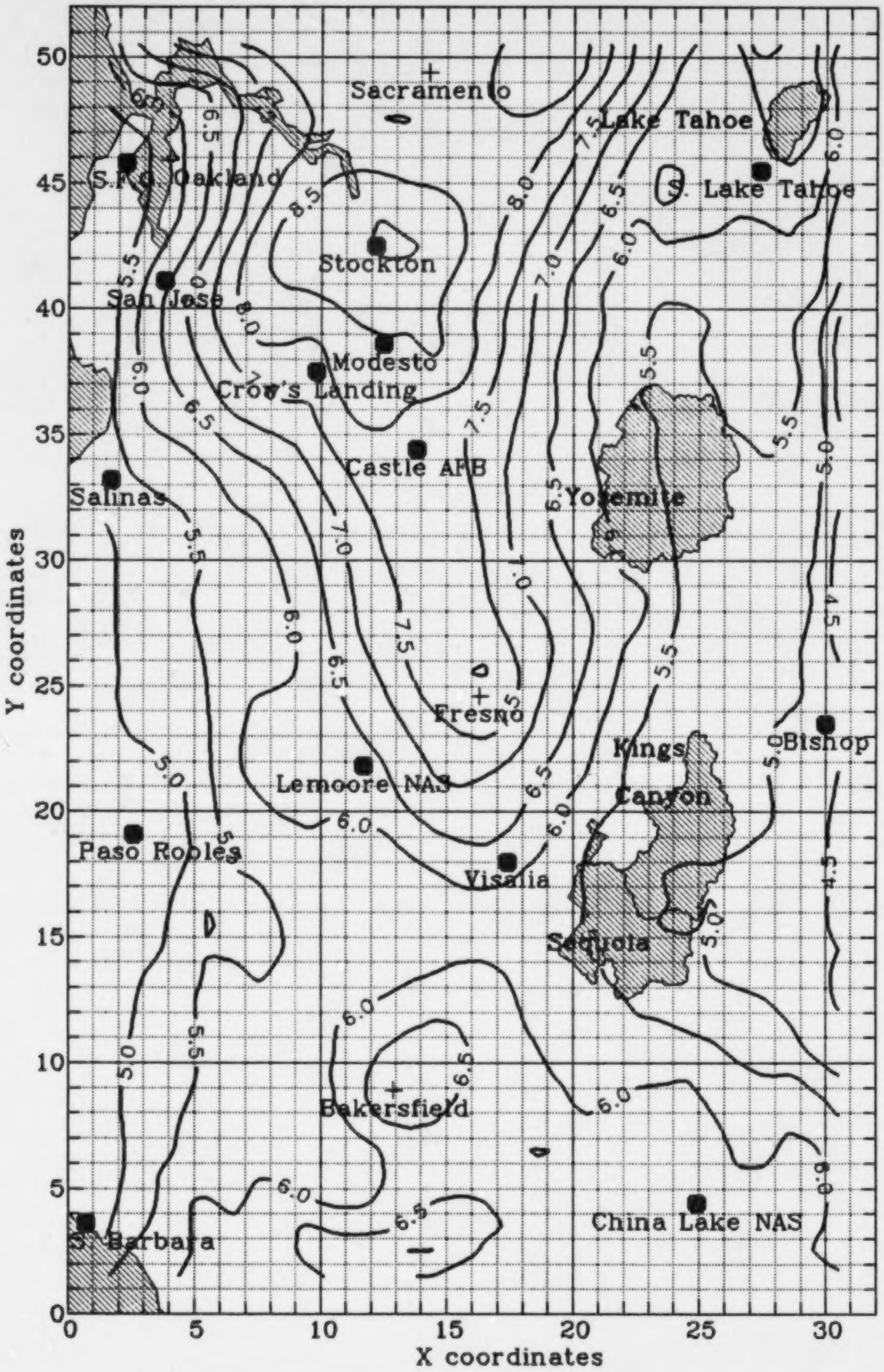

Sacramento
Lake Tahoe
S. Lake Tahoe
S.F. Oakland
Stockton
San Jose
Modesto
Crow's Landing
Castle AFB
Salinas
Yosemite
Fresno
Kings
Canyon
Bishop
Lemoore NAS
Paso Robles
Visalia
Sequoia
Bakersfield
China Lake NAS
S. Barbara
Y coordinates
X coordinates
0
5
10
15
20
25
30
35
40
45
50
4.5
5.0
5.5
6.0
6.5
7.0
7.5
8.0
8.5

Figure 2-1f. Predicted maximum daily mixed-layer ozone concentrations (pphm) for the base case scenario: August 10, 1981.

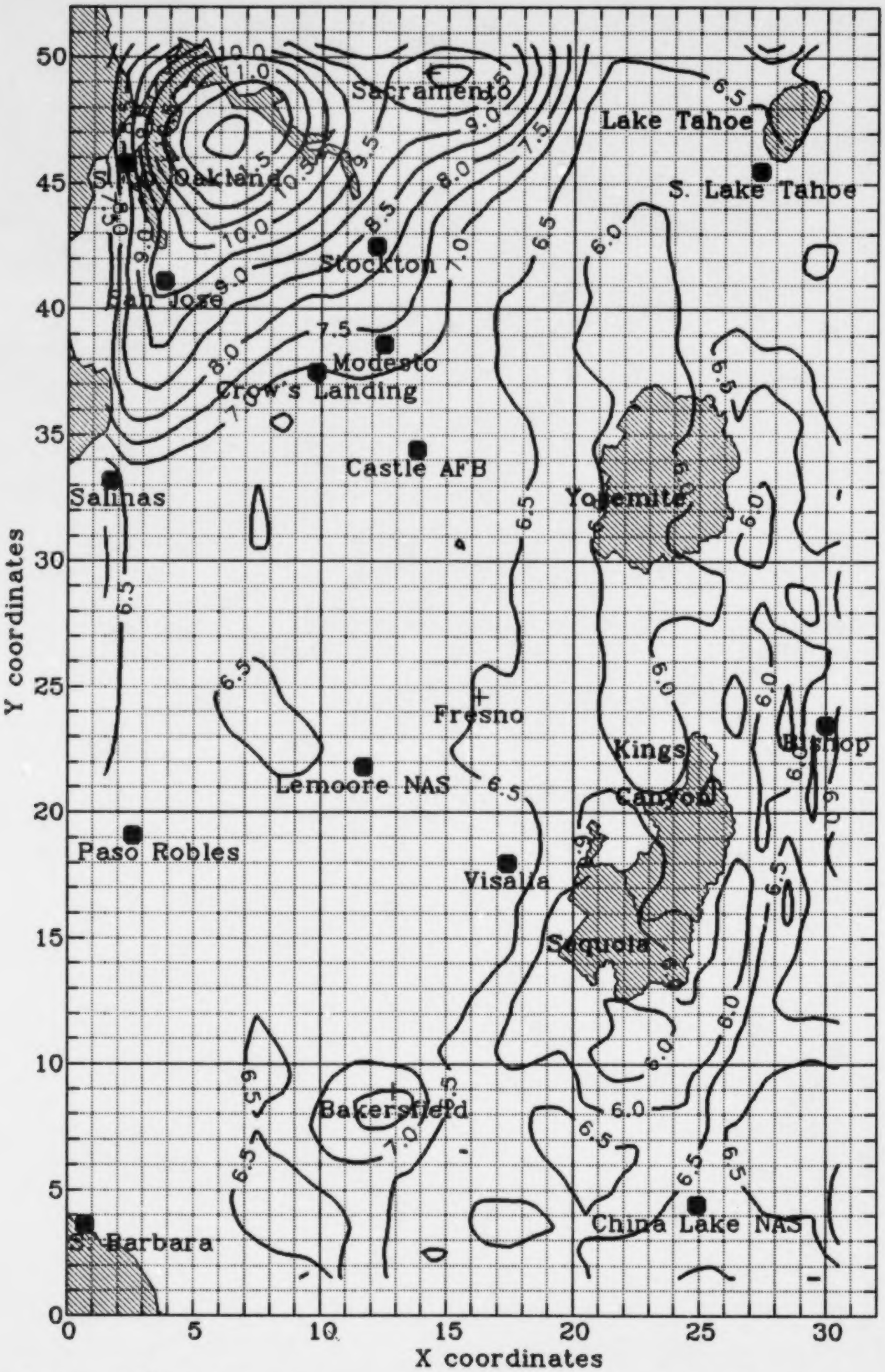
Y coordinates
X coordinates
Sacramento
Lake Tahoe
S. Lake Tahoe
S.F.
Oakland
Stockton
San Jose
Modesto
Crow's Landing
Castle AFB
Salinas
Yosemite
Fresno
Kings
Canyon
Bishop
Lemoore NAS
Paso Robles
Visalia
Sequoia
Bakersfield
China Lake NAS
S. Barbara
0
5
10
15
20
25
30
35
40
45
50
6.0
6.5
7.0
7.5
8.0
8.5
9.0
9.5
10.0
10.5
11.0

Figure 2–2a. Predicted maximum daily mixed–layer ozone concentrations (pphm) for climate sensitivity scenario #1 (temp. and water increase): August 5, 1981.

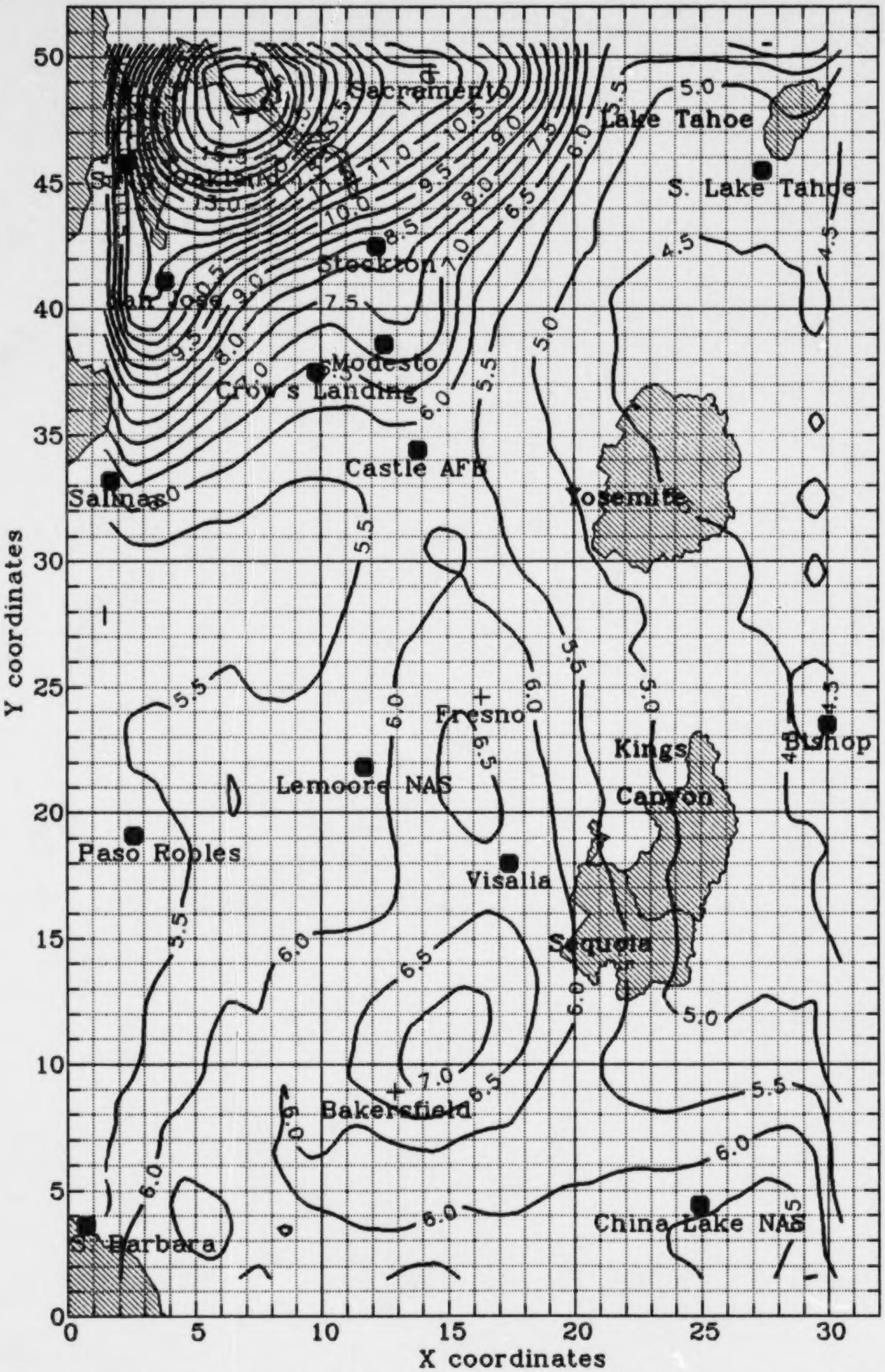
Sacramento
Lake Tahoe
S. Lake Tahoe
S.F. Oakland
San Jose
Stockton
Modesto
Crow's Landing
Castle AFB
Salinas
Yosemite
Fresno
Kings Canyon
Bishop
Lemoore NAS
Paso Robles
Visalia
Sequoia
Bakersfield
China Lake NAS
S. Barbara
Y coordinates
X coordinates
0
5
10
15
20
25
30
35
40
45
50
0
5
10
15
20
25
30
5.0
4.5
5.5
6.0
6.5
7.0
7.5
8.0
8.5
9.0
9.5
10.0
10.5
11.0

Figure 2-2b. Predicted maximum daily mixed-layer ozone concentrations (pphm) for climate sensitivity scenario #1 (temp. and water increase): August 6, 1981.

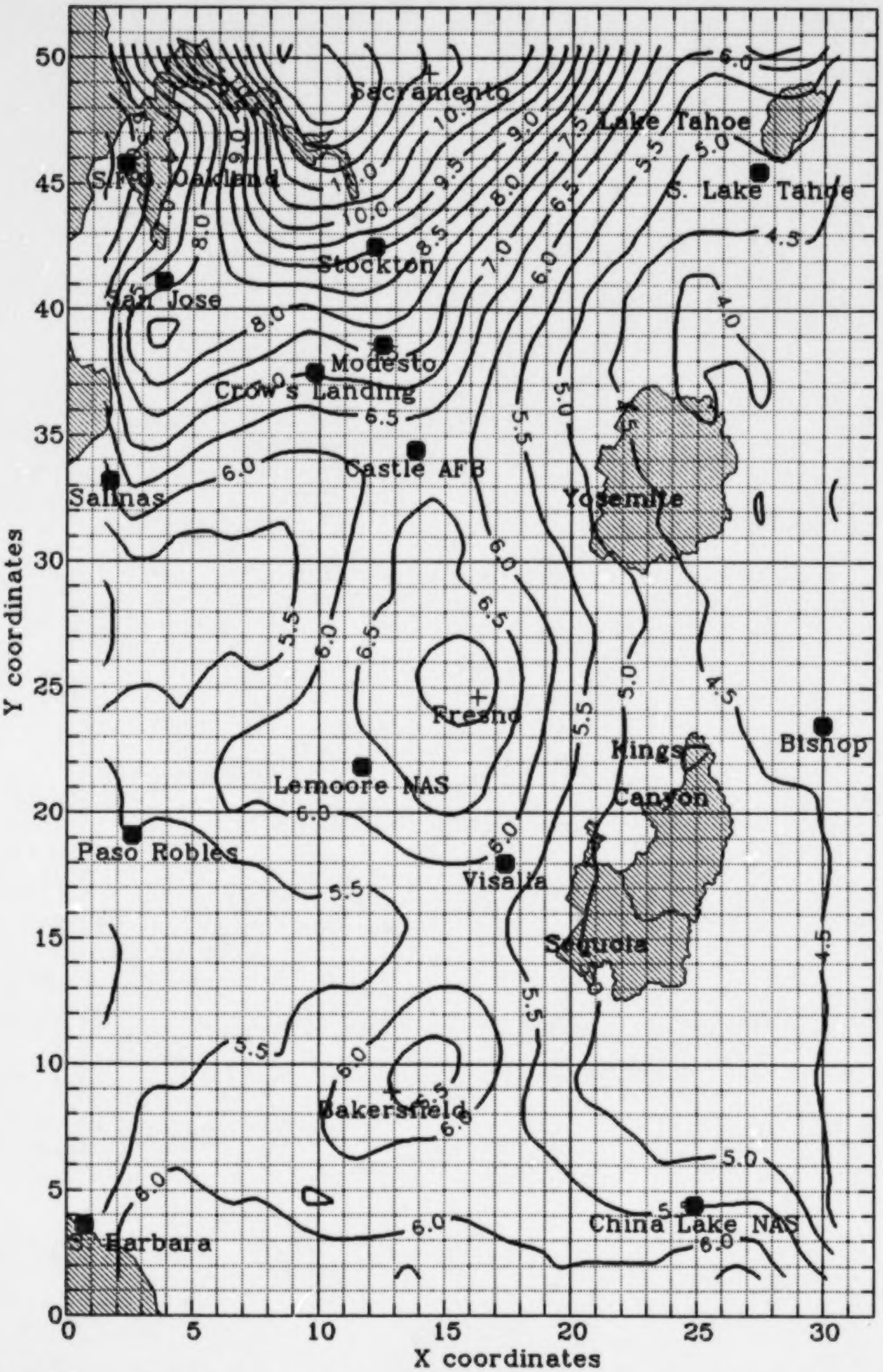
Sacramento
Lake Tahoe
S.F.
Oakland
S. Lake Tahoe
Stockton
San Jose
Modesto
Crow's Landing
Castle AFB
Salinas
Yosemite
Fresno
Kings Canyon
Bishop
Lemoore NAS
Paso Robles
Visalia
Sequoia
Bakersfield
China Lake NAS
S. Barbara
10.5
10.0
9.5
9.0
8.5
8.0
7.5
7.0
6.5
6.0
5.5
5.0
4.5
4.0
Y coordinates
X coordinates
0
5
10
15
20
25
30
35
40
45
50

Figure 2-2c. Predicted maximum daily mixed-layer ozone concentrations (pphm) for climate sensitivity scenario #1 (temp. and water increase): August 7, 1981.

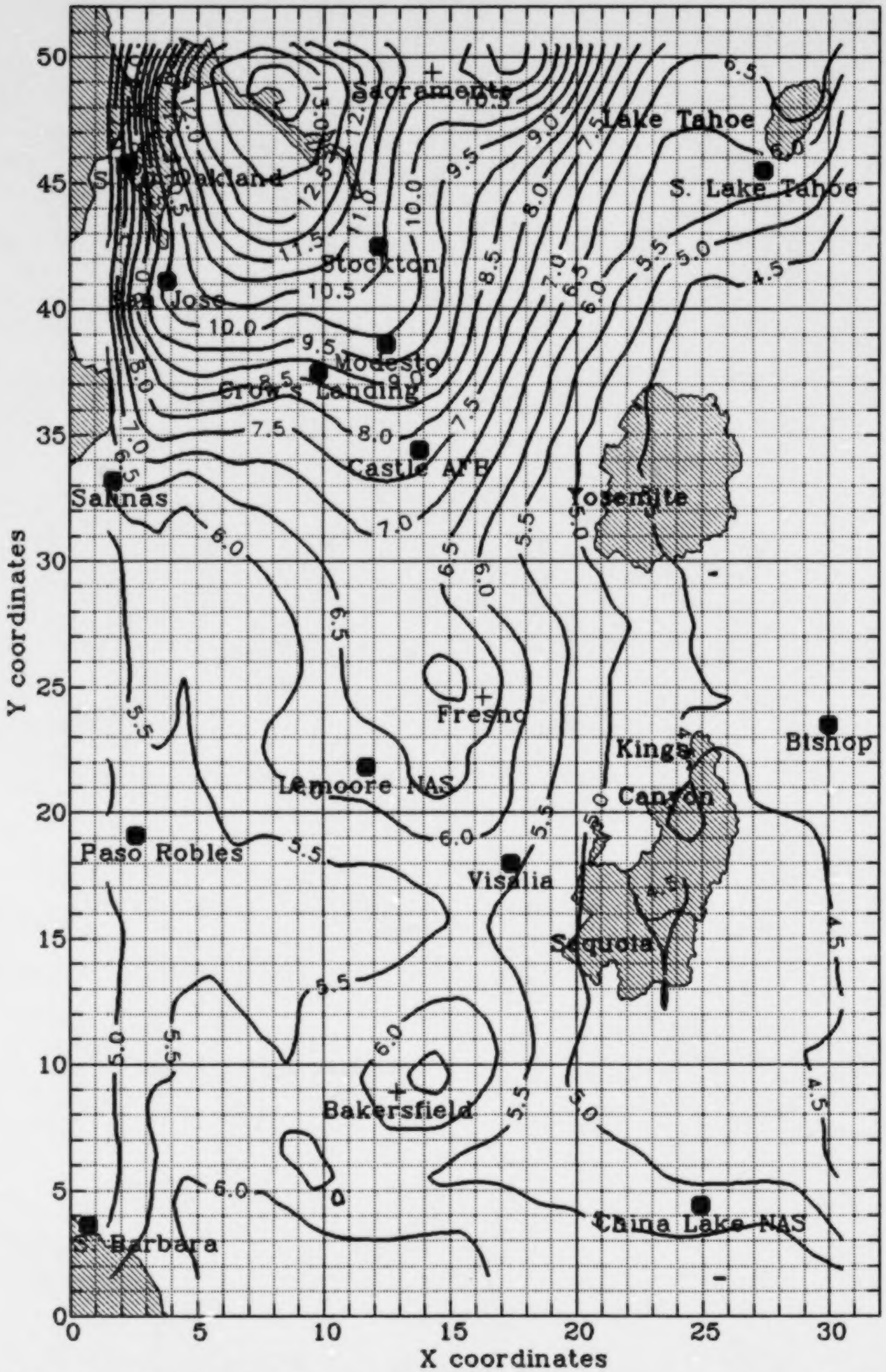
Sacramento
Lake Tahoe
S. Lake Tahoe
S.F.
Oakland
Stockton
San Jose
Modesto
Crow's Landing
Castle AFB
Salinas
Yosemite
Fresno
Bishop
Kings Canyon
Lemoore NAS
Paso Robles
Visalia
Sequoia
Bakersfield
China Lake NAS
S. Barbara
Y coordinates
X coordinates
0
5
10
15
20
25
30
35
40
45
50
12.0
12.5
11.5
11.0
10.5
10.0
9.5
9.0
8.5
8.0
7.5
7.0
6.5
6.0
5.5
5.0
4.5

Figure 2-2d. Predicted maximum daily mixed-layer ozone concentrations (pphm) for climate sensitivity scenario #1 (temp. and water increase): August 8, 1981.

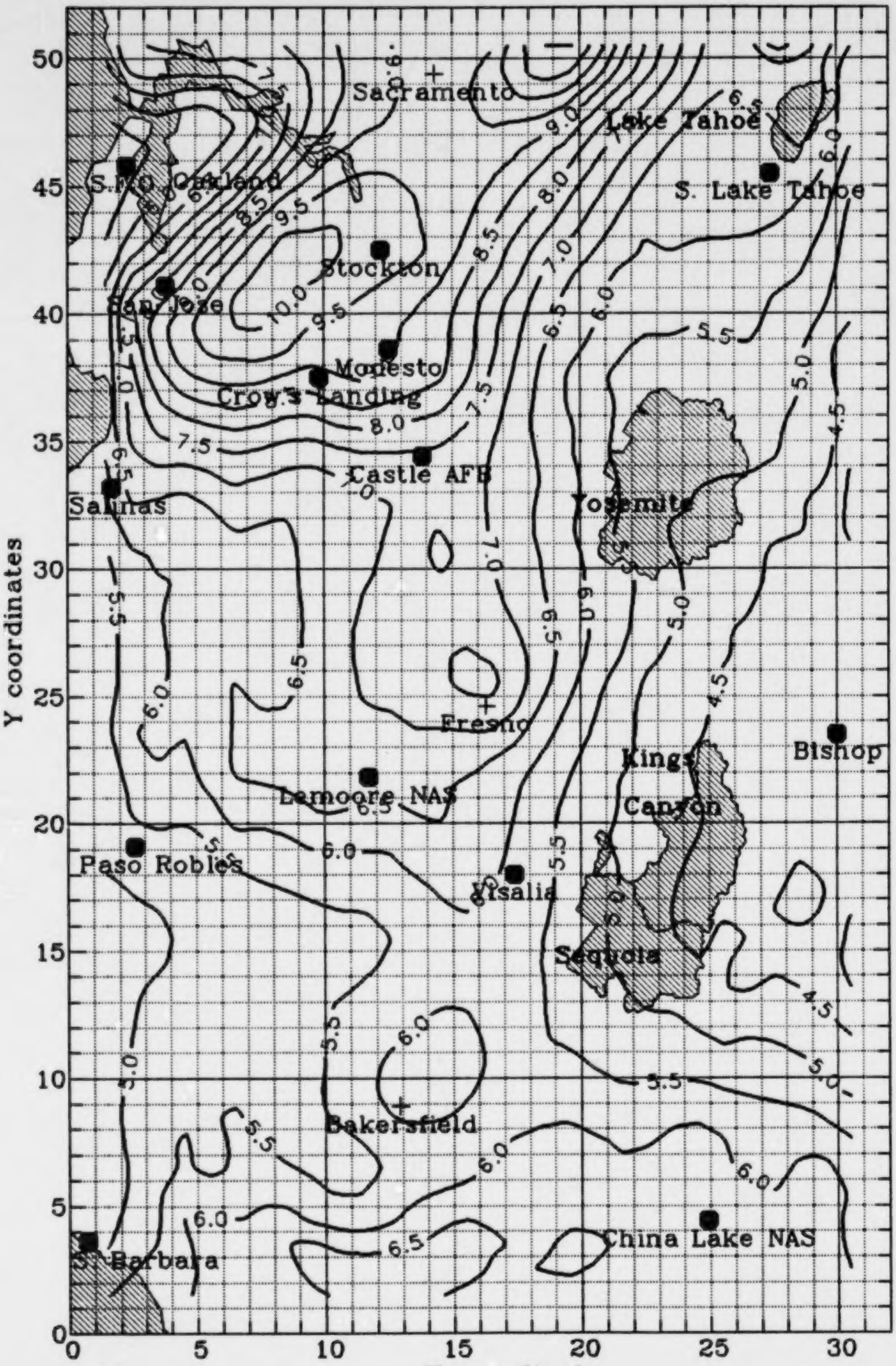
Sacramento
Lake Tahoe
S. Lake Tahoe
S.FO Oakland
Stockton
San Jose
Modesto
Crow's Landing
Castle AFB
Salinas
Yosemite
Fresno
Kings Canyon
Bishop
Lemoore NAS
Paso Robles
Visalia
Sequoia
Bakersfield
China Lake NAS
St Barbara
Y coordinates
X coordinates
0
5
10
15
20
25
30
35
40
45
50

Figure 2-2e. Predicted maximum daily mixed-layer ozone concentrations (pphm) for climate sensitivity scenario #1 (temp. and water increase): August 9, 1981.

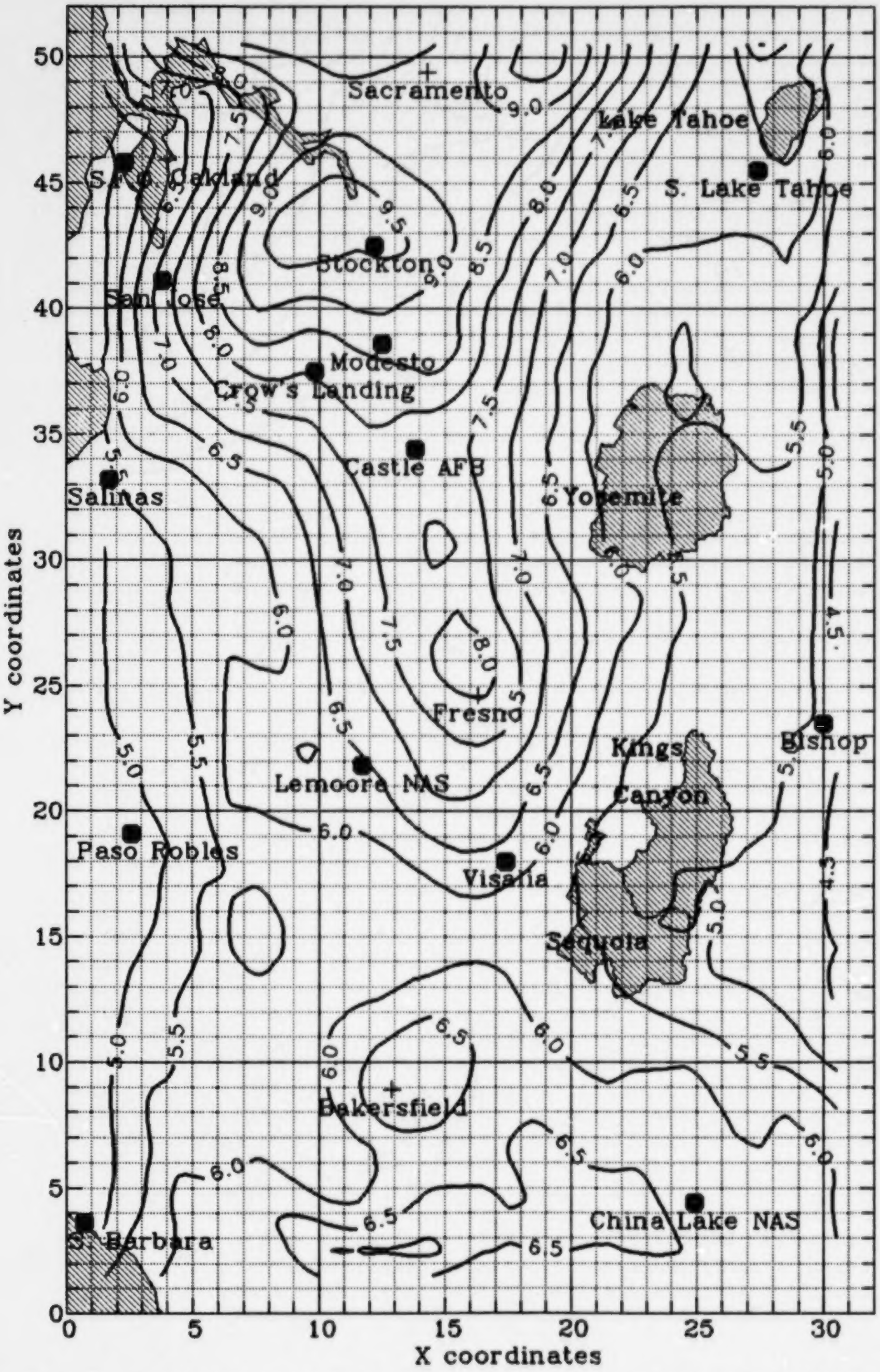
Y coordinates
X coordinates
0
5
10
15
20
25
30
35
40
45
50
Sacramento
Lake Tahoe
S. Lake Tahoe
S.F.
Oakland
Stockton
San Jose
Modesto
Crow's Landing
Castle AFB
Salinas
Yosemite
Fresno
Kings Canyon
Bishop
Lemoore NAS
Paso Robles
Visalia
Sequoia
Bakersfield
China Lake NAS
S. Barbara
9.0
9.5
8.5
8.0
7.5
7.0
6.5
6.0
5.5
5.0
4.5

Figure 2-2f. Predicted maximum daily mixed-layer ozone concentrations (pphm) for climate sensitivity scenario #1 (temp. and water increase): August 10, 1981.

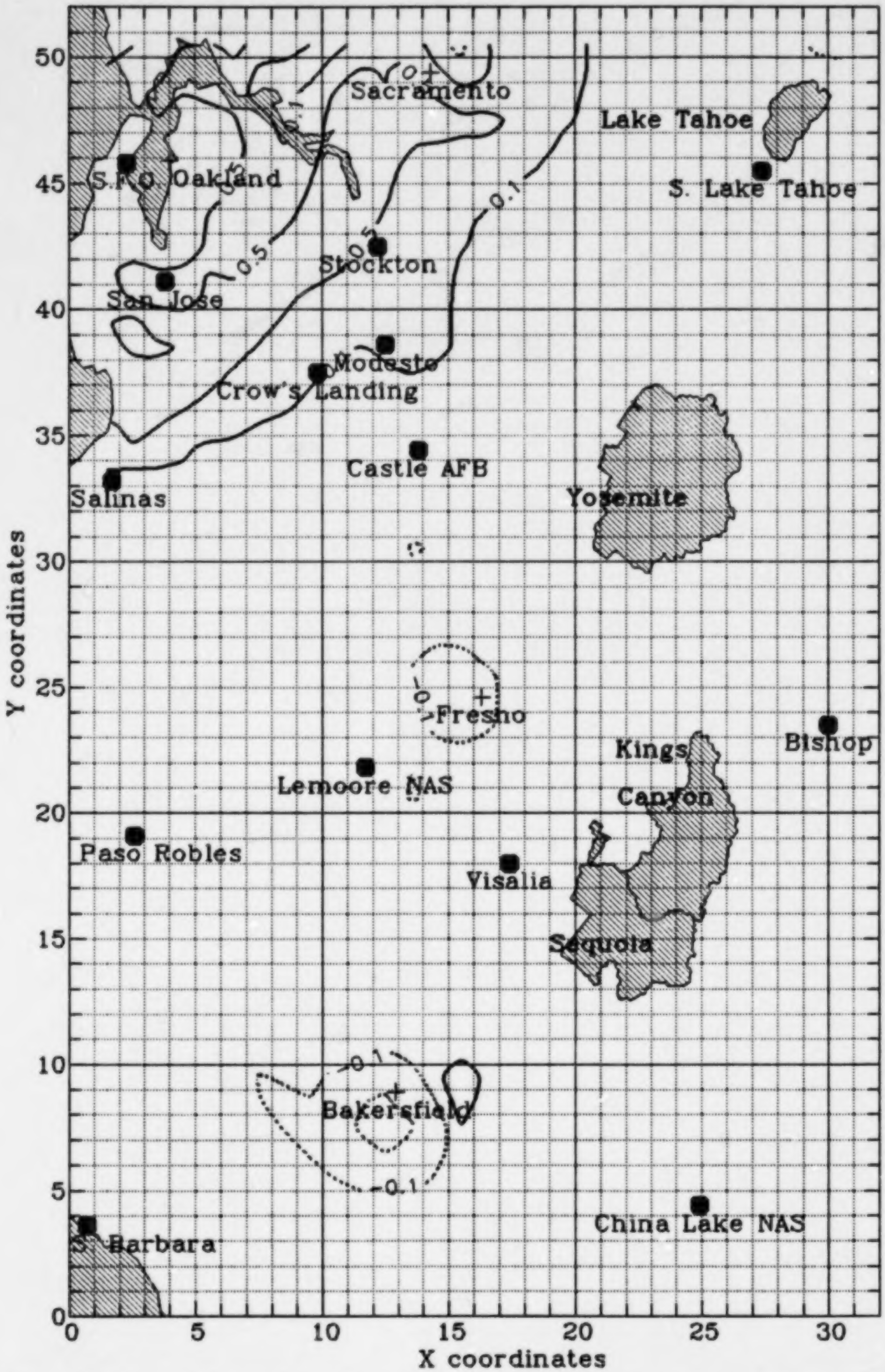
Y coordinates
X coordinates
0
5
10
15
20
25
30
35
40
45
50
S.F.O. Oakland
Sacramento
Lake Tahoe
S. Lake Tahoe
Stockton
San Jose
Modesto
Crow's Landing
Salinas
Castle AFB
Yosemite
Fresno
Kings Canyon
Bishop
Lemoore NAS
Paso Robles
Visalia
Sequoia
Bakersfield
China Lake NAS
S. Barbara
0.1
0.5
-0.1

Figure 2–3a. Differences in maximum daily ozone concentrations (pphm) (climate sensitivity senario#1 – base case): August 5,1981.

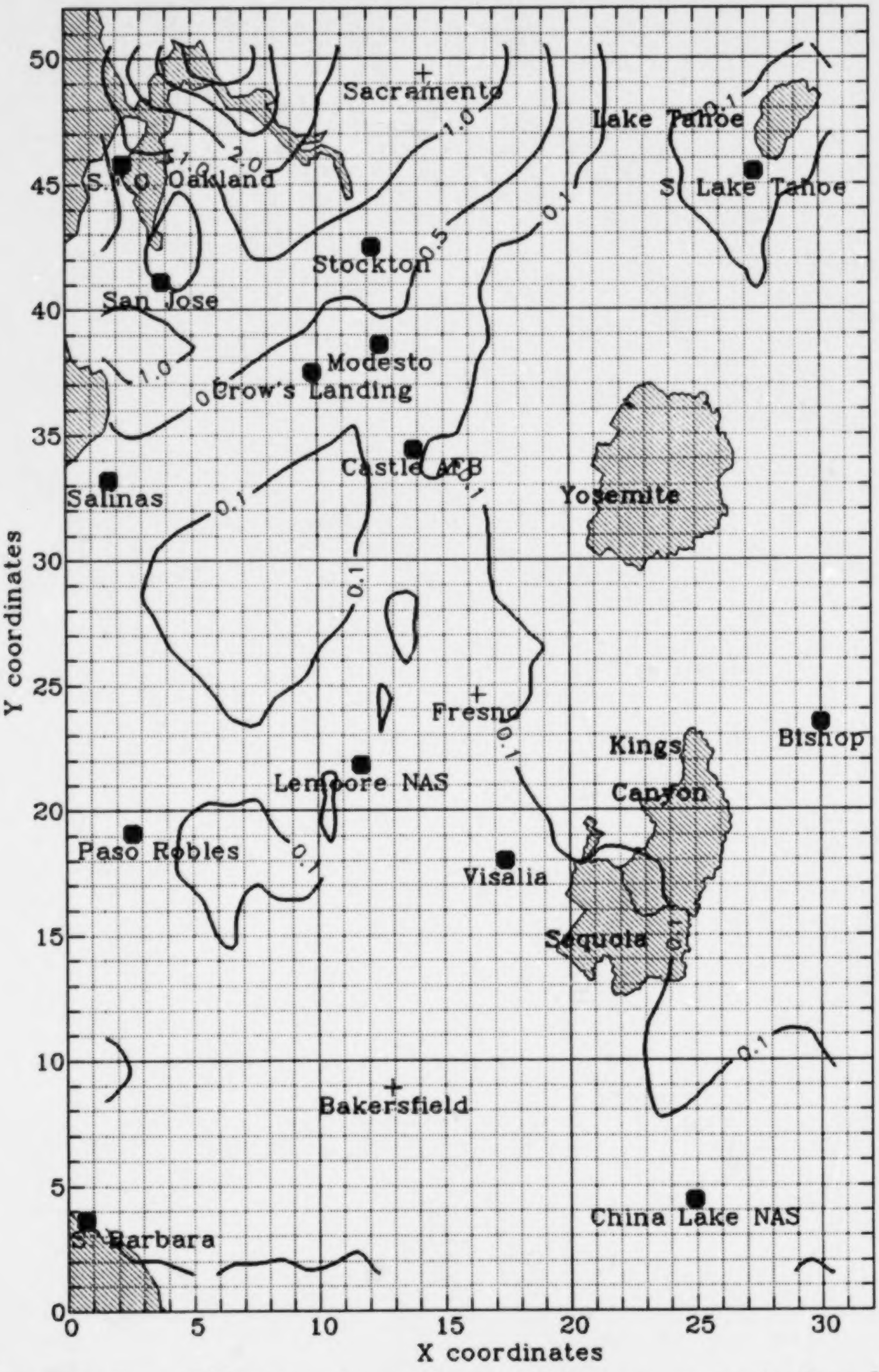
Y coordinates
X coordinates
0
5
10
15
20
25
30
35
40
45
50
Sacramento
S.F. Oakland
Lake Tahoe
S. Lake Tahoe
Stockton
San Jose
Modesto
Crow's Landing
Castle AFB
Salinas
Yosemite
Fresno
Kings
Canyon
Bishop
Lemoore NAS
Paso Robles
Visalia
Sequoia
Bakersfield
China Lake NAS
S. Barbara
1.0
2.0
0.5
0.1

Figure 2–3b. Differences in maximum daily ozone concentrations (pphm) (climate sensitivity senario#1 – base case): August 6,1981.

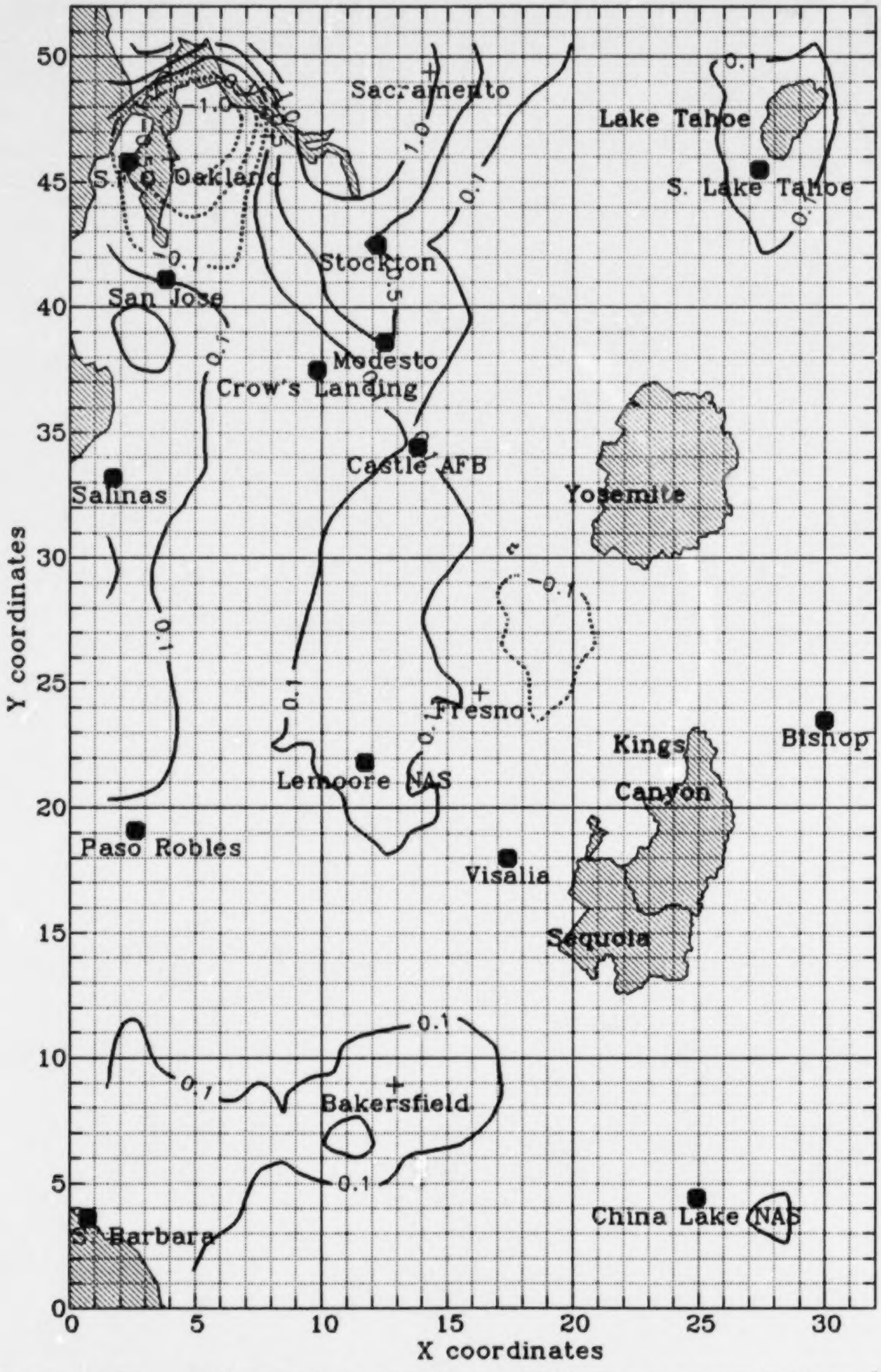
Sacramento
Lake Tahoe
S. Lake Tahoe
S.F.
Oakland
Stockton
San Jose
Modesto
Crow's Landing
Castle AFB
Salinas
Yosemite
Fresno
Kings
Canyon
Bishop
Lemoore NAS
Paso Robles
Visalia
Sequoia
Bakersfield
China Lake NAS
S. Barbara
0.1
-1.0
-0.1
1.0
0.5
-0.1
Y coordinates
X coordinates
0
5
10
15
20
25
30
35
40
45
50

Figure 2–3c. Differences in maximum daily ozone concentrations (pphm) (climate sensitivity senario#1 – base case): August 7,1981.

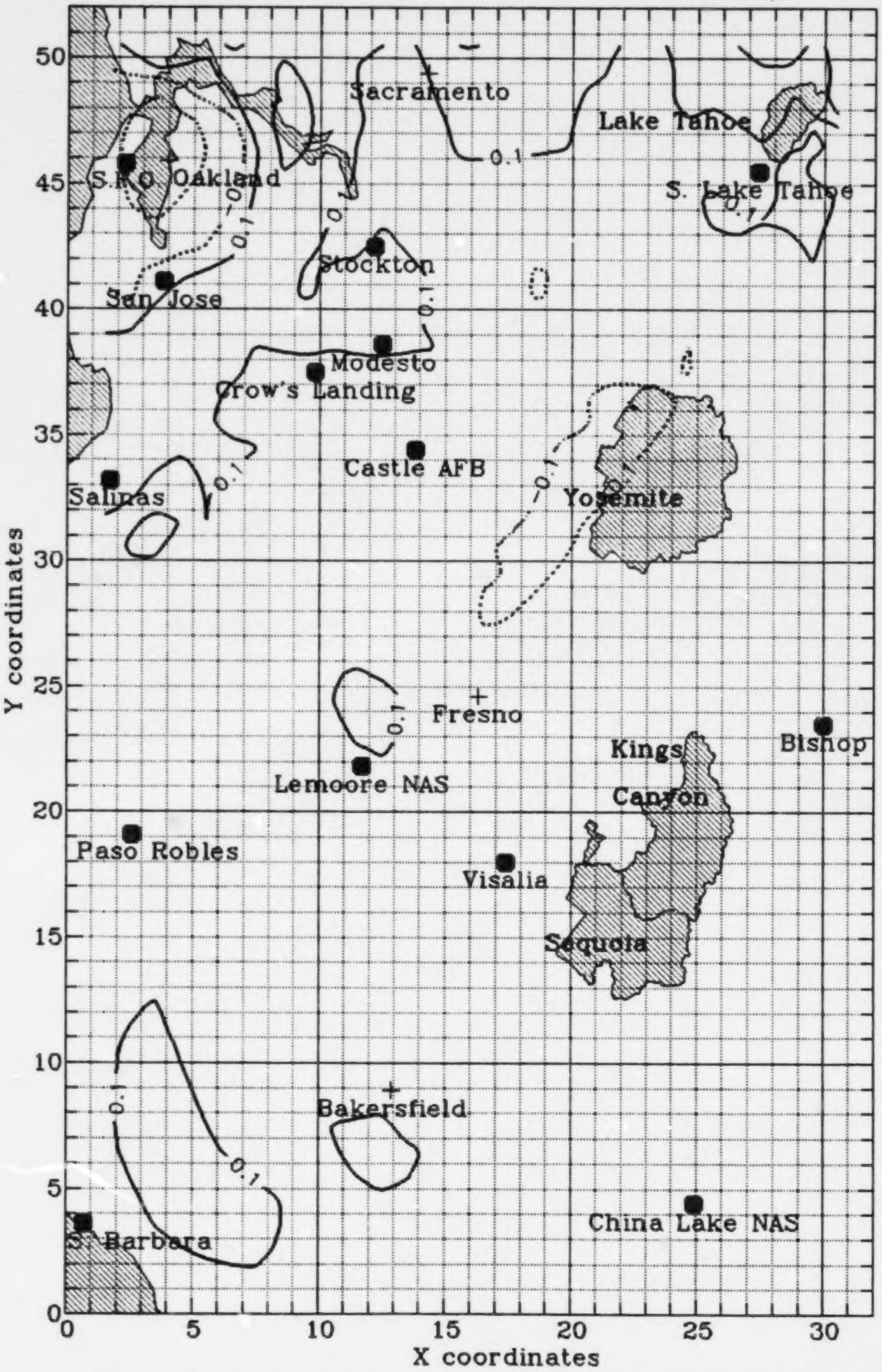
Sacramento
Lake Tahoe
S.F.O. Oakland
S. Lake Tahoe
Stockton
San Jose
Modesto
Crow's Landing
Castle AFB
Salinas
Yosemite
Fresno
Bishop
Kings
Canyon
Lemoore NAS
Paso Robles
Visalia
Sequoia
Bakersfield
China Lake NAS
S. Barbara
0.1
-0.1
Y coordinates
X coordinates
0
5
10
15
20
25
30
35
40
45
50

Figure 2-3d. Differences in maximum daily ozone concentrations (pphm) (climate sensitivity senario#1 - base case): August 8,1981.

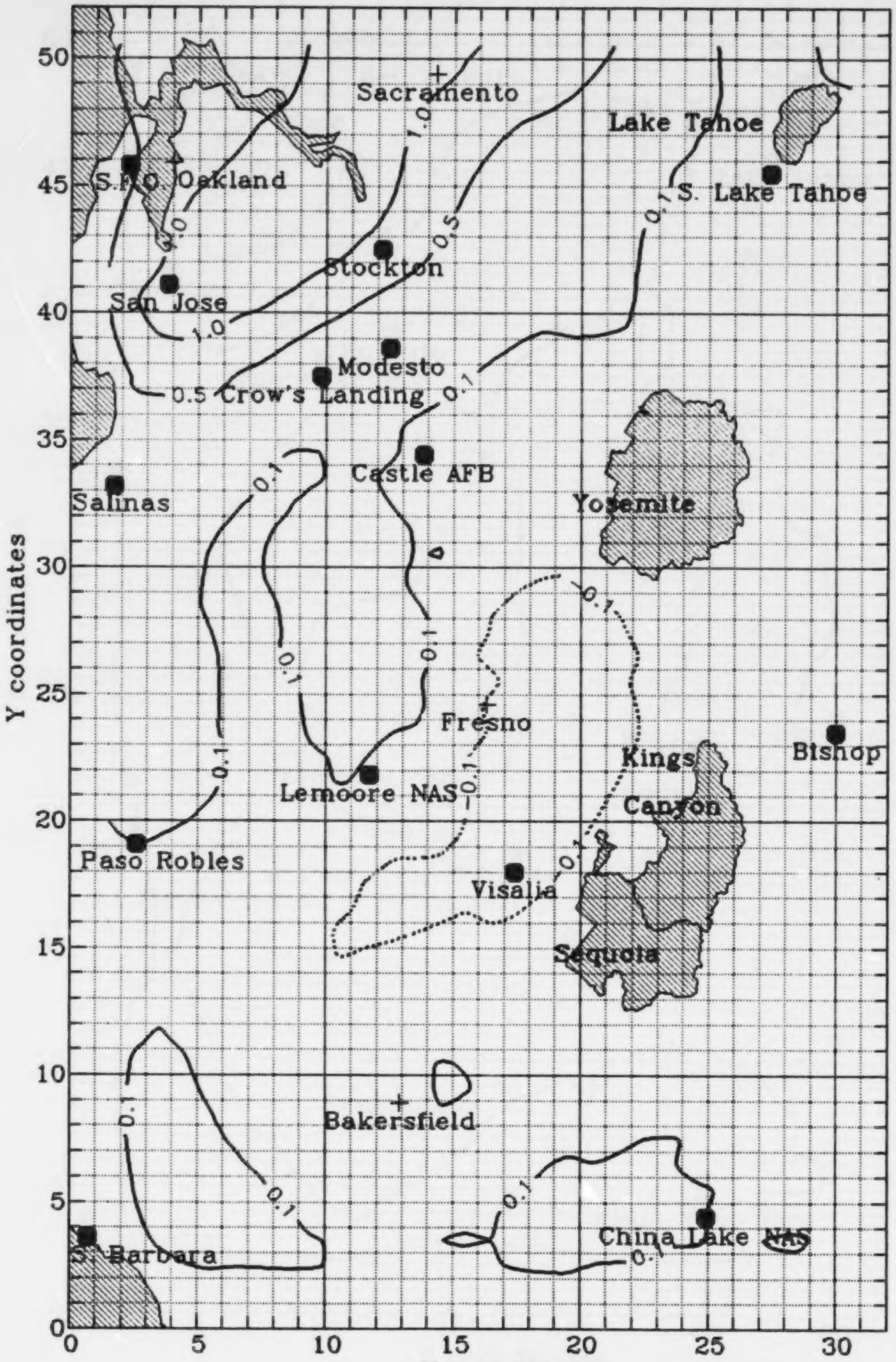
Y coordinates
X coordinates
0
5
10
15
20
25
30
35
40
45
50
0
5
10
15
20
25
30
Sacramento
Lake Tahoe
S.F.
Oakland
S. Lake Tahoe
Stockton
San Jose
Modesto
Crow's Landing
Castle AFB
Salinas
Yosemite
Fresno
Kings
Canyon
Bishop
Lemoore NAS
Paso Robles
Visalia
Sequoia
Bakersfield
China Lake NAS
S. Barbara
1.0
0.5
0.1
-0.1

Figure 2–3e. Differences in maximum daily ozone concentrations (pphm) (climate sensitivity senario#1 – base case): August 9,1981.

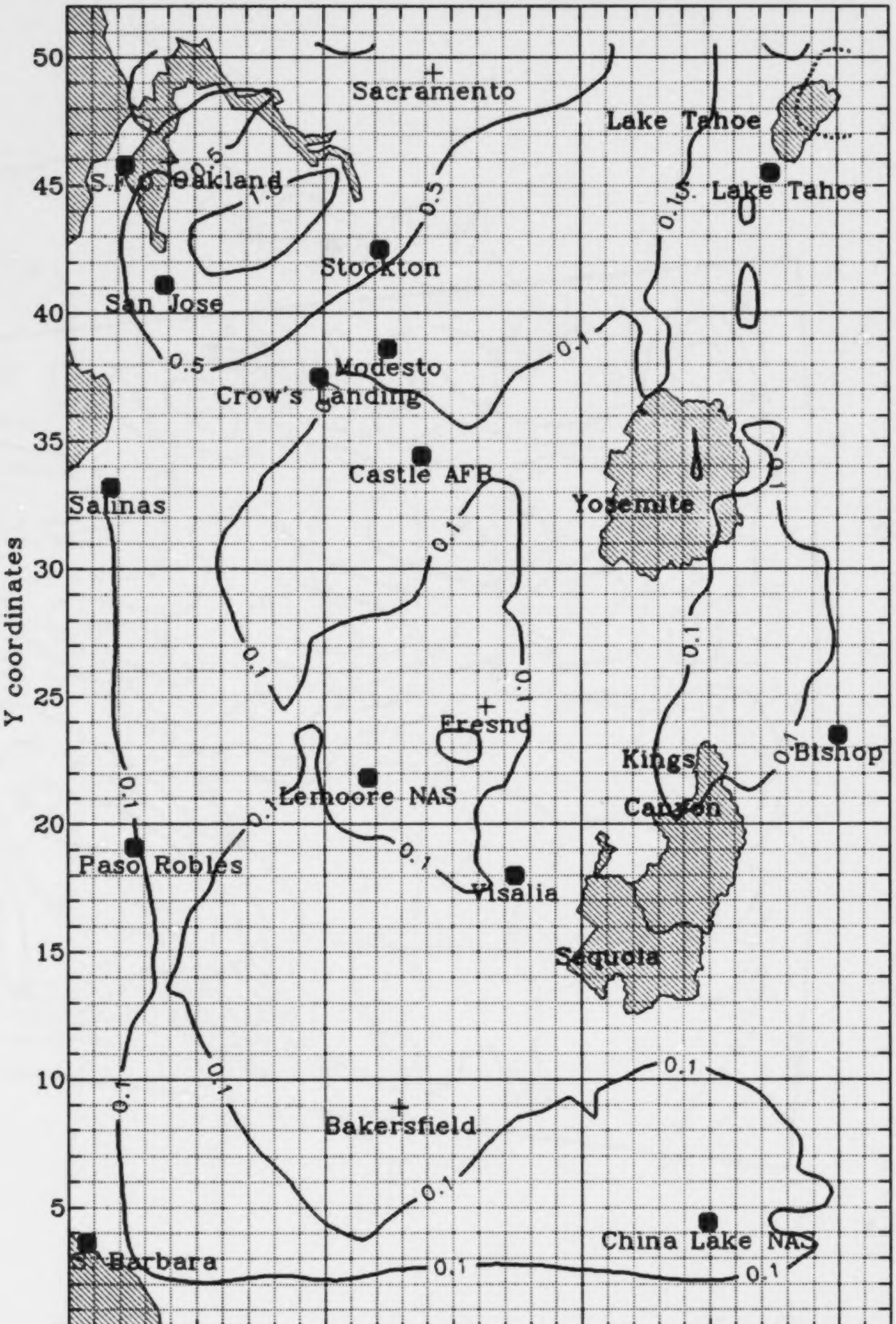
Sacramento
Lake Tahoe
S. Lake Tahoe
S.F.
Oakland
Stockton
San Jose
Modesto
Crow's Landing
Castle AFB
Salinas
Yosemite
Fresno
Kings
Canyon
Bishop
Lemoore NAS
Paso Robles
Visalia
Sequoia
Bakersfield
China Lake NAS
S. Barbara
0.5
1.0
0.1
Y coordinates
X coordinates
0
5
10
15
20
25
30
35
40
45
50

Figure 2-3f. Differences in maximum daily ozone concentrations (pphm) (climate sensitivity senario#1 - base case): August 10,1981.

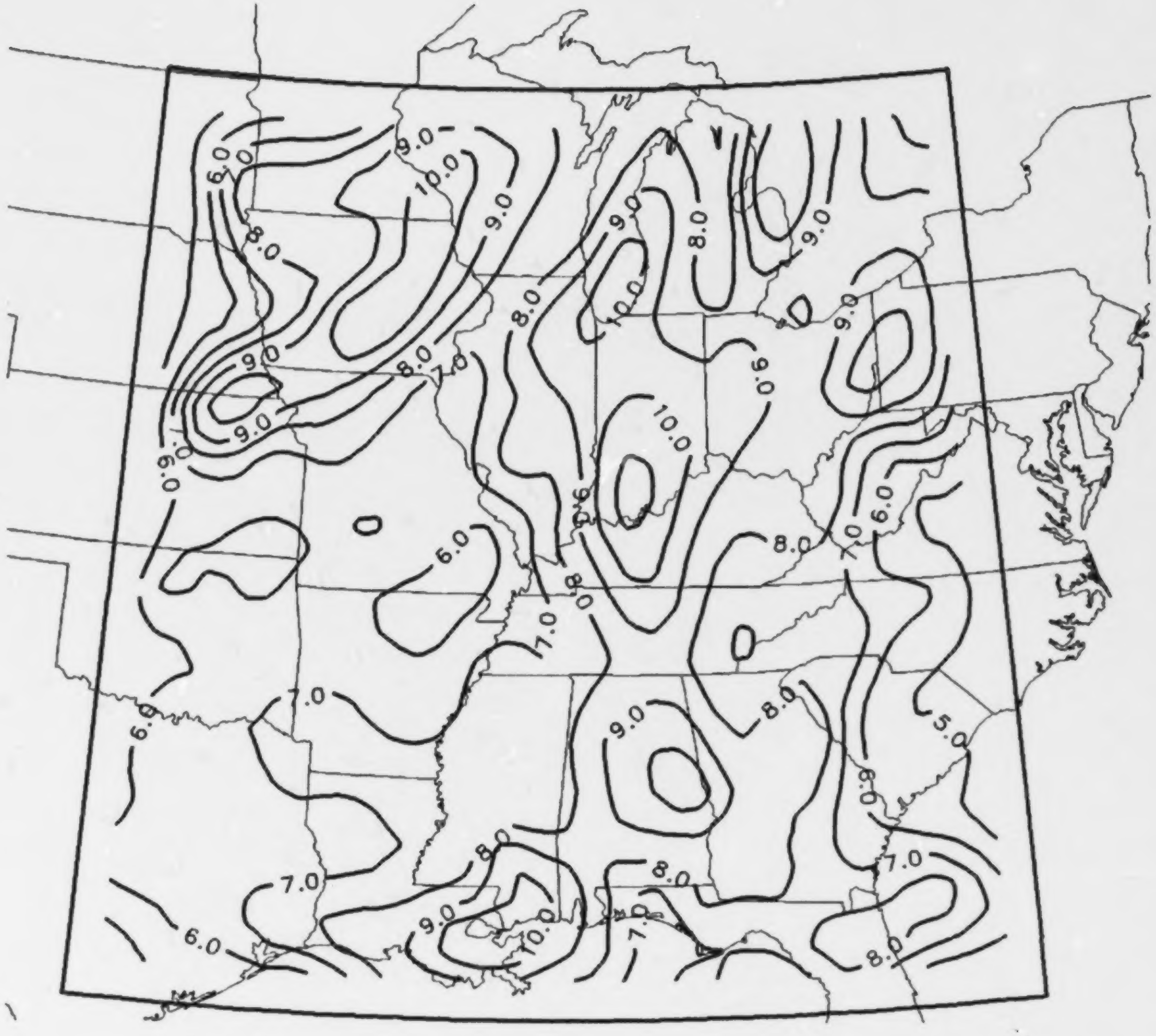
6.0
8.0
9.0
10.0
7.0
5.0

Figure 2-4a. Predicted maximum daily mixed-layer ozone concentrations (pphm) for the base case scenario: July 14, 1980.

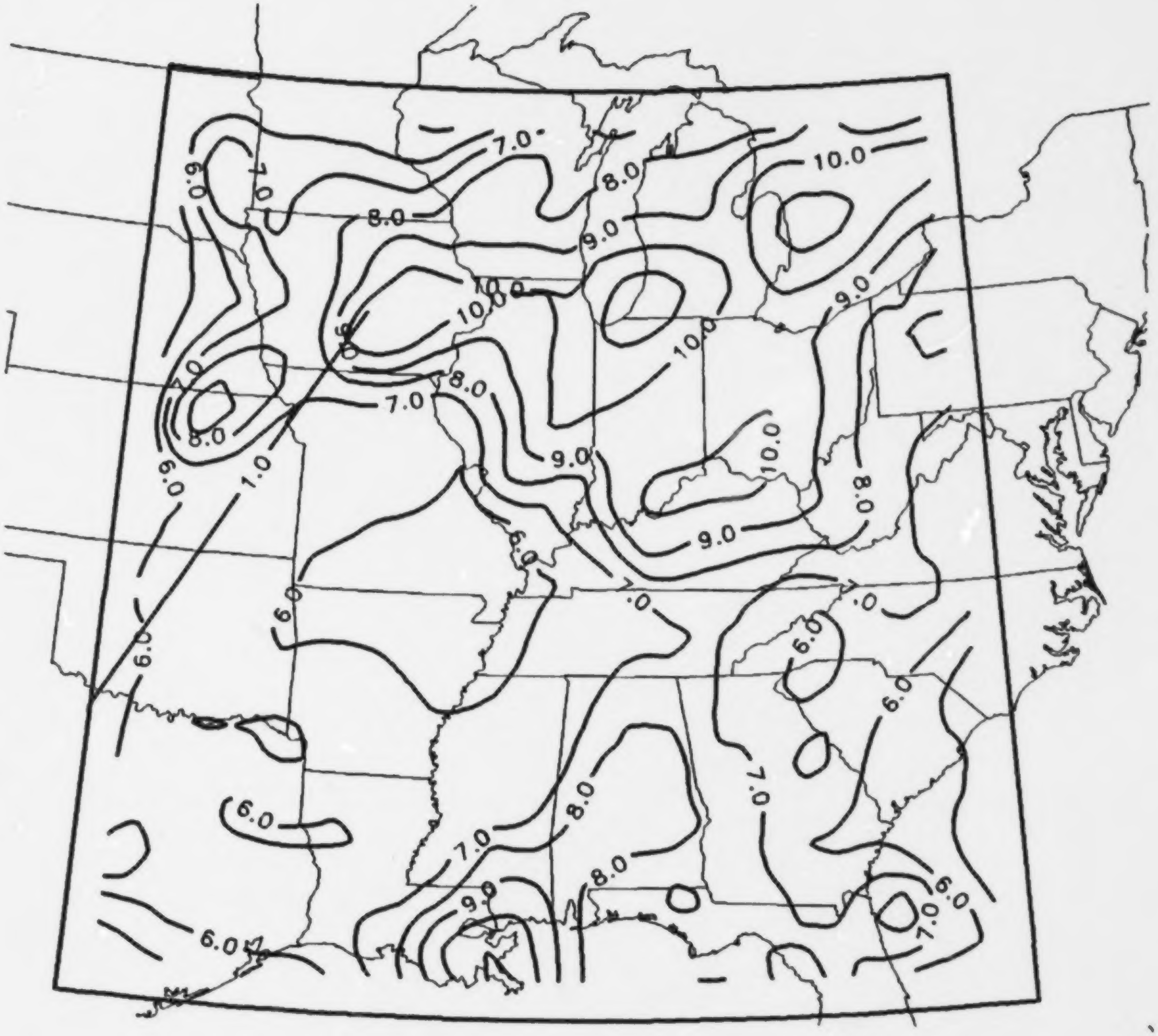
10.0
9.0
8.0
7.0
6.0

Figure 2–4b. Predicted maximum daily mixed–layer ozone concentrations (pphm) for the base case scenario: July 15, 1980.

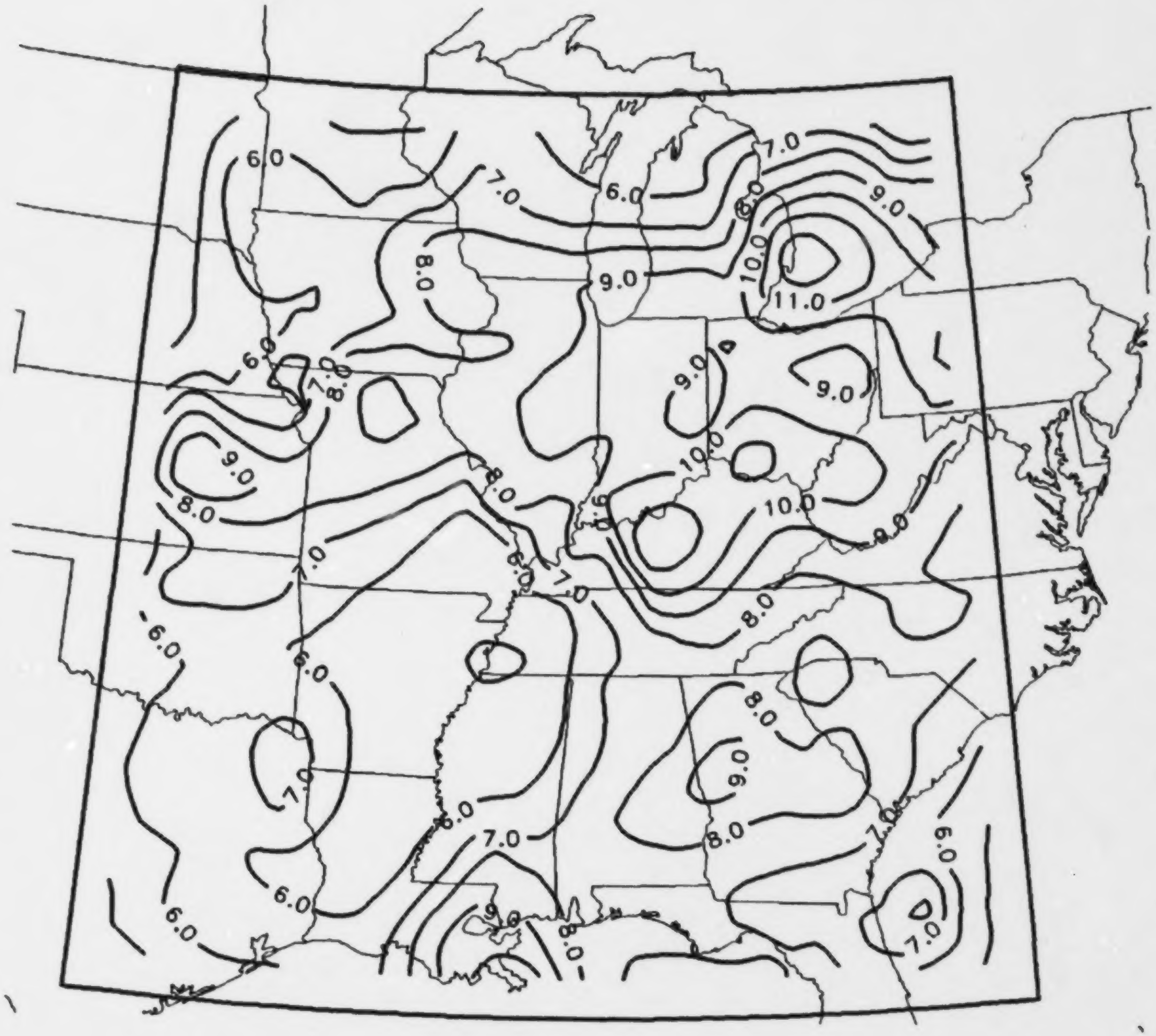
6.0
7.0
6.0
7.0
9.0
11.0
10.0
9.0
8.0
9.0
9.0
10.0
10.0
8.0
7.0
8.0
6.0
9.0
8.0
9.0
8.0
7.0
6.0
7.0
8.0
9.0
8.0
7.0
6.0
6.0
9.0
8.0
6.0
7.0

Figure 2–4c. Predicted maximum daily mixed–layer ozone concentrations (pphm) for the base case scenario: July 16, 1980.

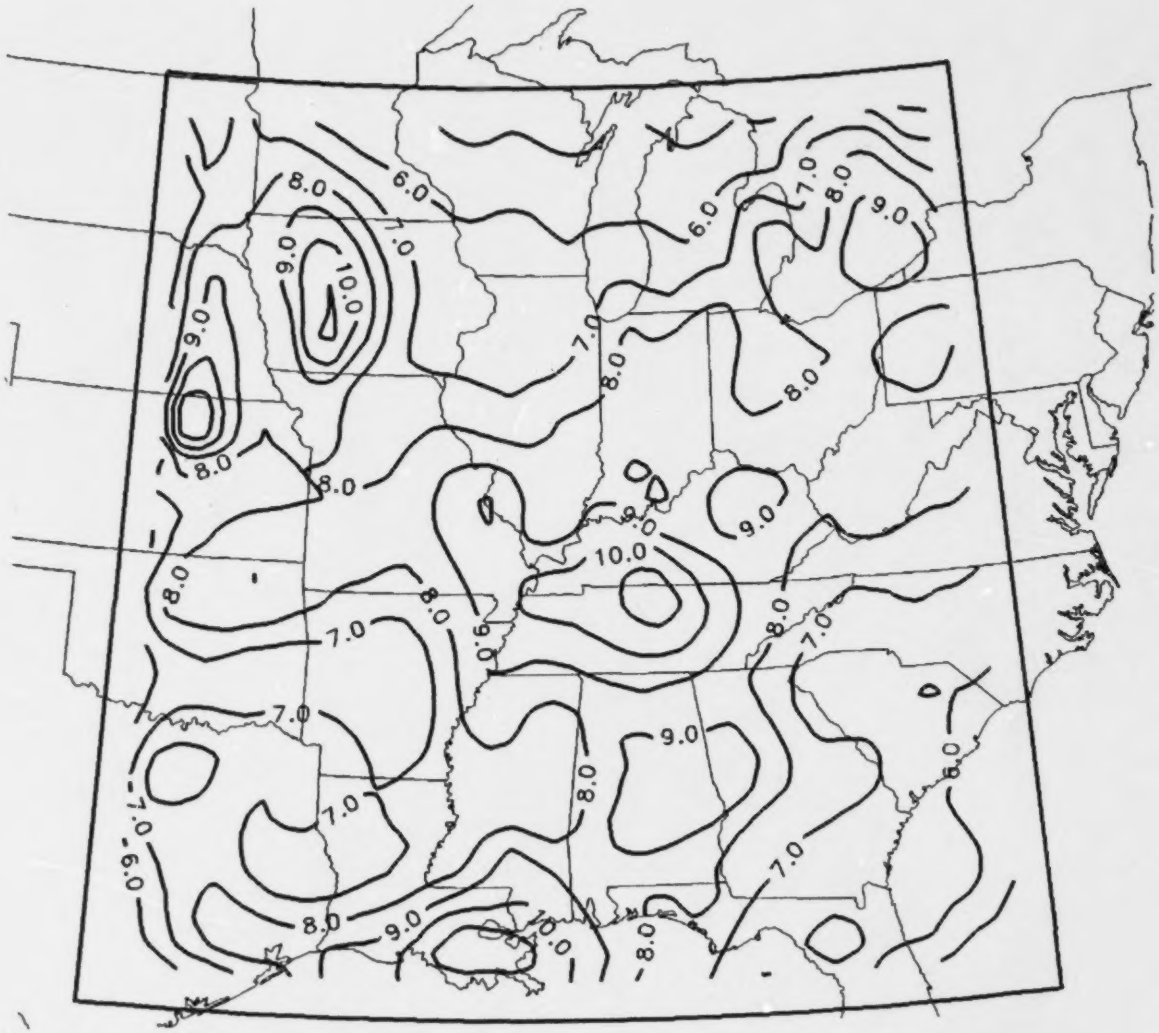
8.0
6.0
6.0
7.0
8.0
9.0
9.0
10.0
7.0
9.0
7.0
8.0
8.0
8.0
8.0
9.0
10.0
9.0
8.0
8.0
7.0
9.0
8.0
7.0
7.0
9.0
8.0
6.0
7.0
6.0
7.0
8.0
9.0
10.0
8.0
7.0

Figure 2-4d. Predicted maximum daily mixed-layer ozone concentrations (pphm) for the base case scenario: July 17, 1980.

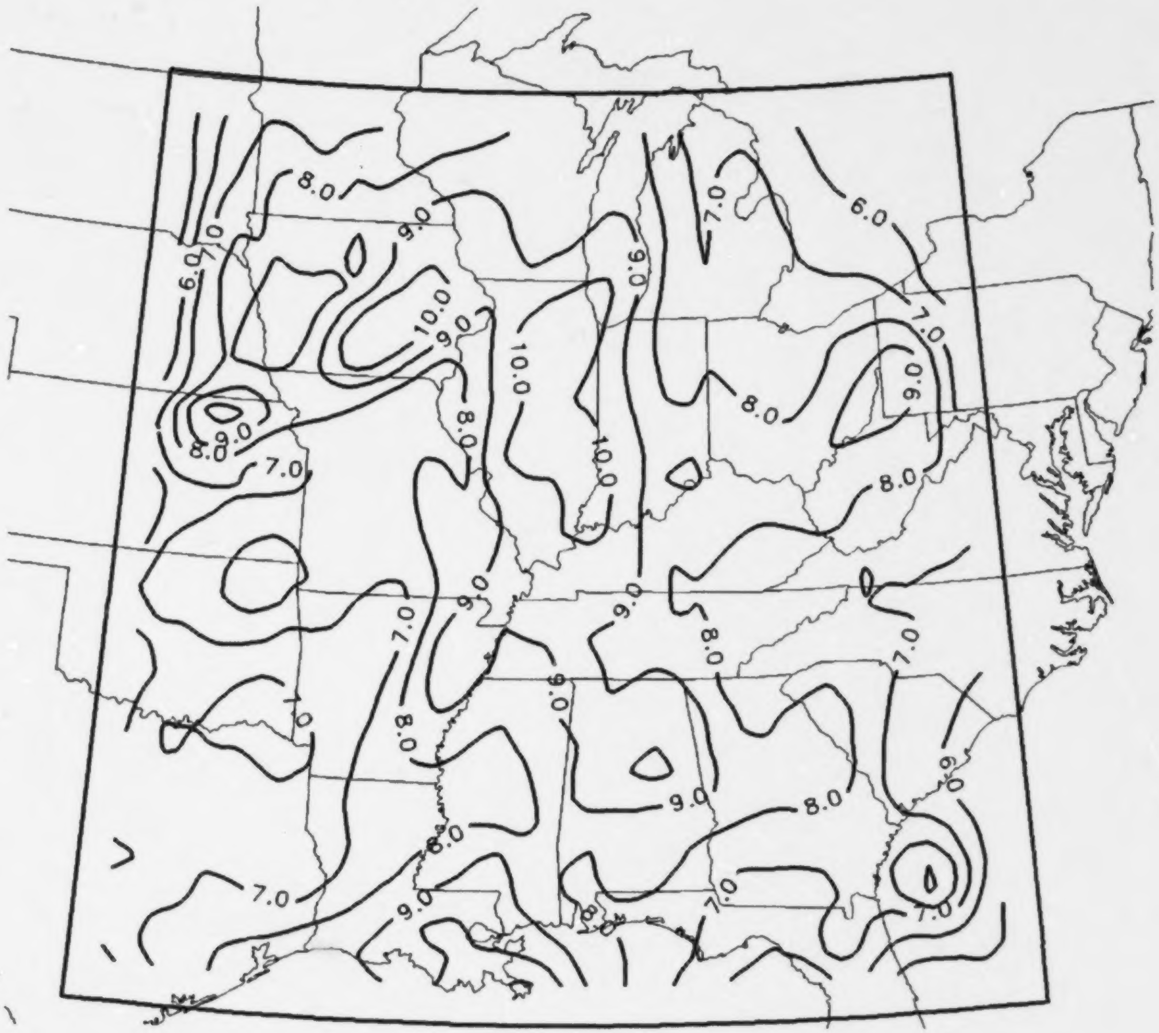
6.0
7.0
8.0
9.0
10.0

Figure 2–4e. Predicted maximum daily mixed–layer ozone concentrations (pphm) for the base case scenario: July 18, 1980.

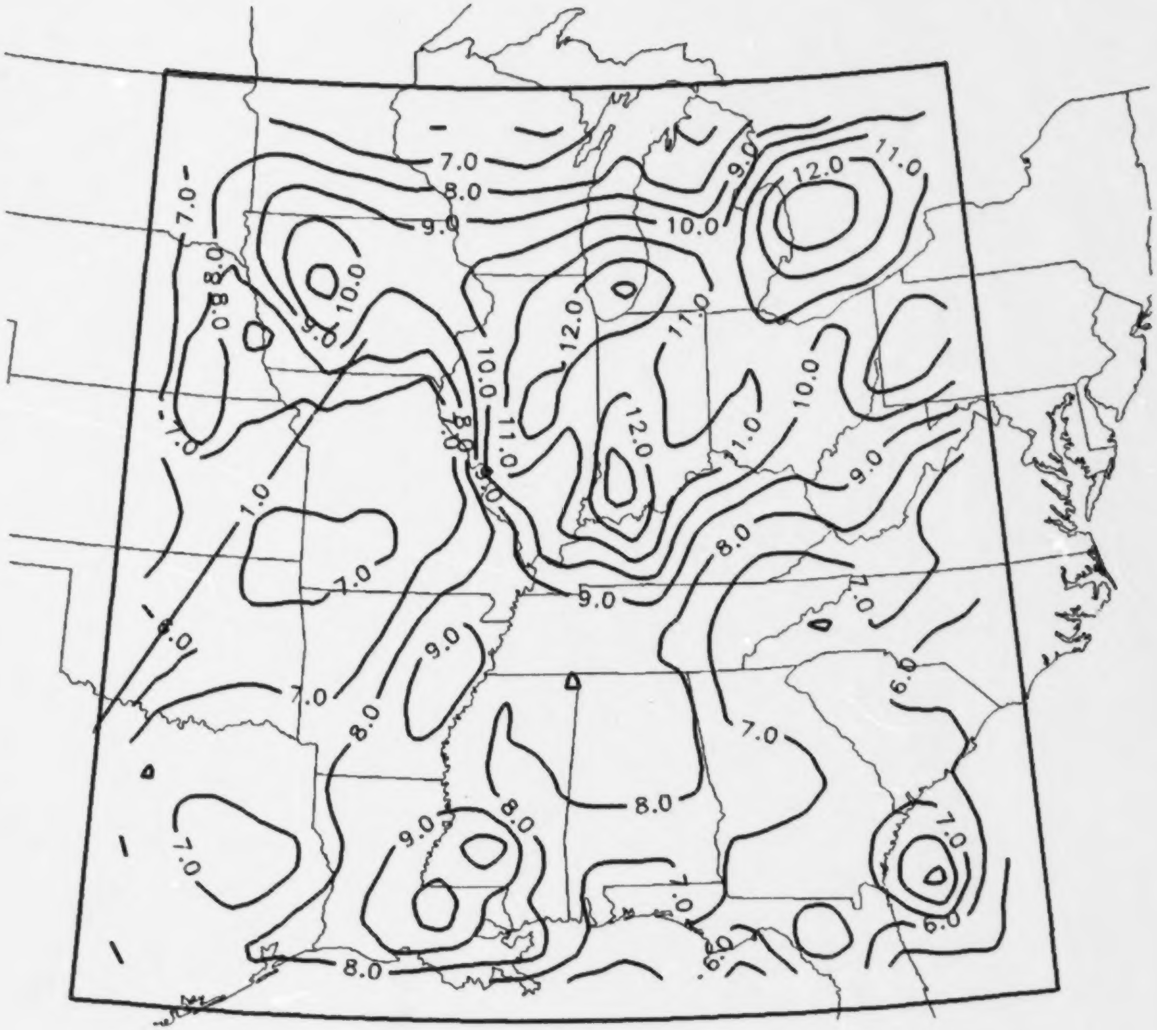
7.0
8.0
9.0
10.0
11.0
12.0
6.0

Figure 2–4f. Predicted maximum daily mixed–layer ozone concentrations (pphm) for the base case scenario: July 19, 1980.

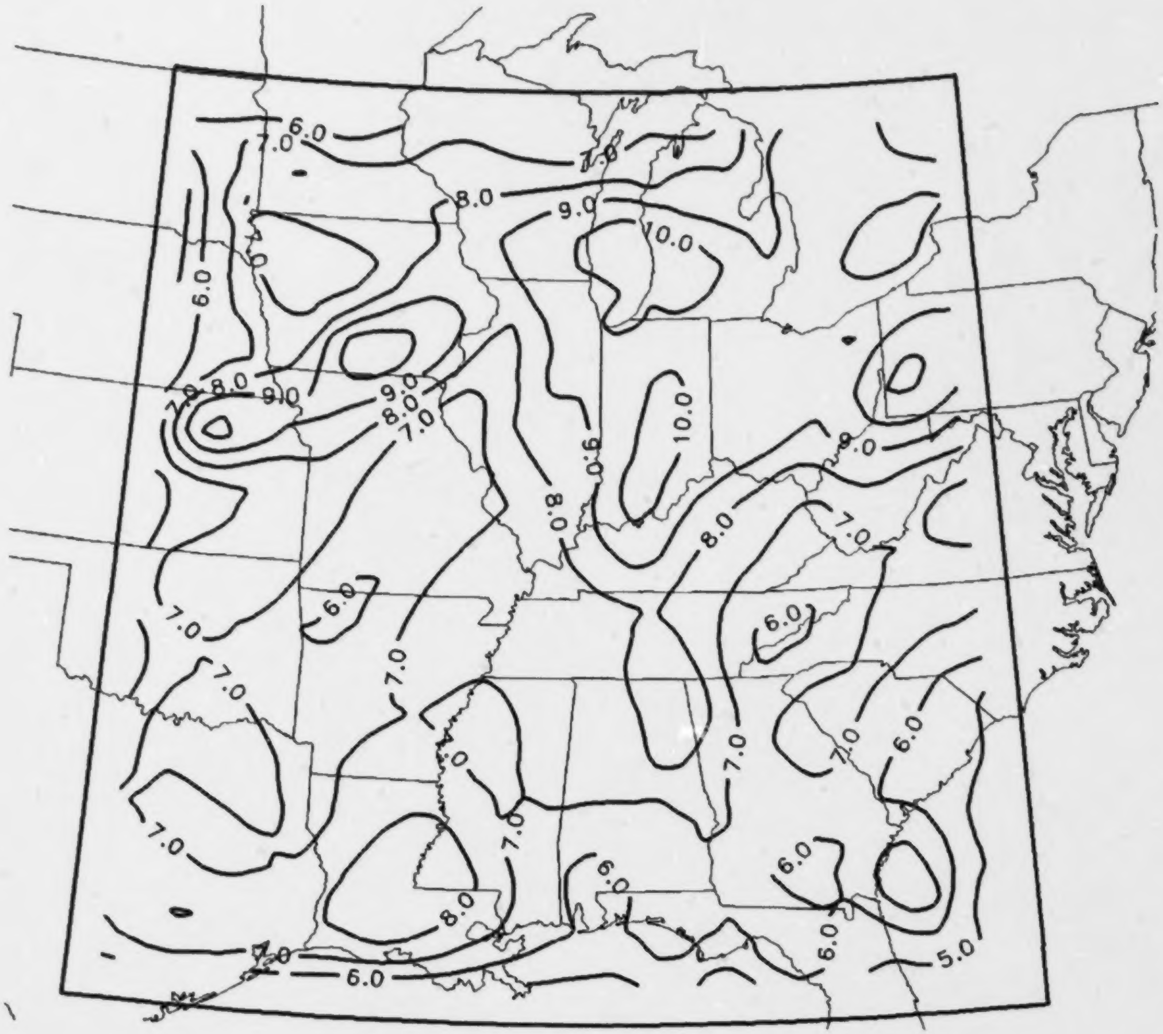
6.0
7.0
8.0
9.0
10.0
5.0

Figure 2–4g. Predicted maximum daily mixed–layer ozone concentrations (pphm) for the base case scenario: July 20, 1980.

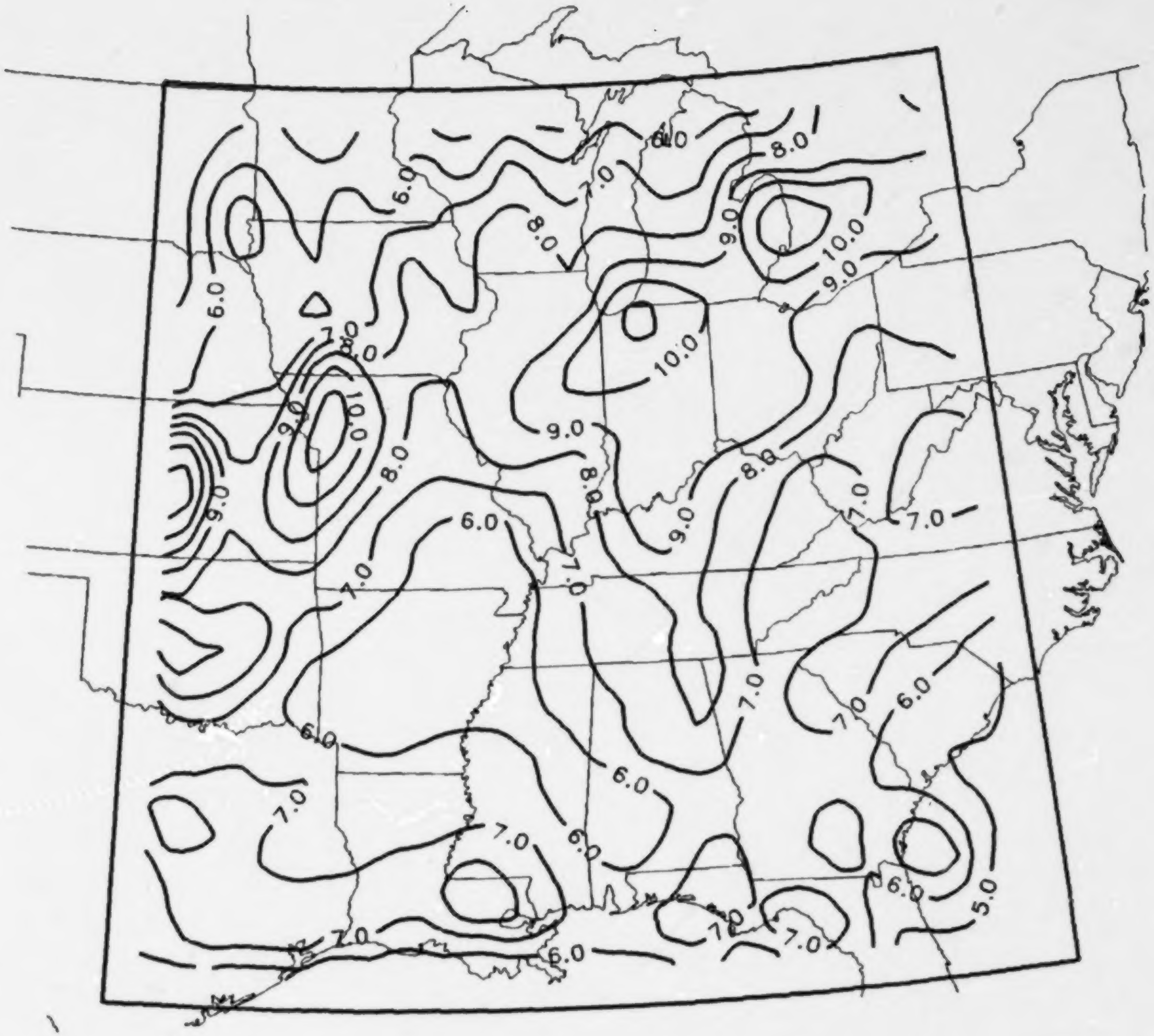
5.0
6.0
7.0
8.0
9.0
10.0

Figure 2–4h. Predicted maximum daily mixed–layer ozone concentrations (pphm) for the base case scenario: July 21, 1980.

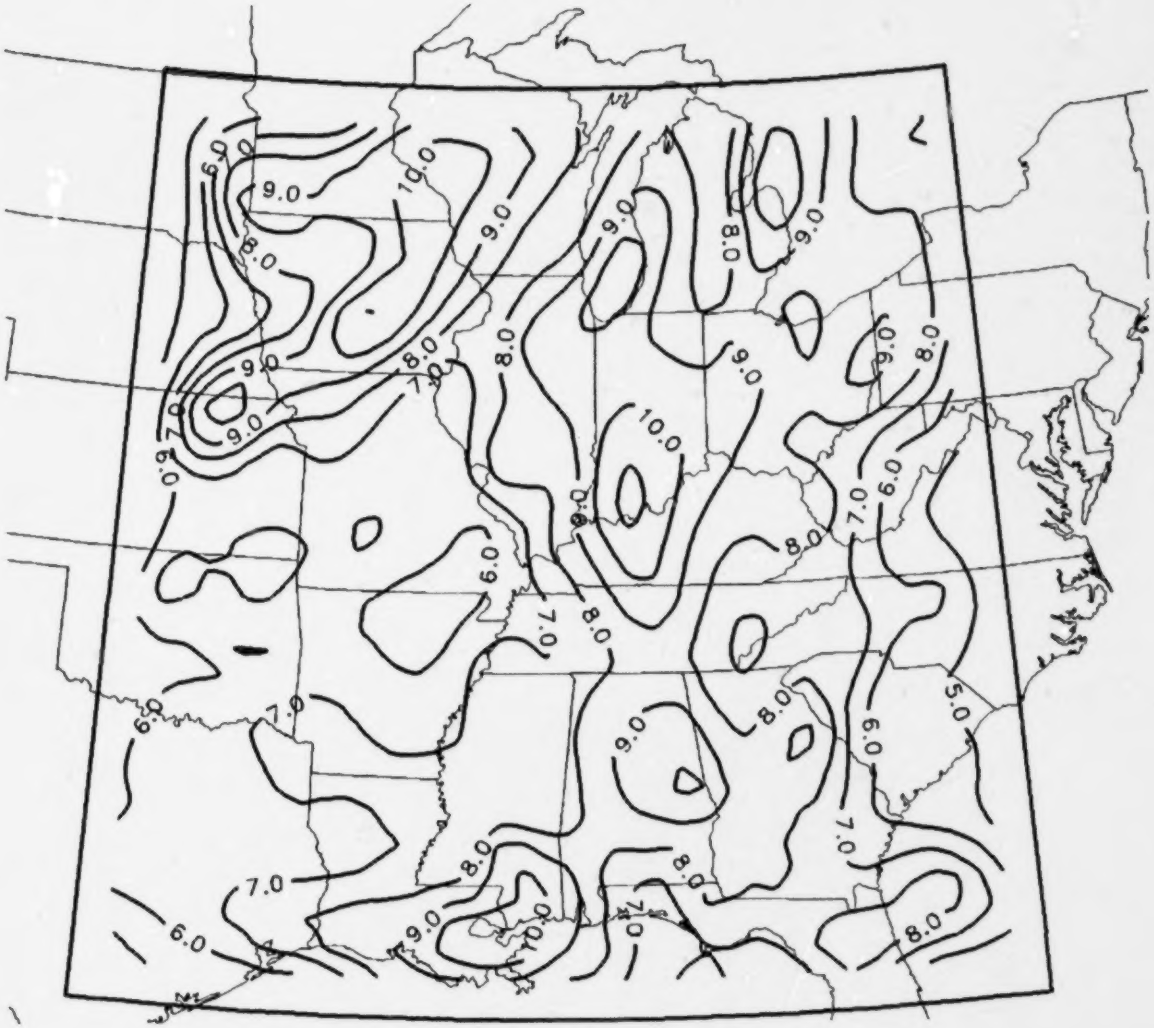
5.0
6.0
7.0
8.0
9.0
10.0

Figure 2–5a. Predicted maximum daily mixed–layer ozone concentrations (pphm) for climate sensitivity scenario#1: July 14, 1980.

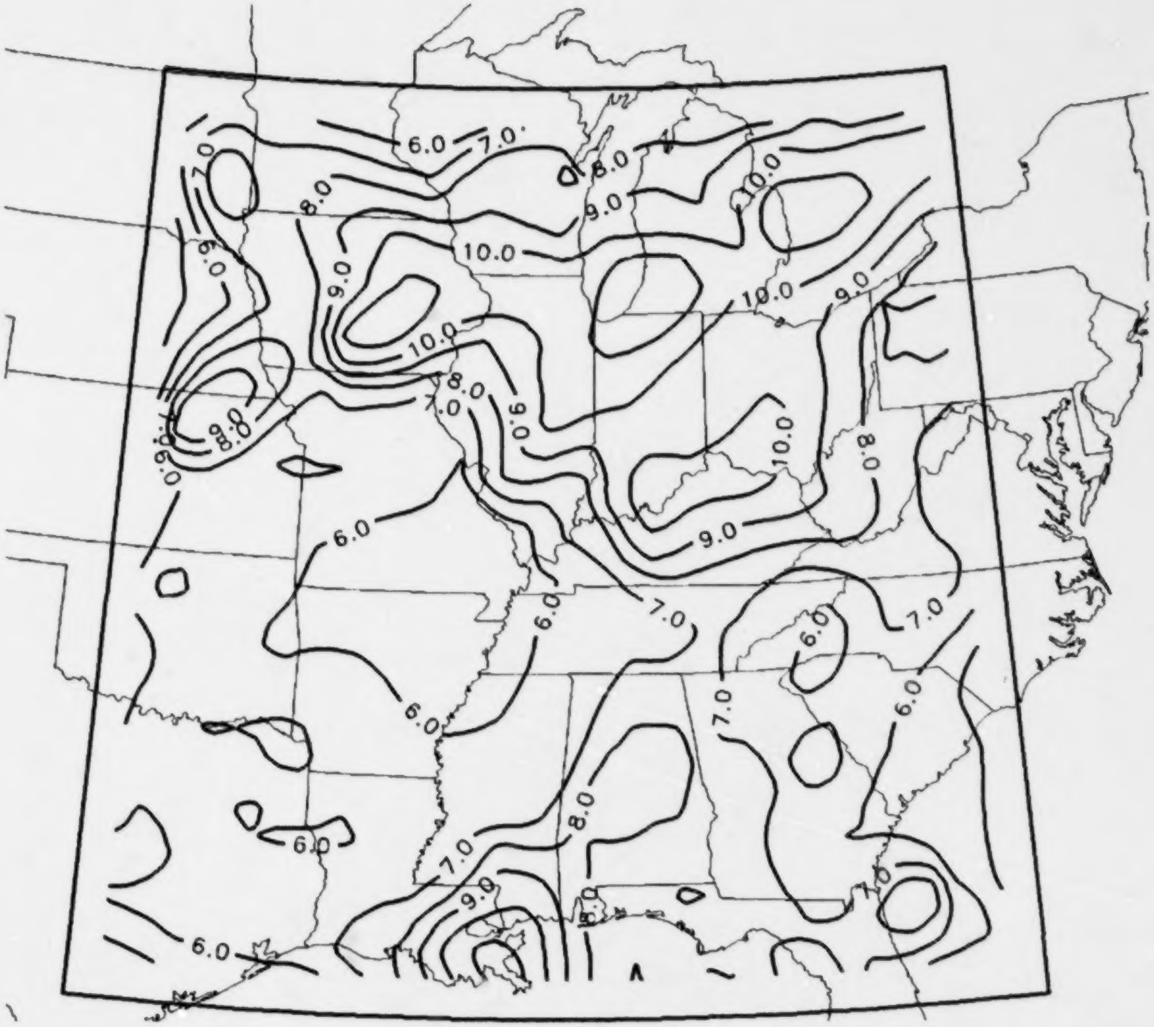

Figure 2–5b. Predicted maximum daily mixed–layer ozone concentrations (pphm) for climate sensitivity scenario#1: July 15, 1980.

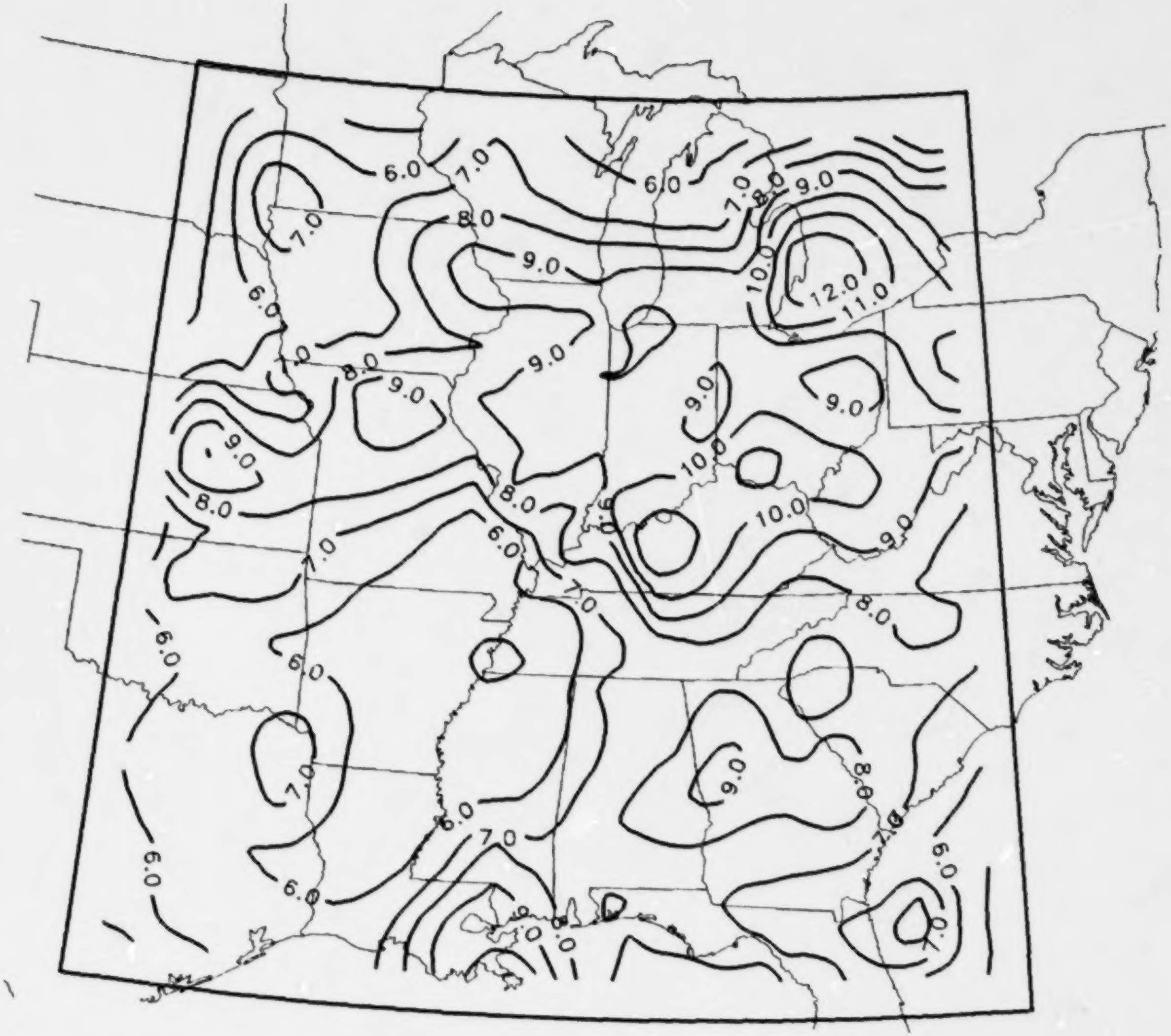
6.0
7.0
6.0
7.0
8.0
9.0
12.0
11.0
10.0
7.0
6.0
9.0
8.0
9.0
9.0
9.0
9.0
10.0
10.0
9.0
8.0
7.0
6.0
8.0
7.0
6.0
8.0
6.0
7.0
9.0
8.0
7.0
6.0
6.0
7.0
6.0
6.0
7.0
10.0

Figure 2–5c. Predicted maximum daily mixed–layer ozone concentrations (pphm) for climate sensitivity scenario#1: July 16, 1980.

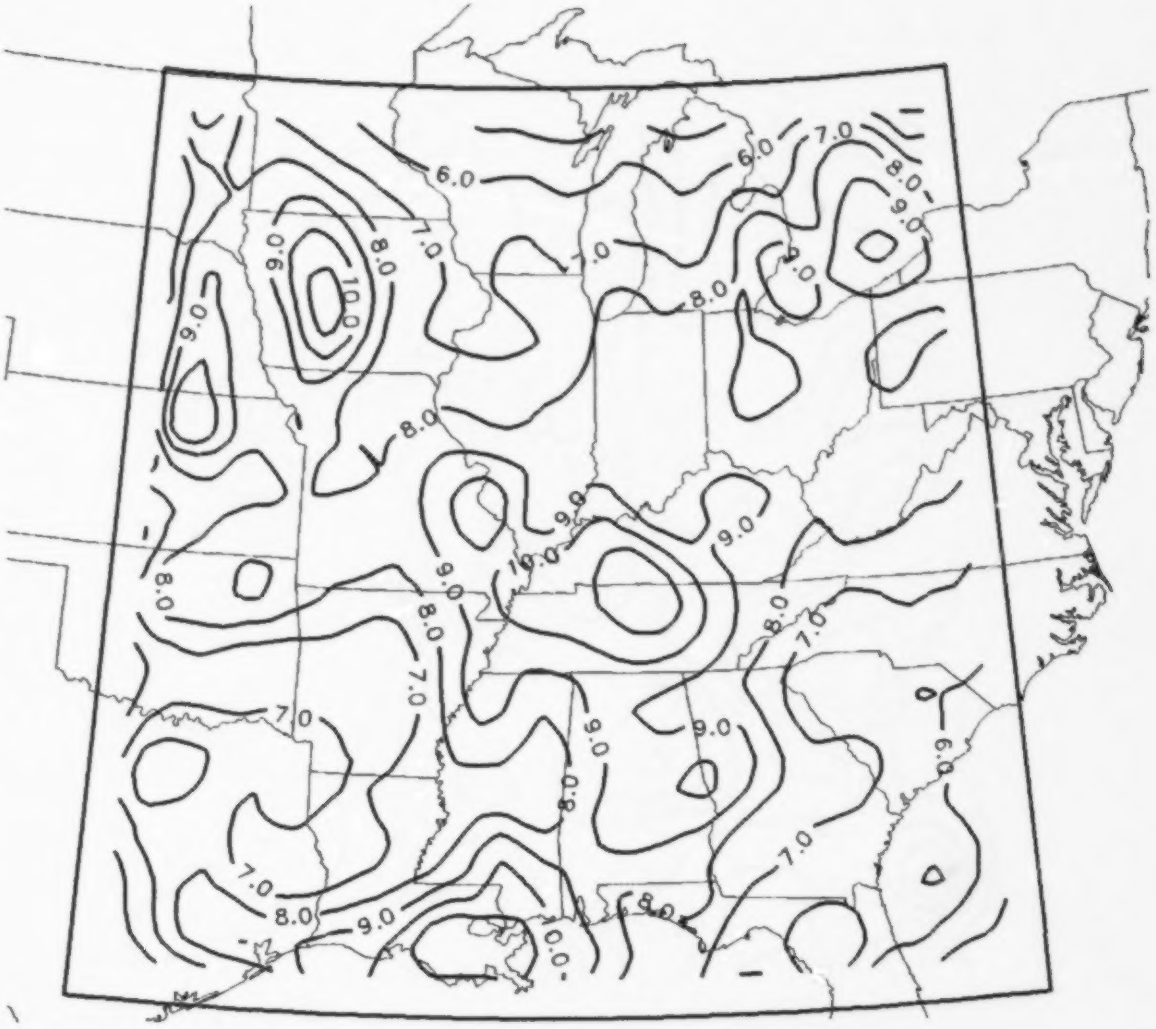

Figure 2–5d. Predicted maximum daily mixed–layer ozone concentrations (pphm) for climate sensitivity scenario#1: July 17, 1980.

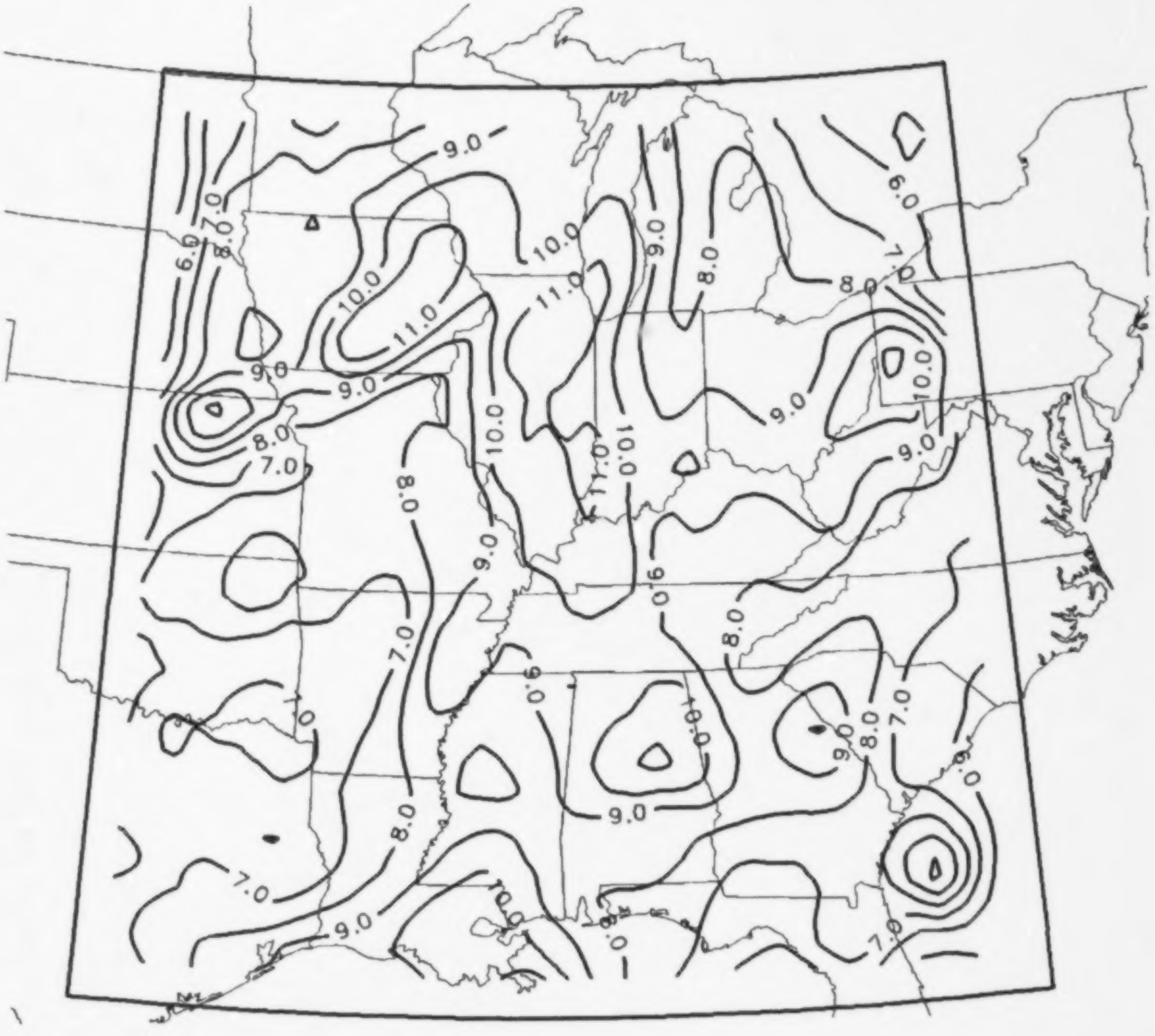
9.0
6.0
7.0
8.0
10.0
11.0
9.0
9.0
9.0
8.0
7.0
10.0
11.0
9.0
8.0
6.0
7.0
8.0
10.0
9.0
10.0
11.0
10.0
9.0
9.0
8.0
9.0
7.0
9.0
8.0
7.0
7.0
10.0
9.0
8.0
7.0
6.0
9.0
8.0
7.0
9.0
10.0
8.0
7.0

Figure 2–5e. Predicted maximum daily mixed–layer ozone concentrations (pphm) for climate sensitivity scenario#1: July 18, 1980.

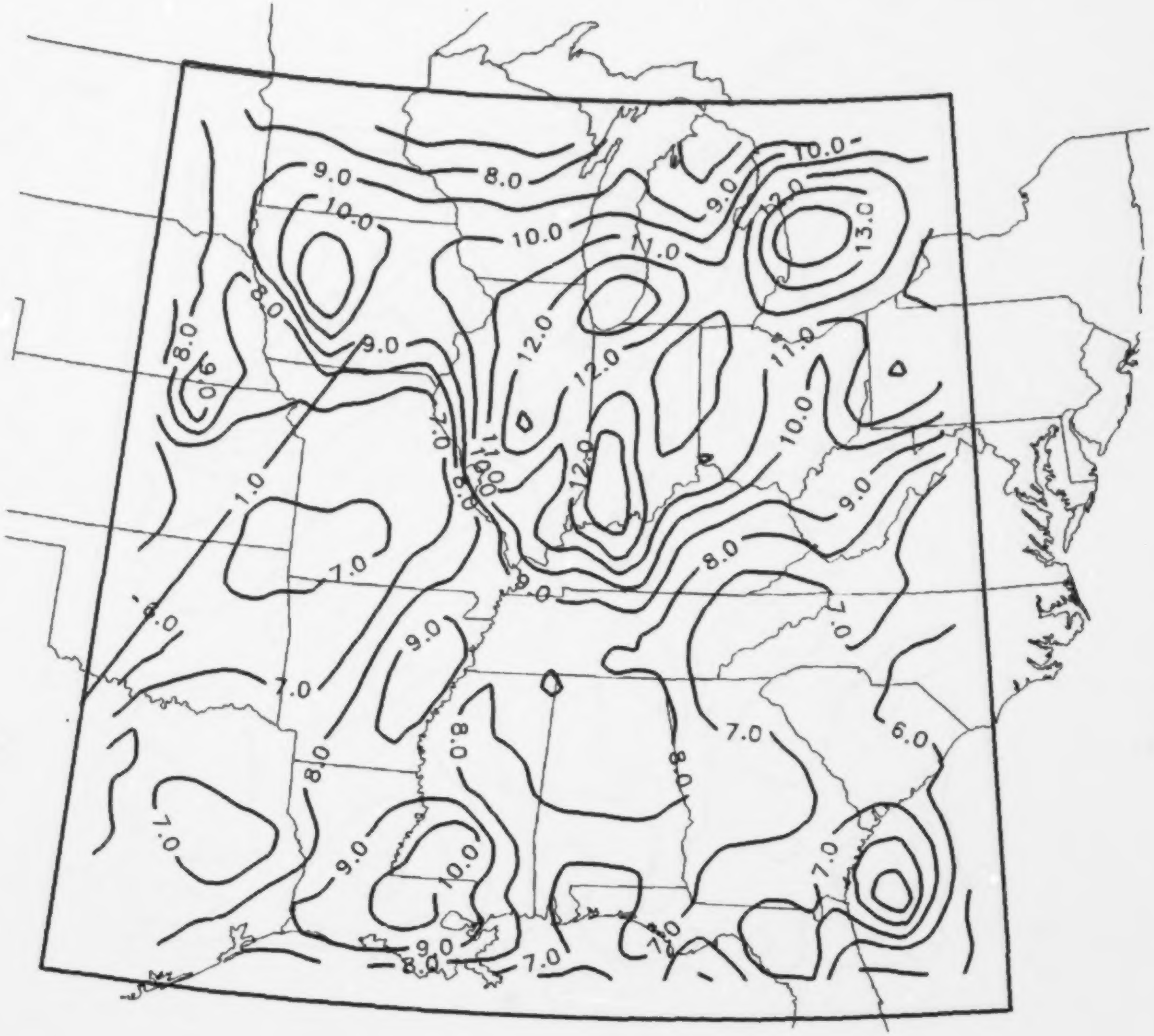
10.0
9.0
8.0
9.0
10.0
10.0
11.0
12.0
13.0
8.0
9.0
8.0
9.0
12.0
12.0
12.0
11.0
10.0
7.0
11.0
10.0
8.0
9.0
1.0
8.0
7.0
9.0
7.0
9.0
6.0
7.0
7.0
6.0
8.0
8.0
8.0
7.0
7.0
9.0
10.0
9.0
8.0
7.0
7.0

Figure 2–5f. Predicted maximum daily mixed–layer ozone concentrations (pphm) for climate sensitivity scenario#1: July 19, 1980.

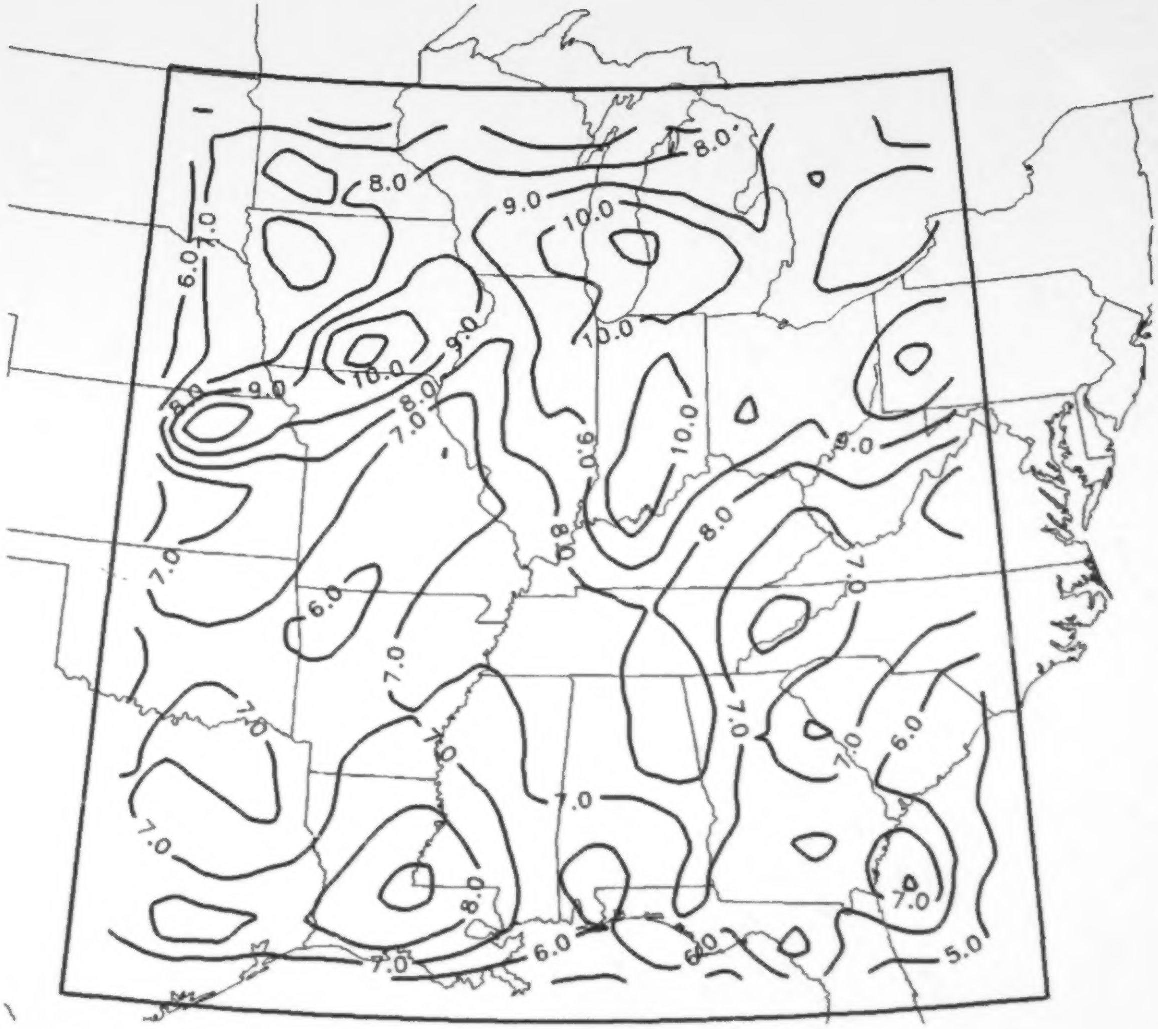

8.0
9.0
10.0
8.0
7.0
6.0
10.0
9.0
9.0
8.0
7.0
10.0
9.0
9.0
8.0
8.0
7.0
6.0
7.0
7.0
7.0
7.0
7.0
7.0
6.0
7.0
8.0
7.0
6.0
6.0
7.0
5.0

Figure 2-5g. Predicted maximum daily mixed-layer ozone concentrations (pphm) for climate sensitivity scenario#1: July 20, 1980.

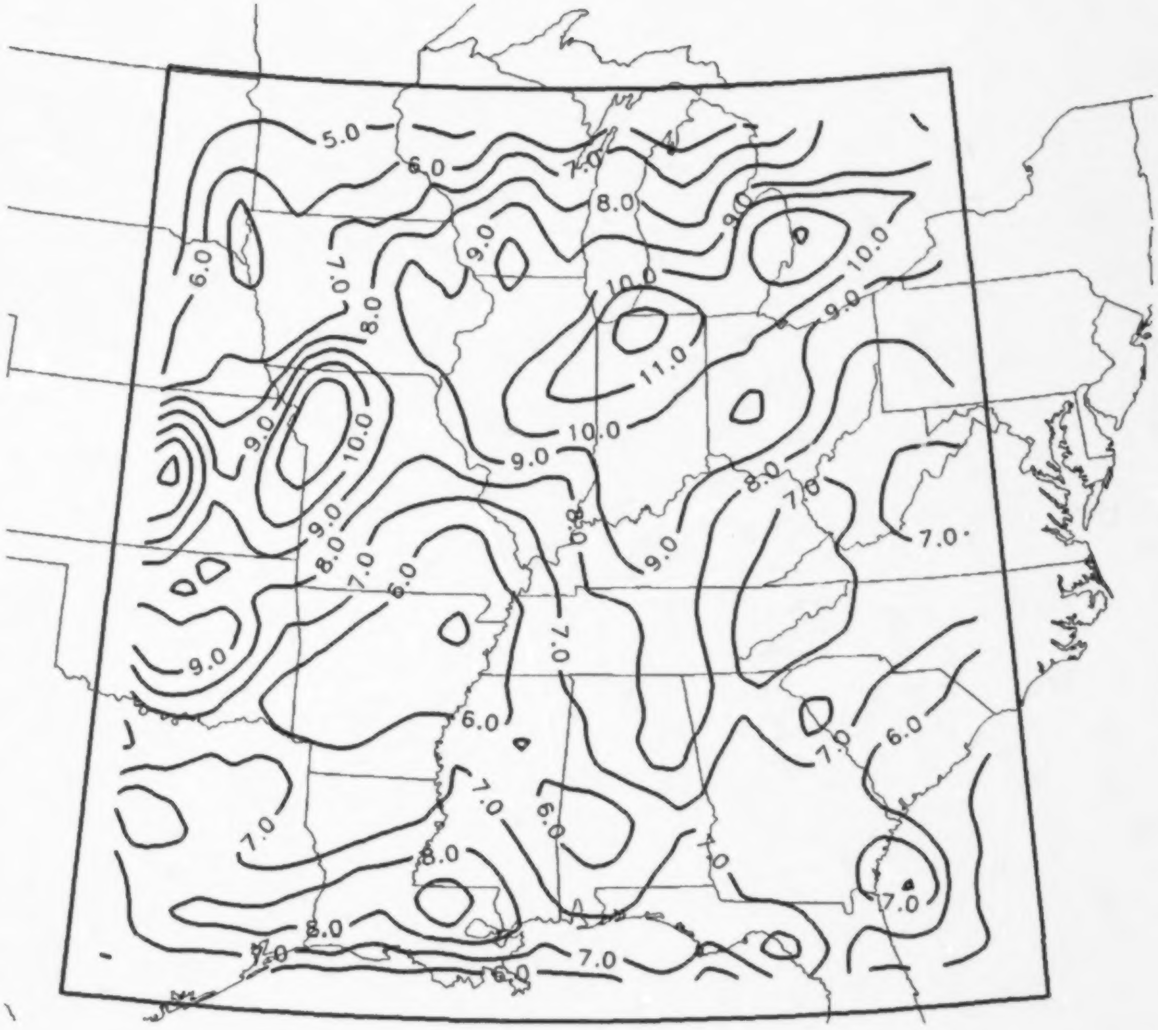
5.0
6.0
7.0
8.0
9.0
9.0
10.0
6.0
7.0
8.0
9.0
10.0
11.0
9.0
10.0
9.0
8.0
7.0
7.0
9.0
9.0
10.0
9.0
8.0
7.0
6.0
9.0
7.0
6.0
7.0
6.0
7.0
6.0
7.0
8.0
7.0
8.0
7.0
6.0
7.0
7.0

Figure 2–5h. Predicted maximum daily mixed–layer ozone concentrations (pphm) for climate sensitivity scenario#1: July 21, 1980.

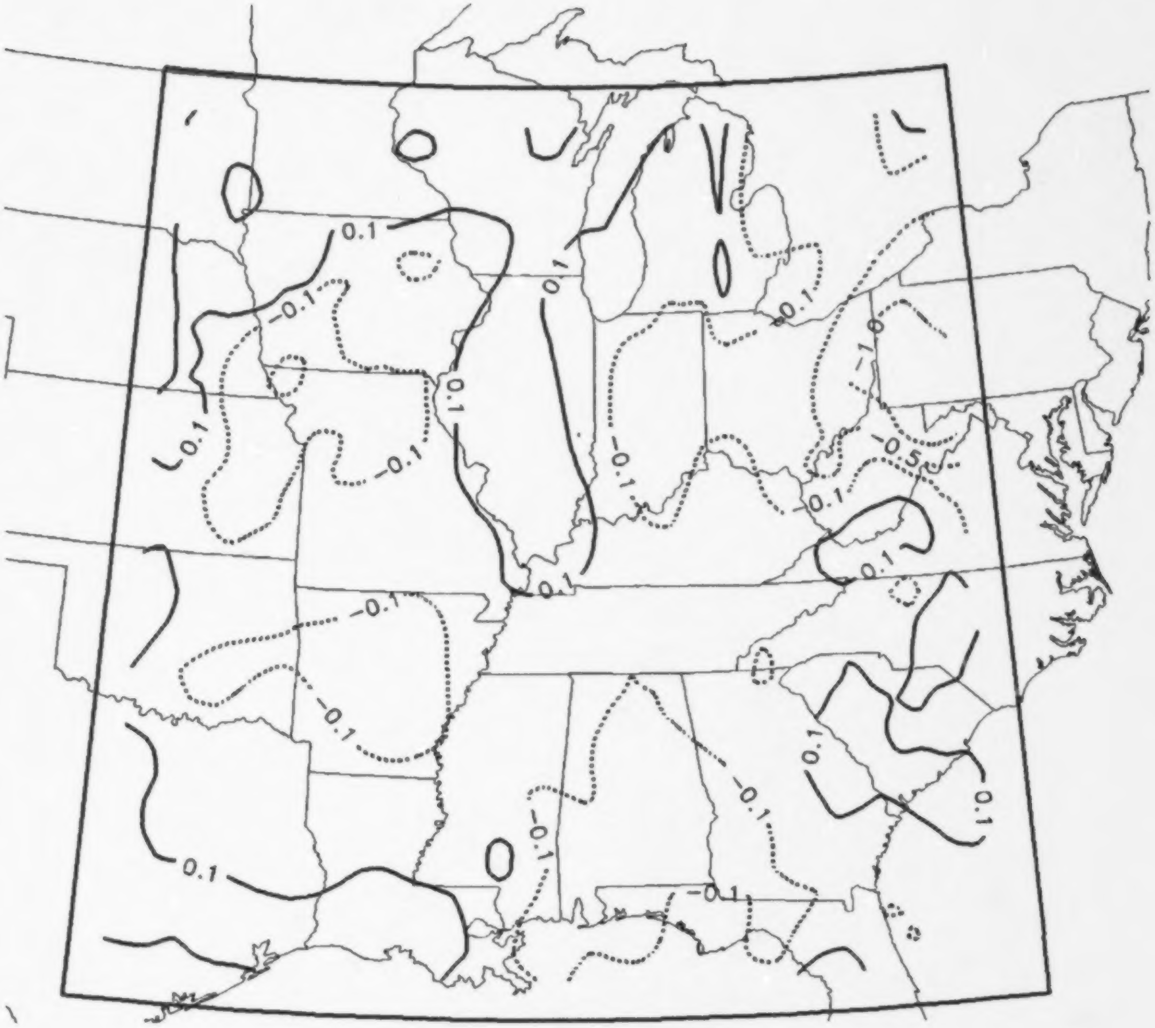
0.1
-0.1
0.1
-0.1
0.1
0.1
-0.1
0.1
0.1
-0.1
-0.1
-1.0
-0.5
-0.1
0.1
-0.1
-0.1
0.1
0.1
-0.1
-0.1
-0.1
0.1

Figure 2–6a. Differences in maximum daily ozone concentrations (pphm) (climate sensitivity scenario#1 – base case): July 14, 1980.

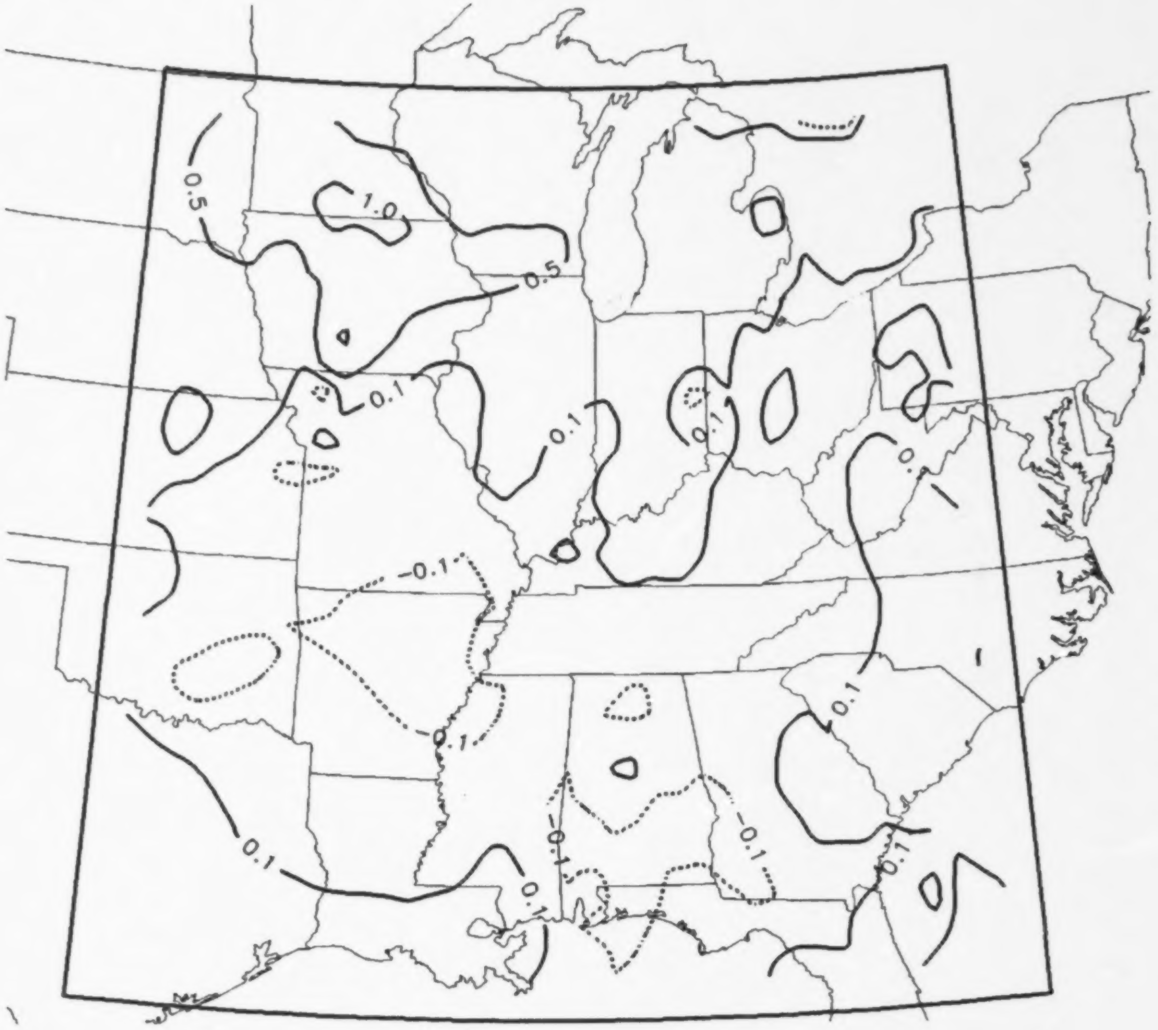
0.5
1.0
0.5
0.1
0.1
0.1
0.1
-0.1
-0.1
0.1
0.1
-0.1
-0.1
0.1
0.1

Figure 2–6b. Differences in maximum daily ozone concentrations (pphm) (climate sensitivity scenario#1 – base case): July 15, 1980.

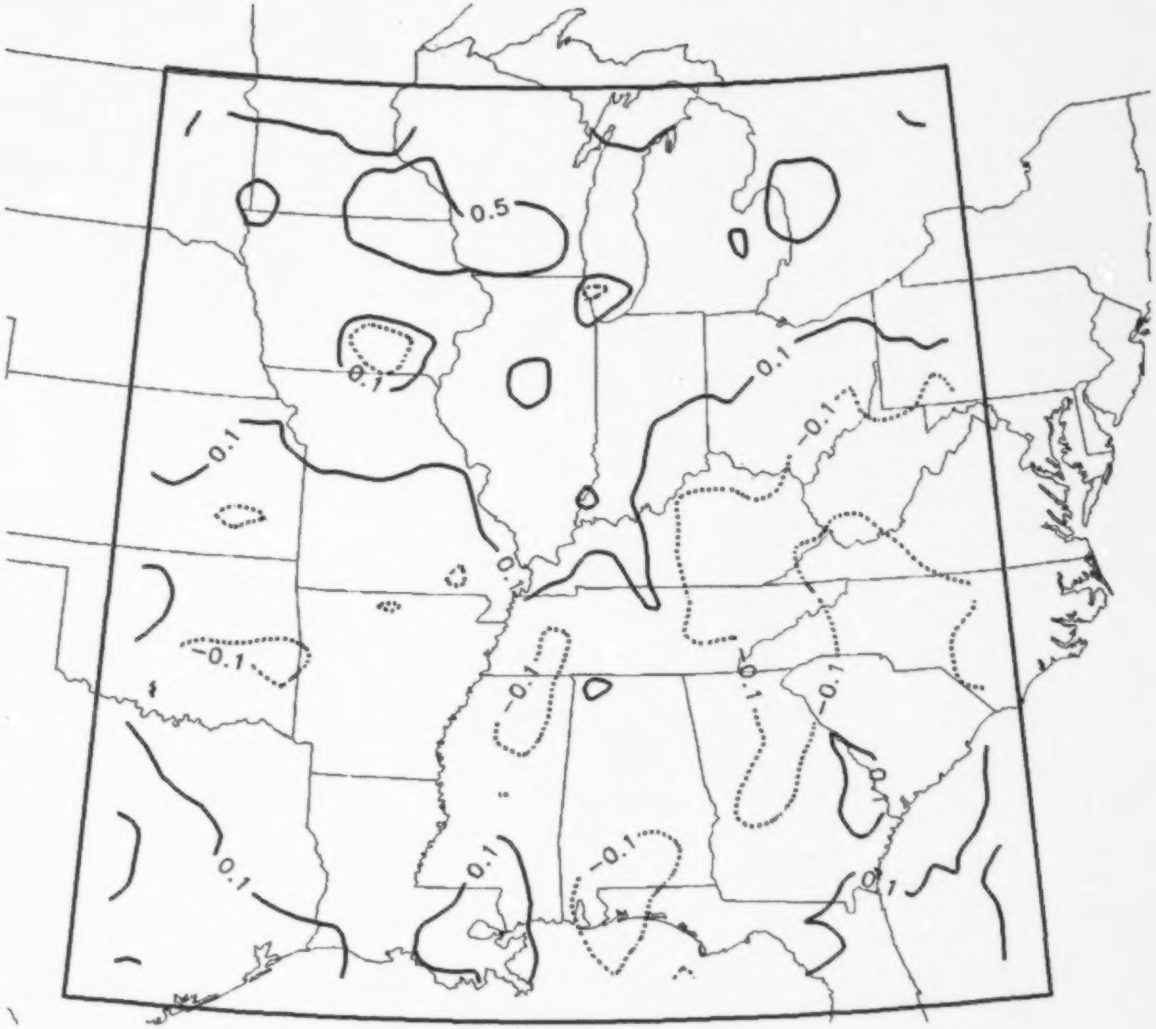

Figure 2–6c. Differences in maximum daily ozone concentrations (pphm) (climate sensitivity scenario#1 – base case): July 16, 1980.

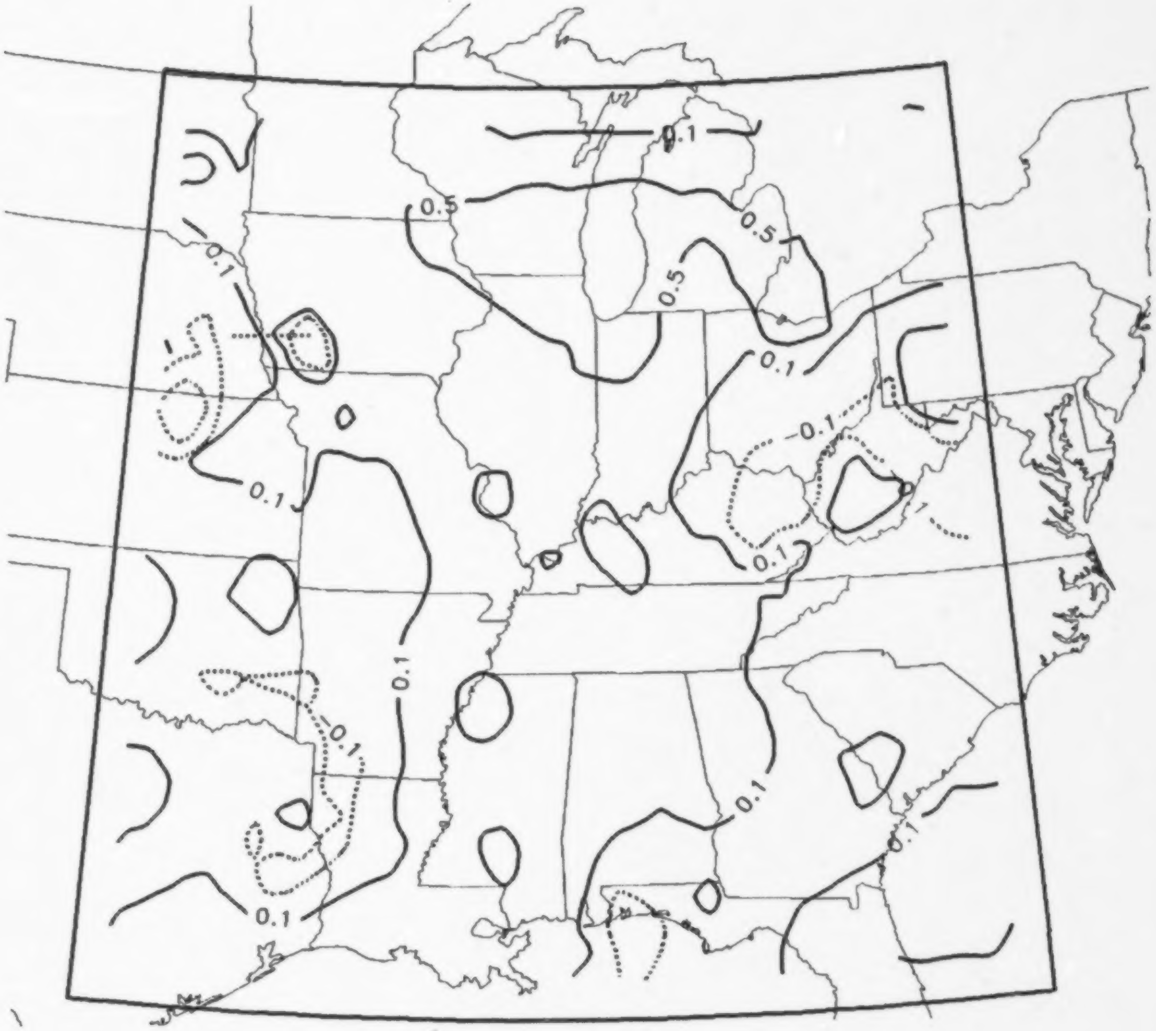
0.1
0.5
0.5
0.5
0.1
-0.1
0.1
0.1
0.1
0.1
0.1
0.1
-0.1
0.1

Figure 2–6d. Differences in maximum daily ozone concentrations (pphm) (climate sensitivity scenario#1 – base case): July 17, 1980.

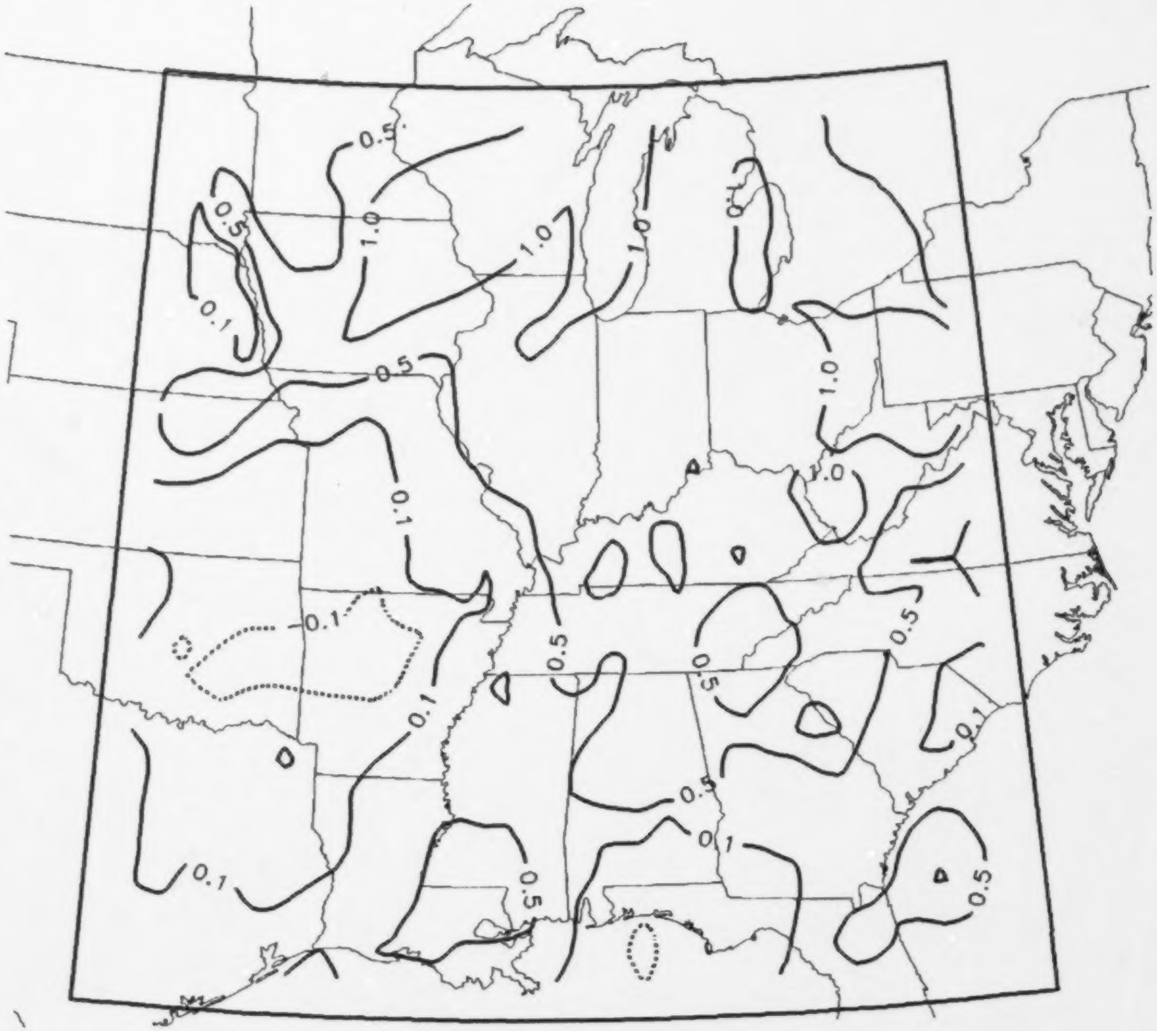
0.5
0.5
0.1
1.0
1.0
1.0
0.1
0.5
1.0
0.1
1.0
-0.1
0.5
0.1
0.5
0.5
0.5
0.1
0.1
0.5
0.1
0.5
0.5

Figure 2–6e. Differences in maximum daily ozone concentrations (pphm) (climate sensitivity scenario#1 – base case): July 18, 1980.

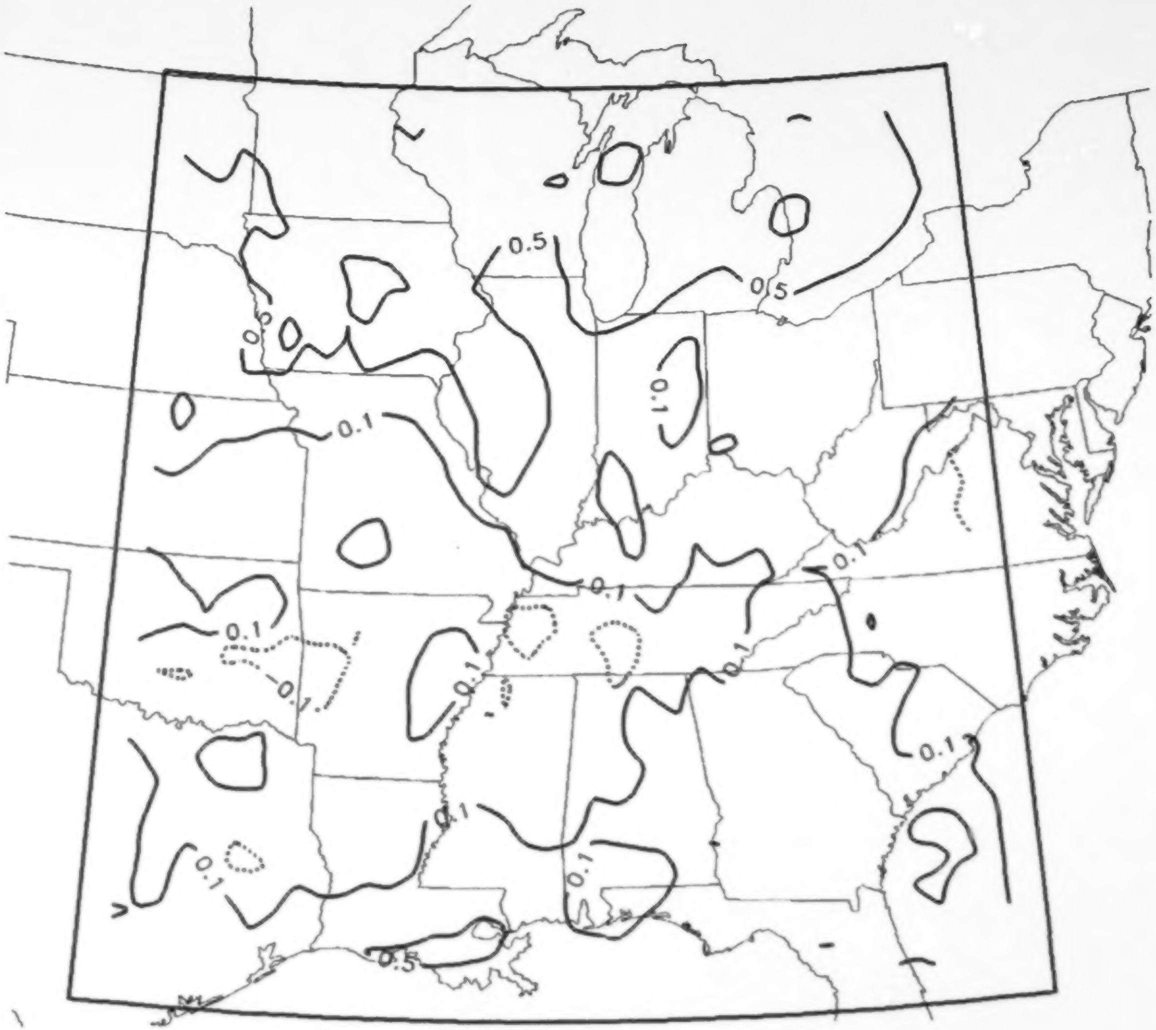
0.5
0.5
0.5
0
0.1
0.1
0.1
0.1
0.1
0.1
-0.1
0.1
0.1
0.1
0.1
0.1
0.5

Figure 2–6f. Differences in maximum daily ozone concentrations (pphm) (climate sensitivity scenario#1 – base case): July 19, 1980.

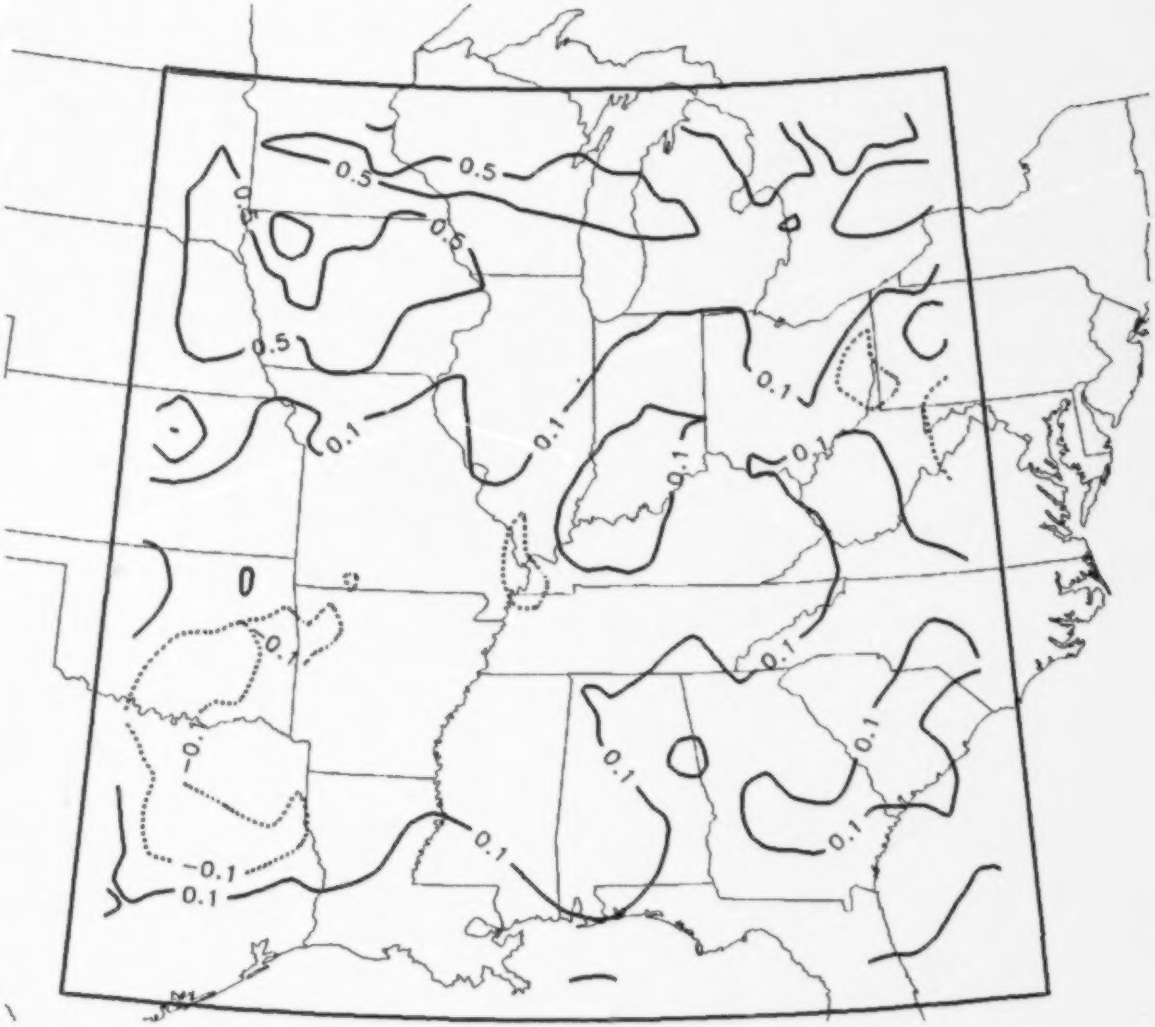
0.5
0.5
0.5
0.5
0.5
0.5
0.1
0.1
0.1
0.1
0.1
0.1
0.1
0.1
0.1
0.1
0.1
-0.1
-0.1
-0.1
0.1

Figure 2–6g. Differences in maximum daily ozone concentrations (pphm) (climate sensitivity scenario#1 – base case): July 20, 1980.

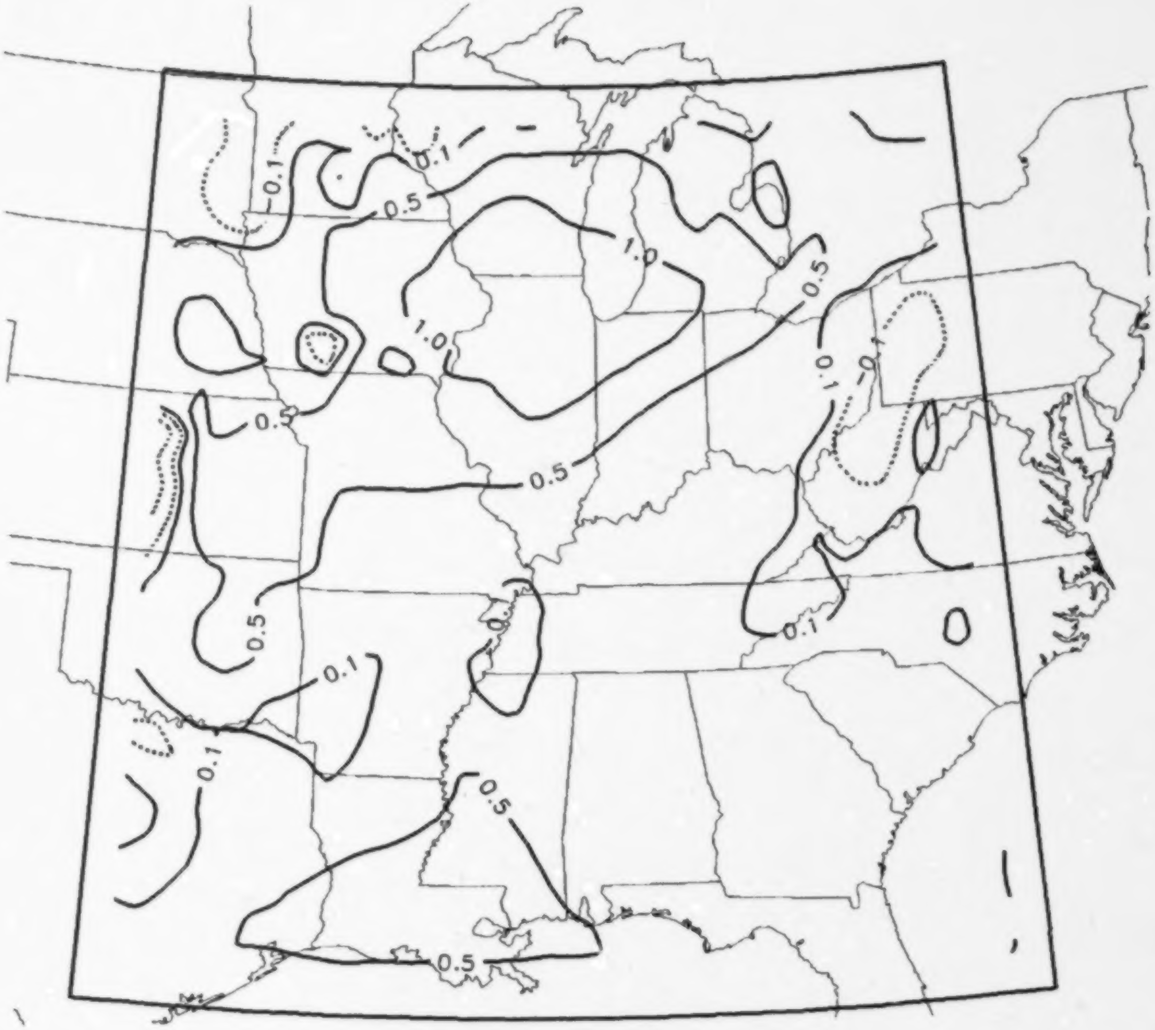
0.1
0.1
0.5
1.0
0.5
1.0
0.5
0.5
0.1
0.1
0.5
0.1
0.1
0.1
0.5
0.5
0.5

Figure 2–6h. Differences in maximum daily ozone concentrations (pphm) (climate sensitivity scenario#1 – base case): July 21, 1980.

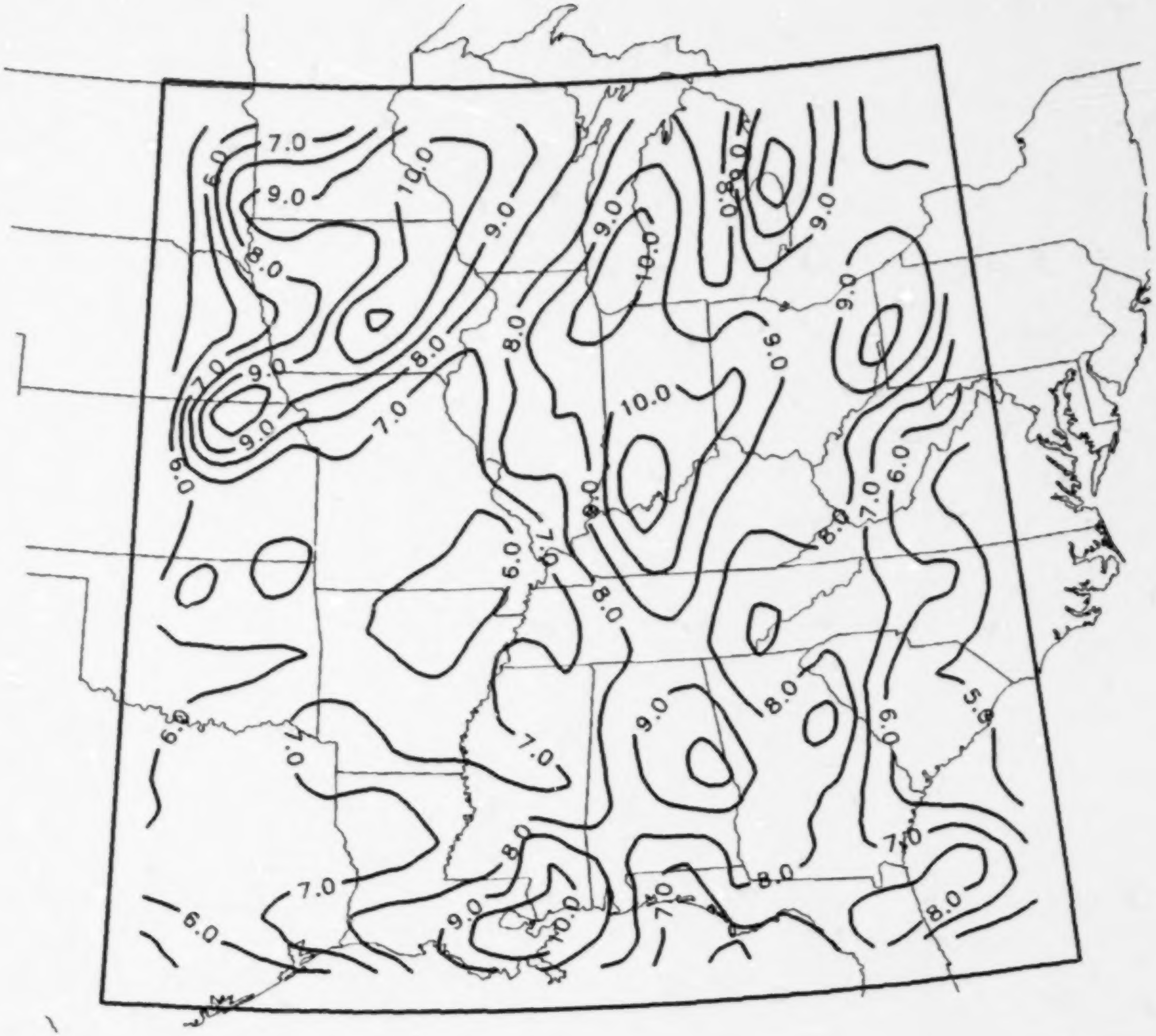
7.0
6.0
9.0
10.0
8.0
5.0

Figure 2–7a. Predicted maximum daily mixed–layer ozone concentrations (pphm) for climate sensitivity scenario#2: July 14, 1980.

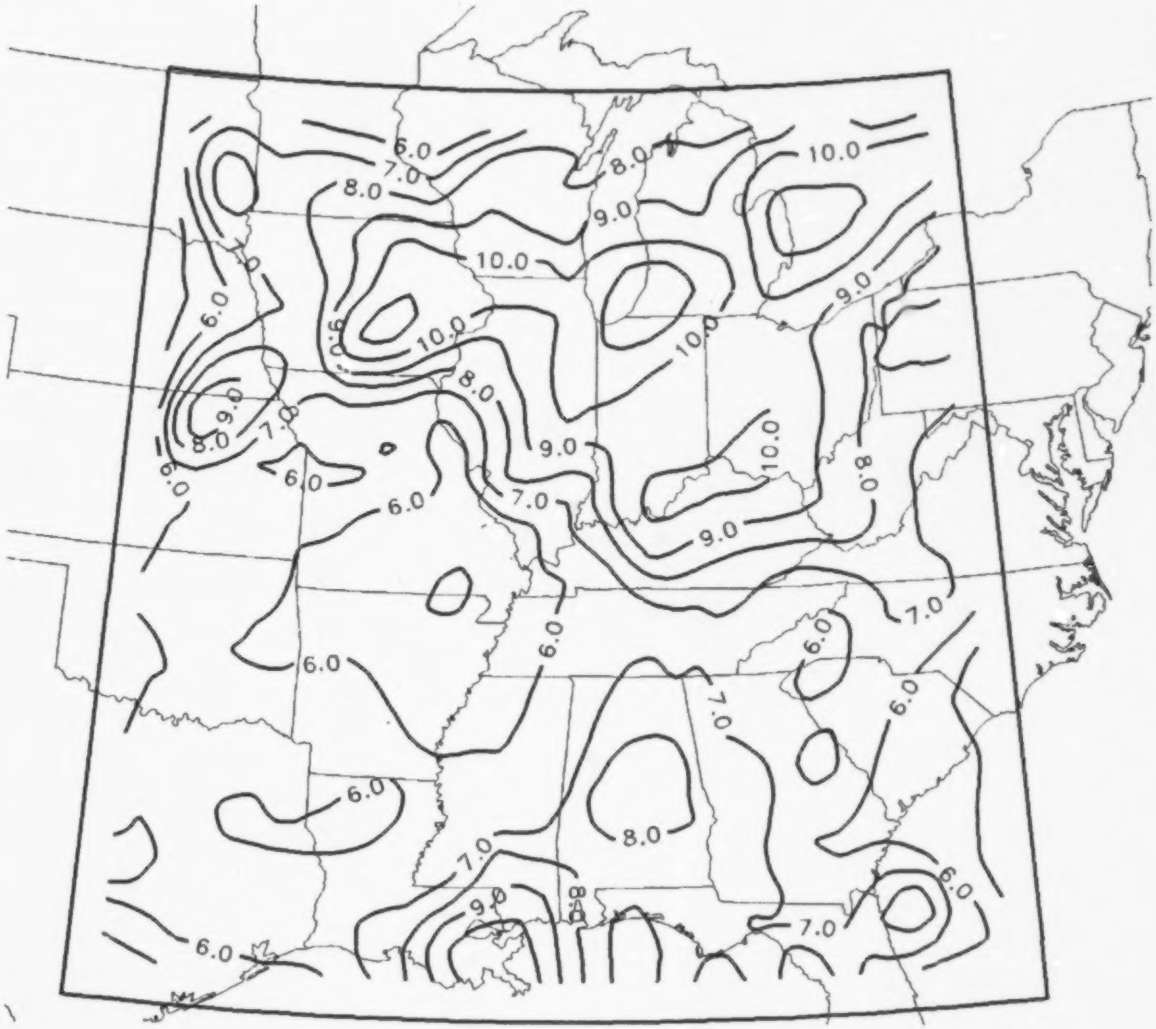

Figure 2–7b. Predicted maximum daily mixed–layer ozone concentrations (pphm) for climate sensitivity scenario#2: July 15, 1980.

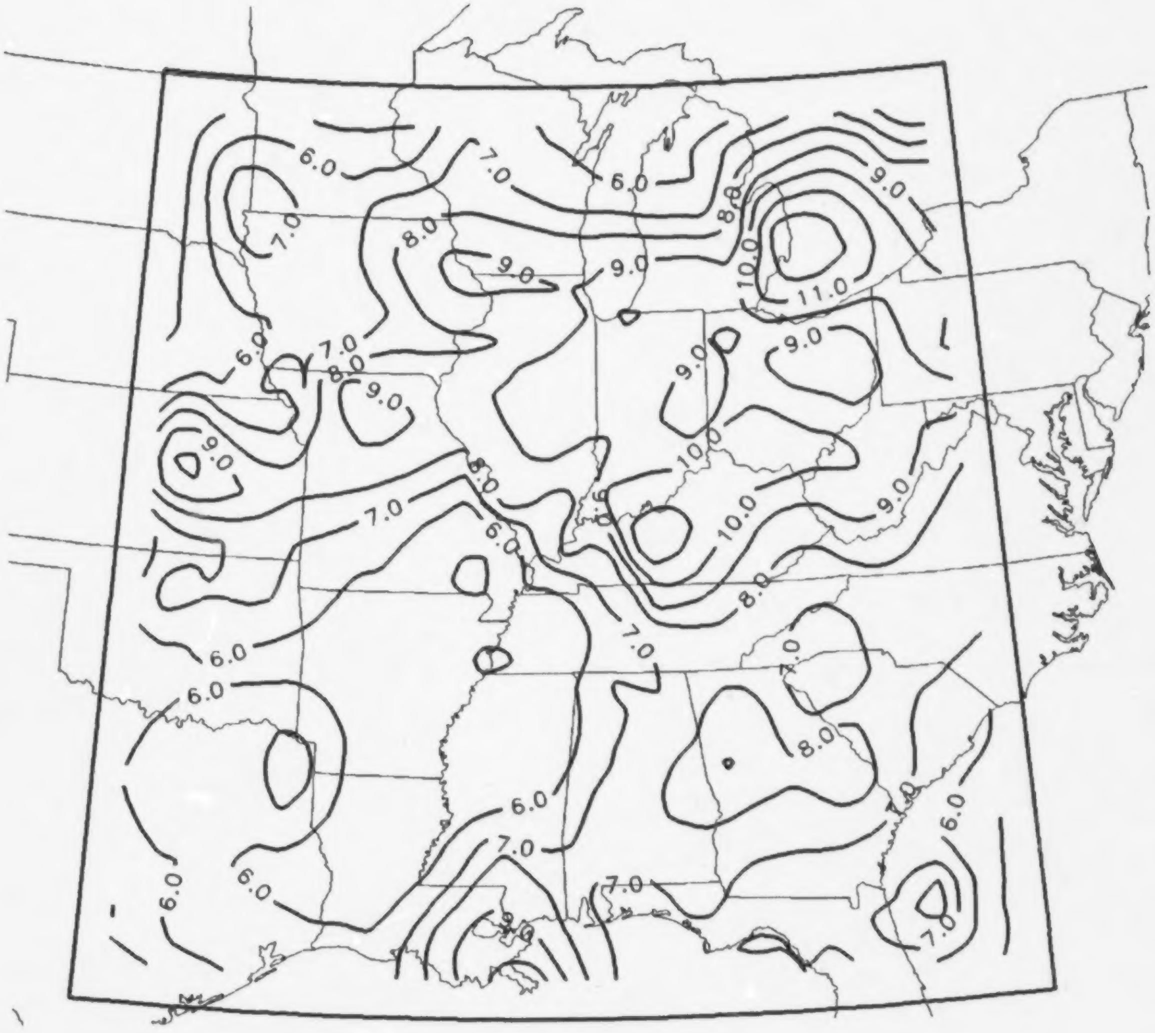
6.0
7.0
8.0
9.0
10.0
11.0

Figure 2–7c. Predicted maximum daily mixed–layer ozone concentrations (pphm) for climate sensitivity scenario#2: July 16, 1980.

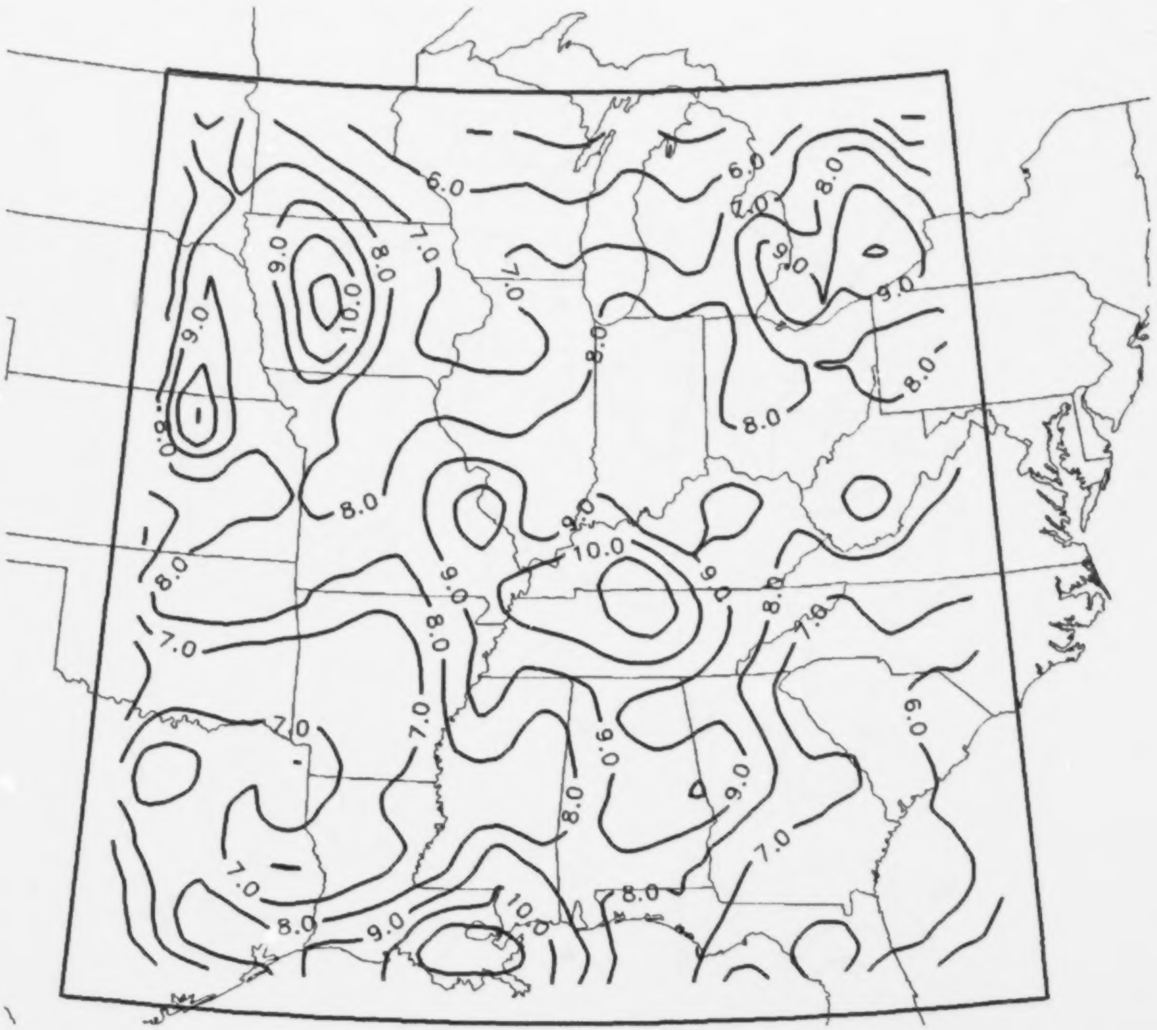
6.0
6.0
7.0
7.0
8.0
9.0
10.0
9.0
8.0
8.0
7.0
8.0
9.0
10.0
9.0
8.0
7.0
8.0
9.0
9.0
8.0
7.0
7.0
8.0
9.0
10.0
8.0
7.0
9.0
6.0

Figure 2–7d. Predicted maximum daily mixed–layer ozone concentrations (pphm) for climate sensitivity scenario#2: July 17, 1980.

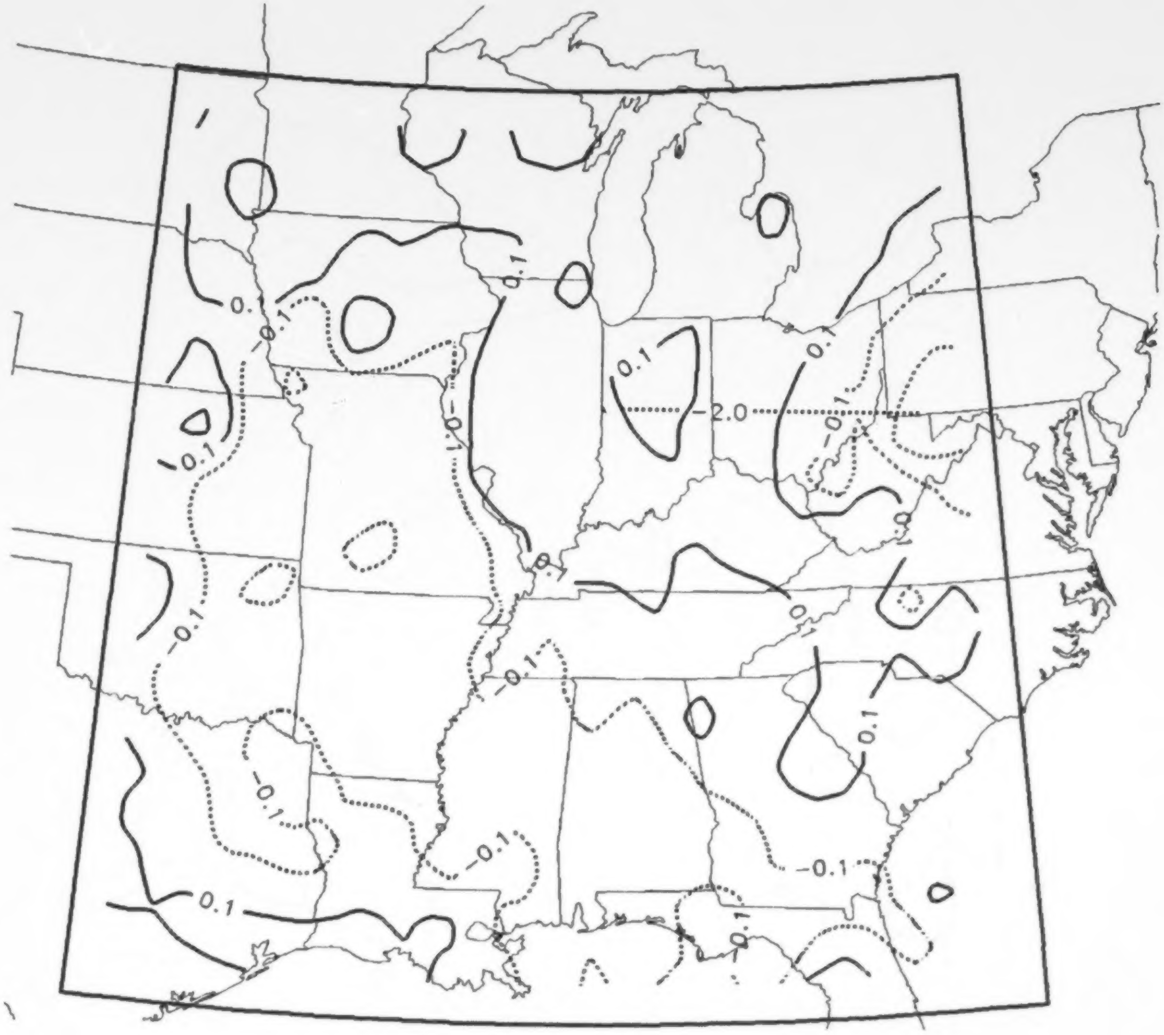
0.1
-0.1
0.1
-0.1
-2.0
0.1
-0.1
0.1
-0.1
-0.1
0.1
-0.1
-0.1
-0.1
-0.1
0.1
0.1
-0.1
-0.1
0.1

Figure 2–8a. Differences in maximum daily ozone concentrations (pphm) (climate sensitivity scenario#2 – base case): July 14, 1980.

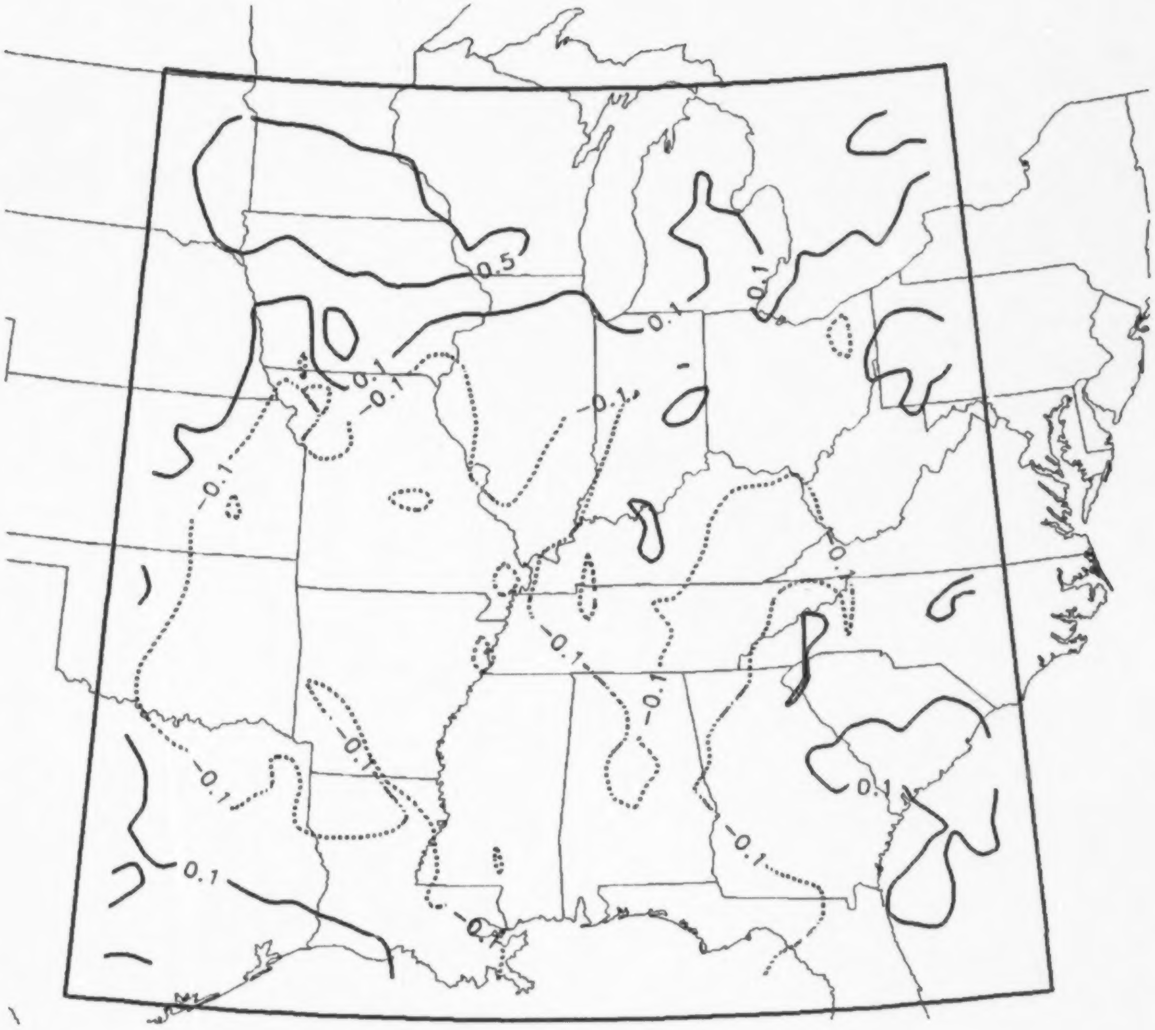
0.5
0.1
0.1
-0.1
-0.1
-0.1
-0.1
0.1
-0.1
-0.1
-0.1
-0.1
-0.1
-0.1
-0.1
0.1
-0.1
0.1
-0.1

Figure 2–8b. Differences in maximum daily ozone concentrations (pphm) (climate sensitivity scenario#2 – base case): July 15, 1980.

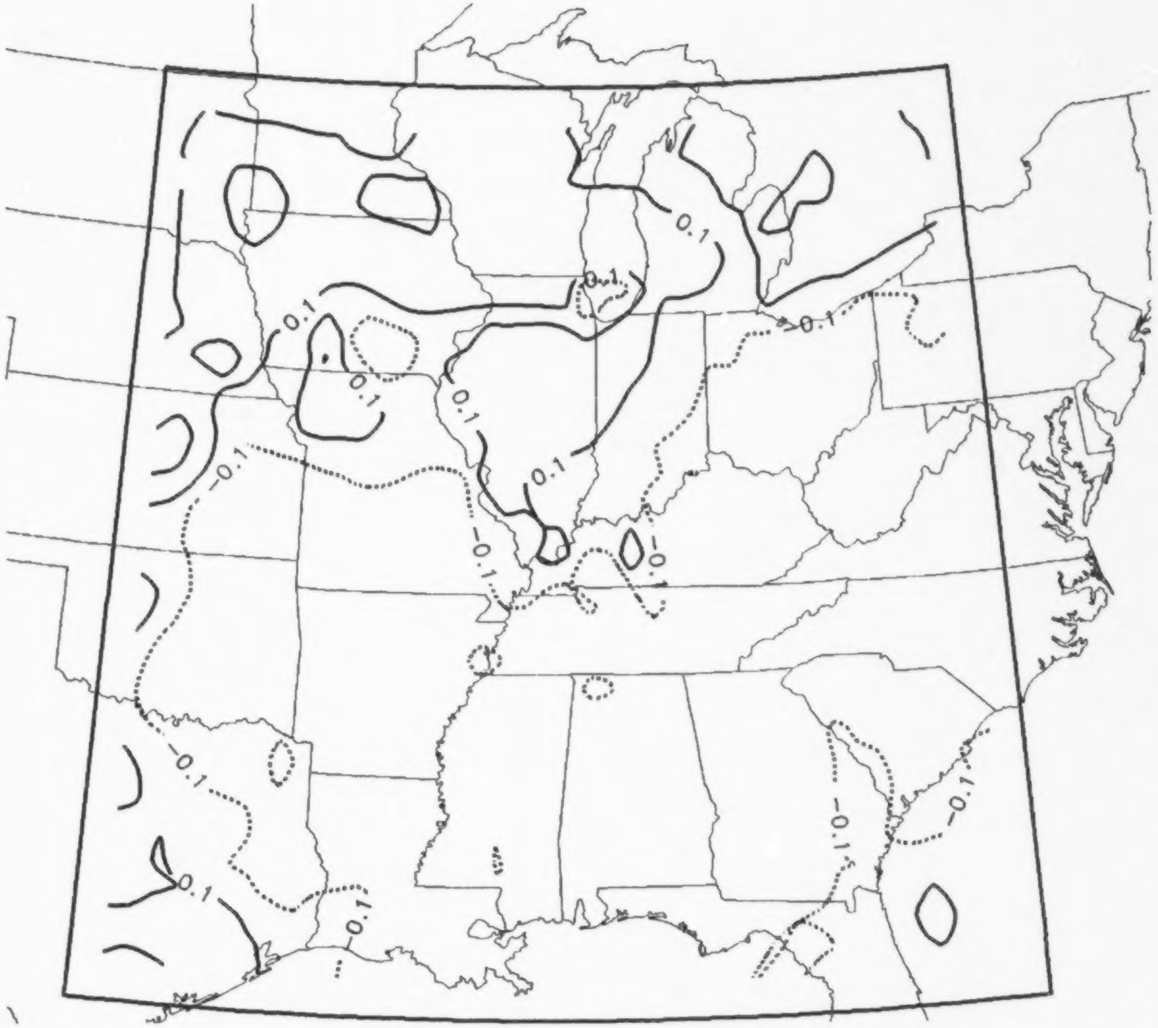
0.1
0.1
0.1
0.1
0.1
0.1
-0.1
-0.1
-0.1
-0.1
-0.1
-0.1
-0.1
0.1
-0.1

Figure 2–8c. Differences in maximum daily ozone concentrations (pphm) (climate sensitivity scenario#2 – base case): July 16, 1980.

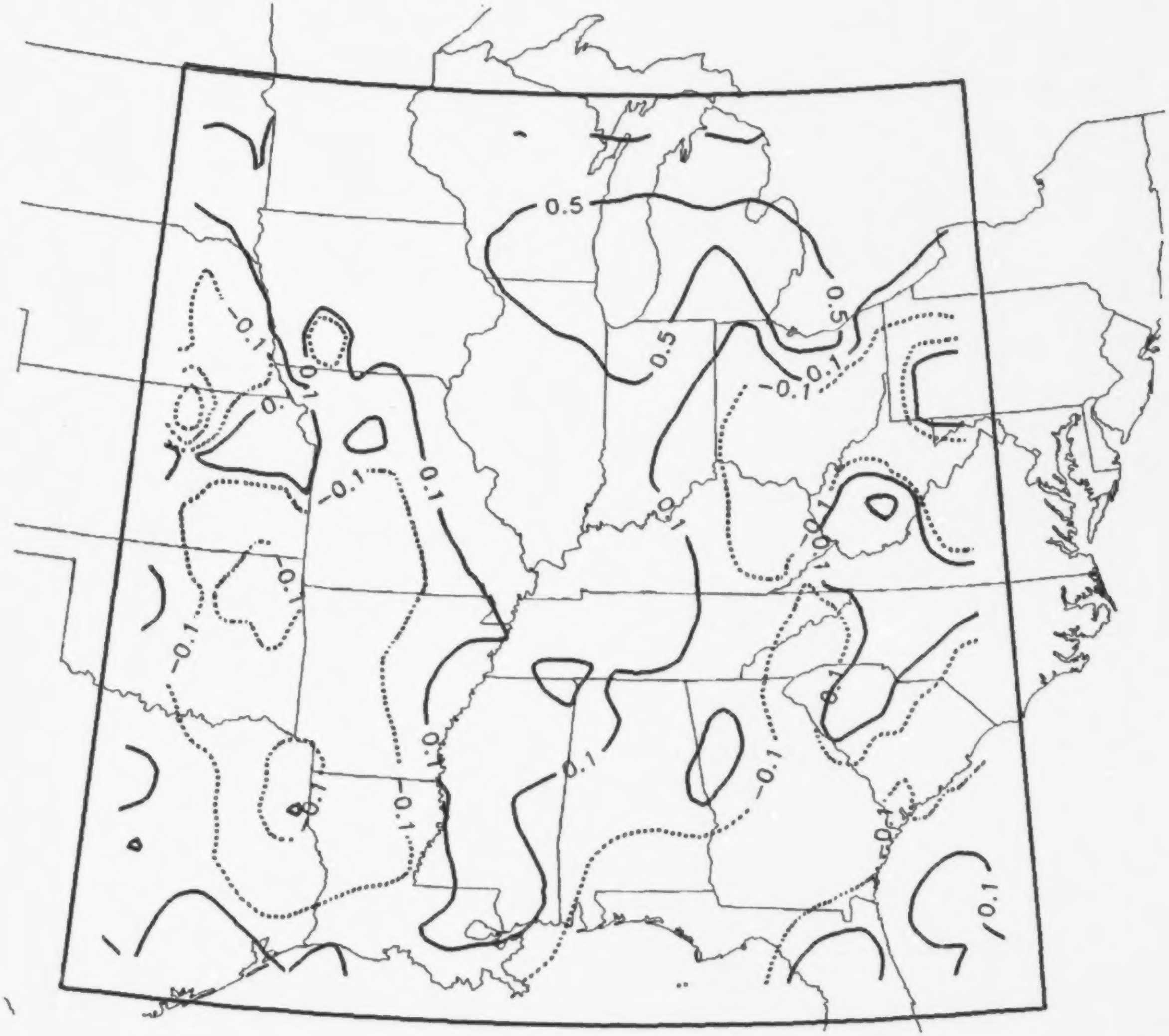
0.5
0.5
0.5
0.5
-0.1
0.1
-0.1
0.1
-0.1
0.1
-0.1
-0.1

Figure 2–8d. Differences in maximum daily ozone concentrations (pphm) (climate sensitivity scenario#2 – base case): July 17, 1980.

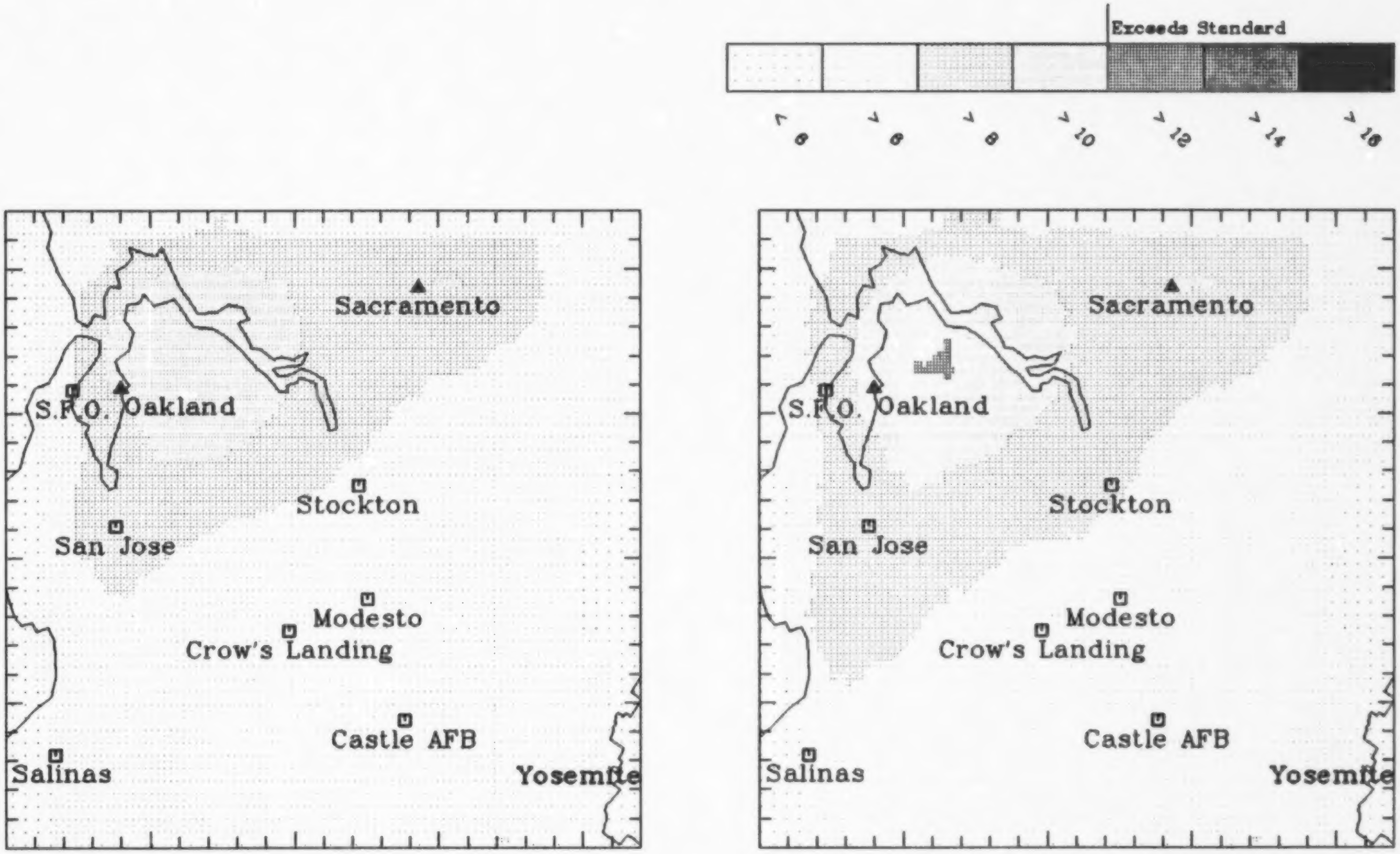
Exceeds Standard
< 6
> 6
> 8
> 10
> 12
> 14
> 16
Sacramento
S.F.O.
Oakland
Stockton
San Jose
Modesto
Crow's Landing
Castle AFB
Salinas
Yosemite

Base Case

Climate Sensitivity Scenario #1

FIGURE 2-9a. **Comparison of predicted maximum daily ozone concentrations (pphm) for the base case and climate sensitivity scenario #1 (temperature and water increase) for August 5, 1981**

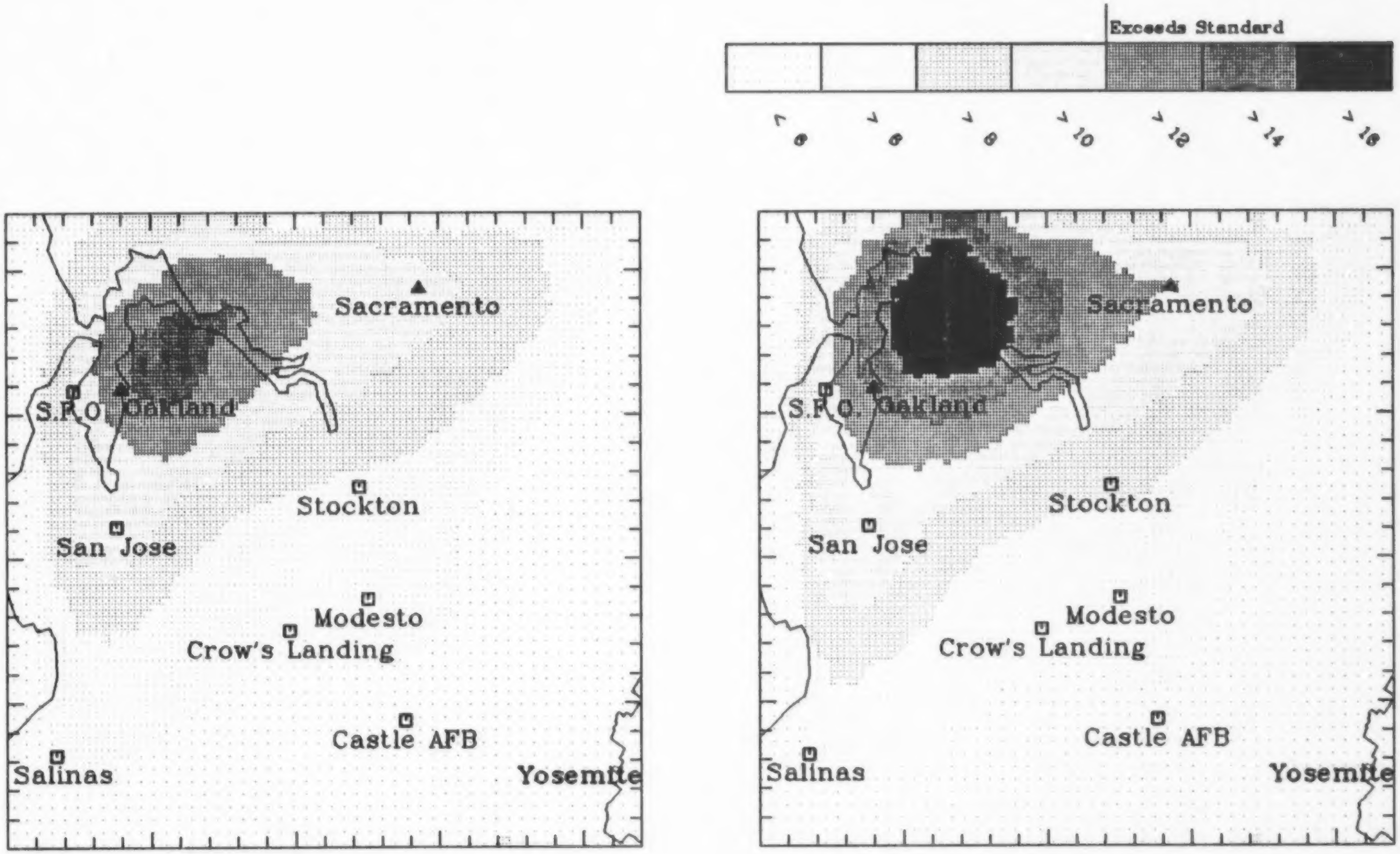
Exceeds Standard
< 6
> 6
> 8
> 10
> 12
> 14
> 16
Sacramento
S.F.O.
Oakland
Stockton
San Jose
Modesto
Crow's Landing
Castle AFB
Salinas
Yosemite

Base Case

Climate Sensitivity Scenario #1

FIGURE 2-9b. **Comparison of predicted maximum daily ozone concentrations (pphm) for the base case and climate sensitivity scenario #1 (temperature and water increase) for August 6, 1981**

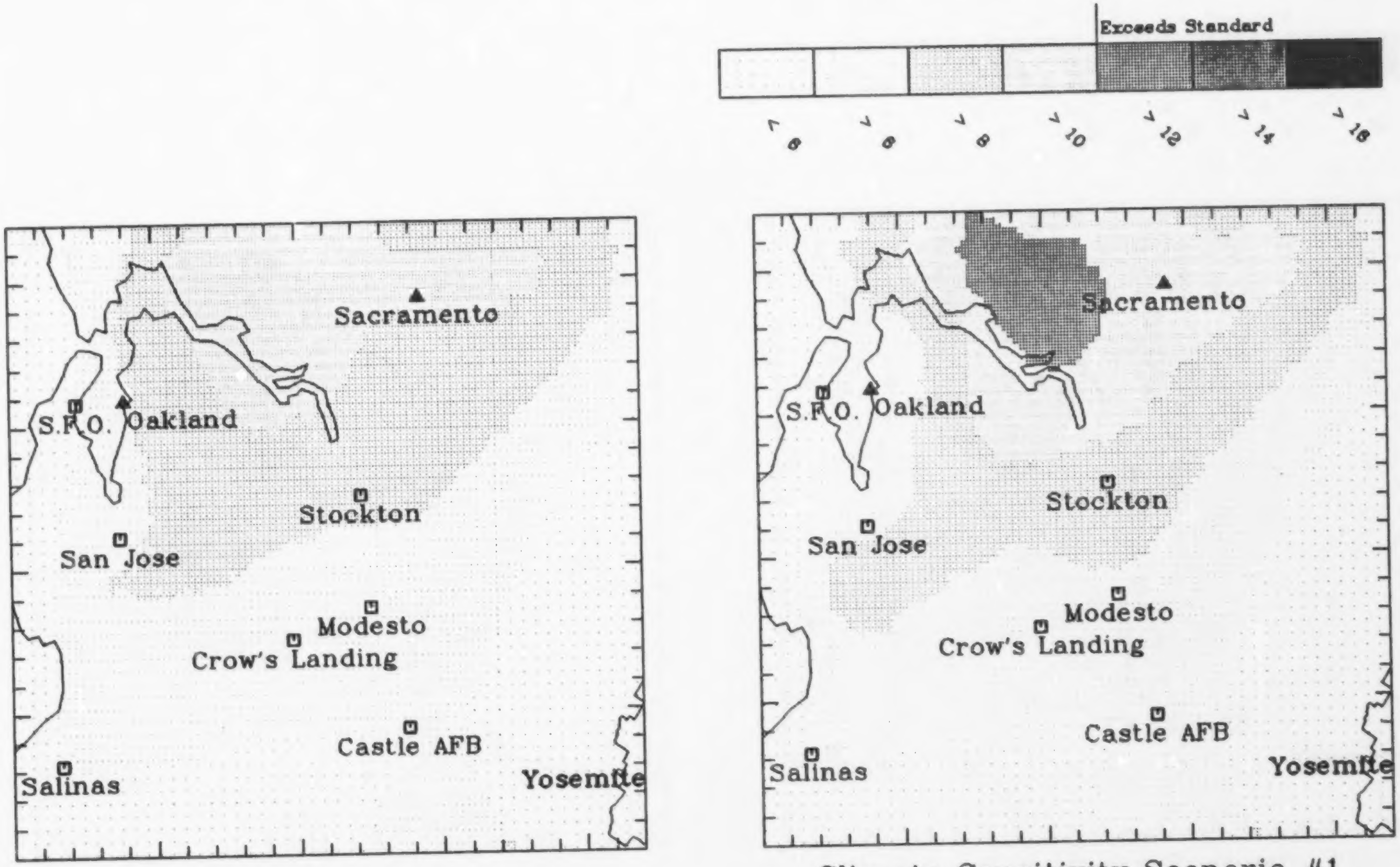
Exceeds Standard
< 6
> 6
> 8
> 10
> 12
> 14
> 16
Sacramento
S.F.O.
Oakland
Stockton
San Jose
Modesto
Crow's Landing
Castle AFB
Salinas
Yosemite

Base Case

Climate Sensitivity Scenario #1

FIGURE 2-9c. **Comparison of predicted maximum daily ozone concentrations (pphm) for the base case and climate sensitivity scenario #1 (temperature and water increase) for August 7, 1981**

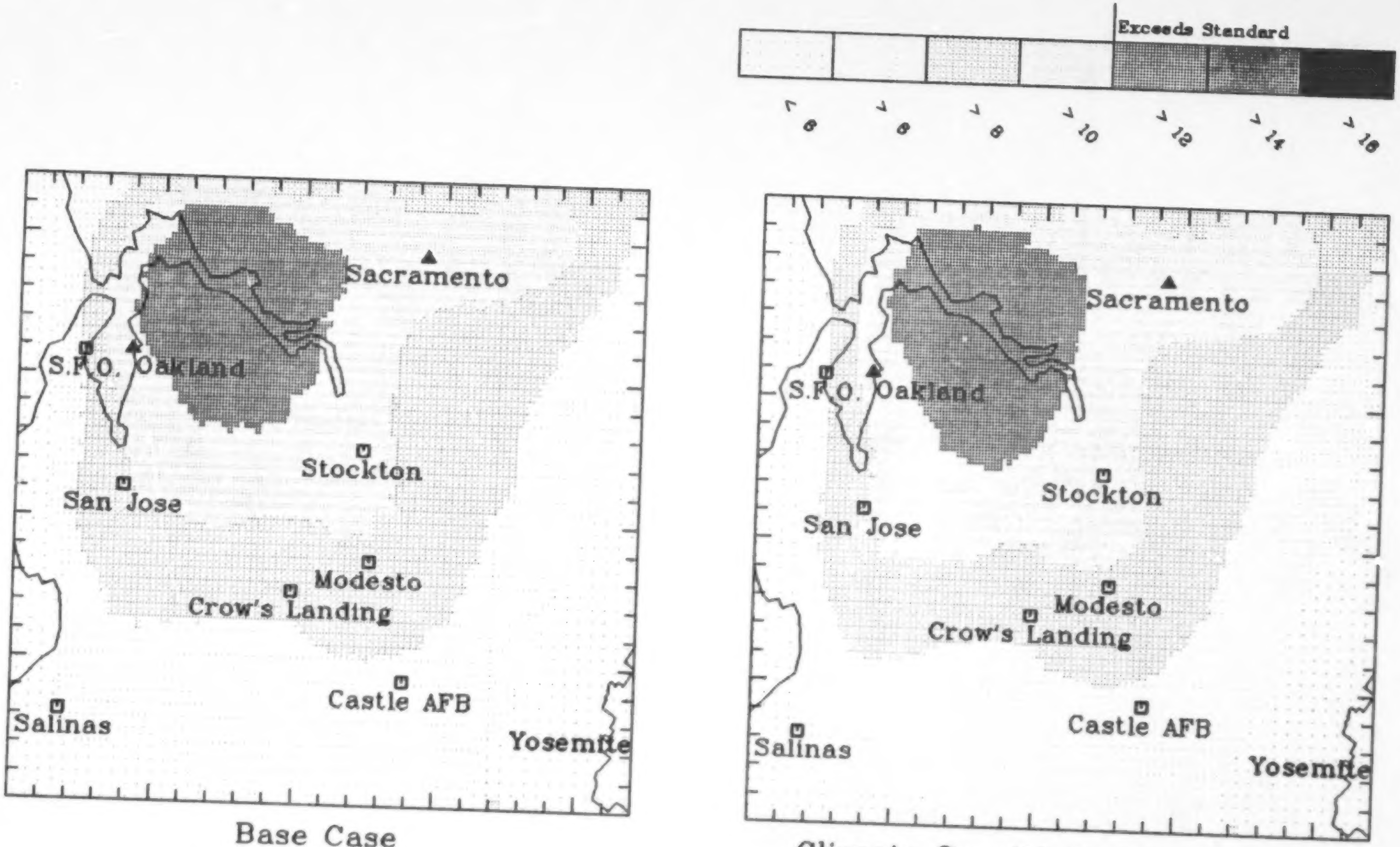
Exceeds Standard
< 6
> 6
> 8
> 10
> 12
> 14
> 16
Sacramento
S.F.O.
Oakland
Stockton
San Jose
Modesto
Crow's Landing
Castle AFB
Salinas
Yosemite

Base Case

Climate Sensitivity Scenario #1

FIGURE 2-9d. **Comparison of predicted maximum daily ozone concentrations (pphm) for the base case and climate sensitivity scenario #1 (temperature and water increase) for August 8, 1981**

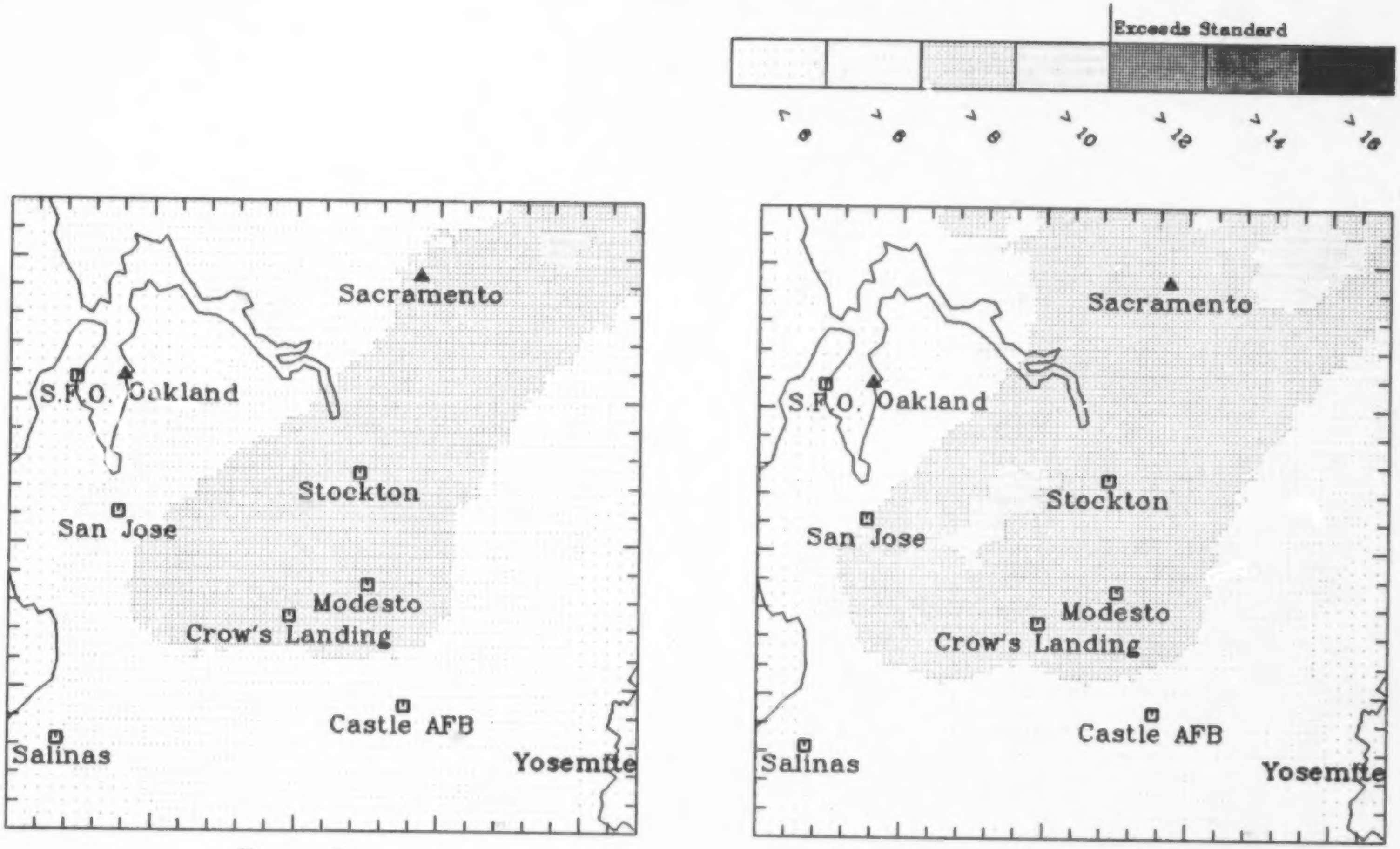
Exceeds Standard
< 6
> 6
> 8
> 10
> 12
> 14
> 16
Sacramento
S.F.O.
Oakland
Stockton
San Jose
Modesto
Crow's Landing
Castle AFB
Salinas
Yosemite

Base Case

Climate Sensitivity Scenario #1

FIGURE 2-9e. Comparison of predicted maximum daily ozone concentrations (pphm) for the base case and climate sensitivity scenario #1 (temperature and water increase) for August 9, 1981

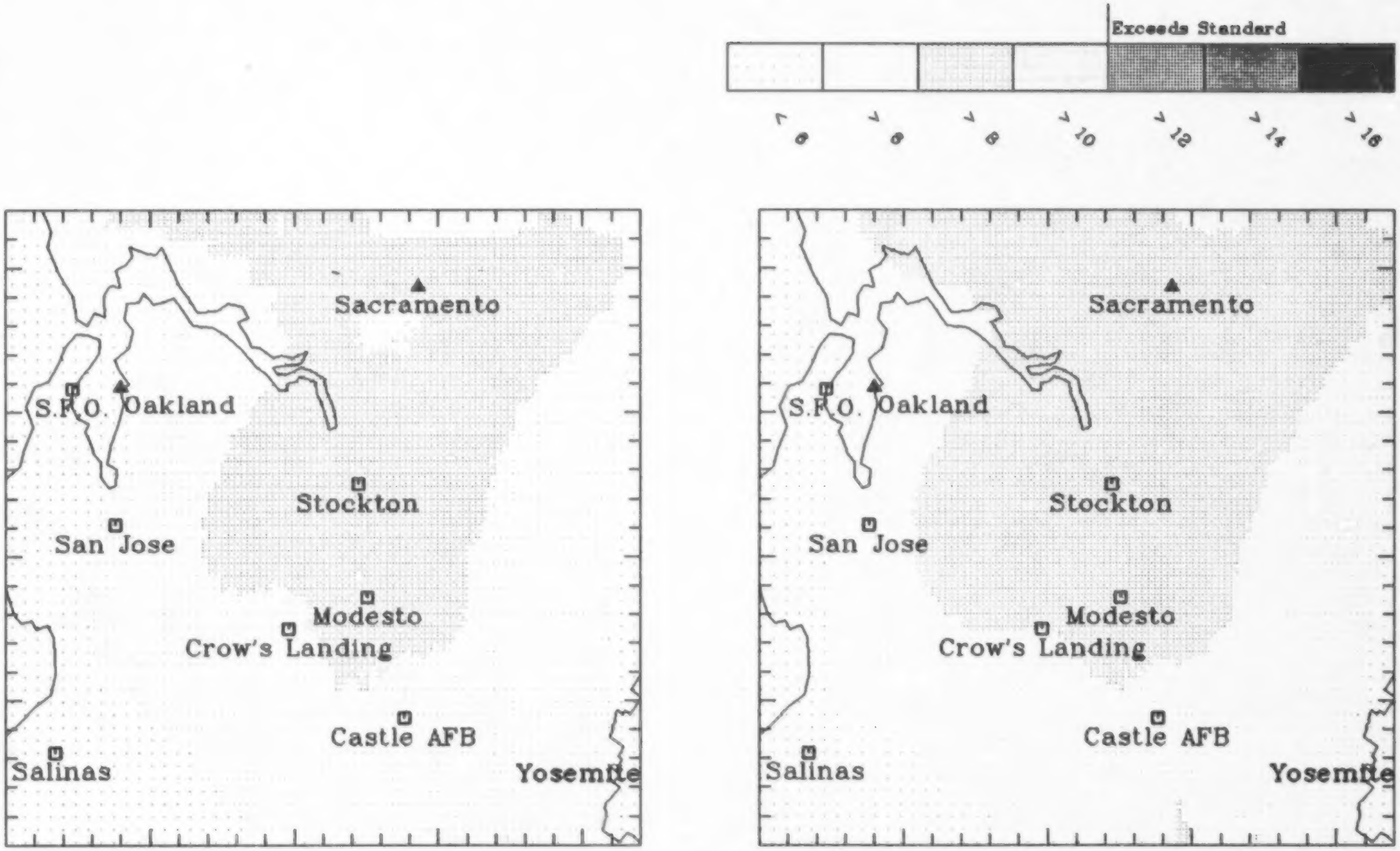
Exceeds Standard
< 6
> 6
> 8
> 10
> 12
> 14
> 16
S.F.O.
Oakland
Sacramento
Stockton
San Jose
Modesto
Crow's Landing
Castle AFB
Salinas
Yosemite

Base Case

Climate Sensitivity Scenario #1

FIGURE 2-9f. **Comparison of predicted maximum daily ozone concentrations (pphm) for the base case and climate sensitivity scenario #1 (temperature and water increase) for August 10, 1981**

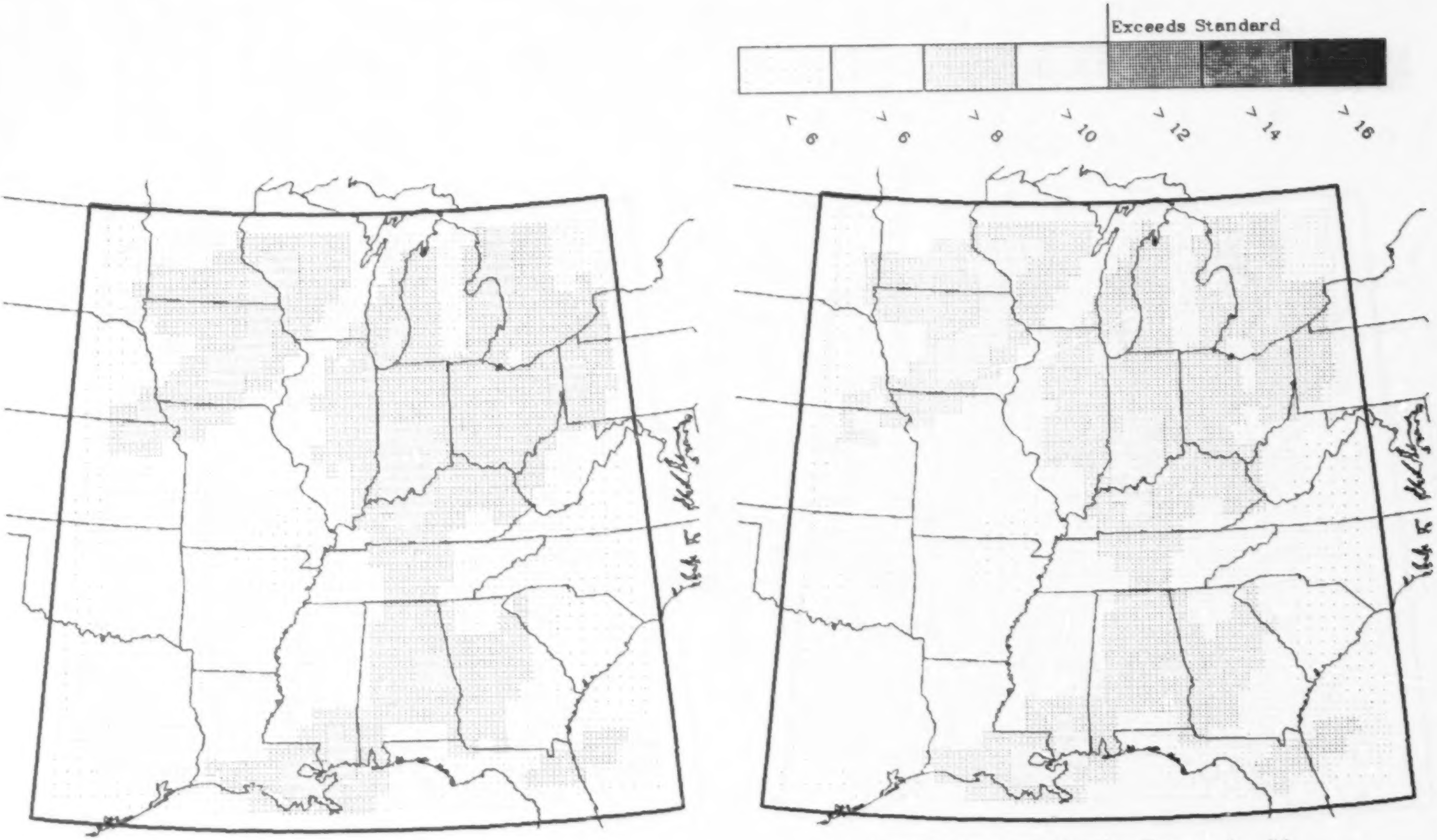
Exceeds Standard
< 6
> 6
> 8
> 10
> 12
> 14
> 16

Base Case

Climate Sensitivity Scenario #1

FIGURE 2-10a, **Comparison of predicted maximum daily ozone concentrations (pphm) for the base case and climate sensitivity scenario #1 (temperature and water increase) for July 14, 1980**

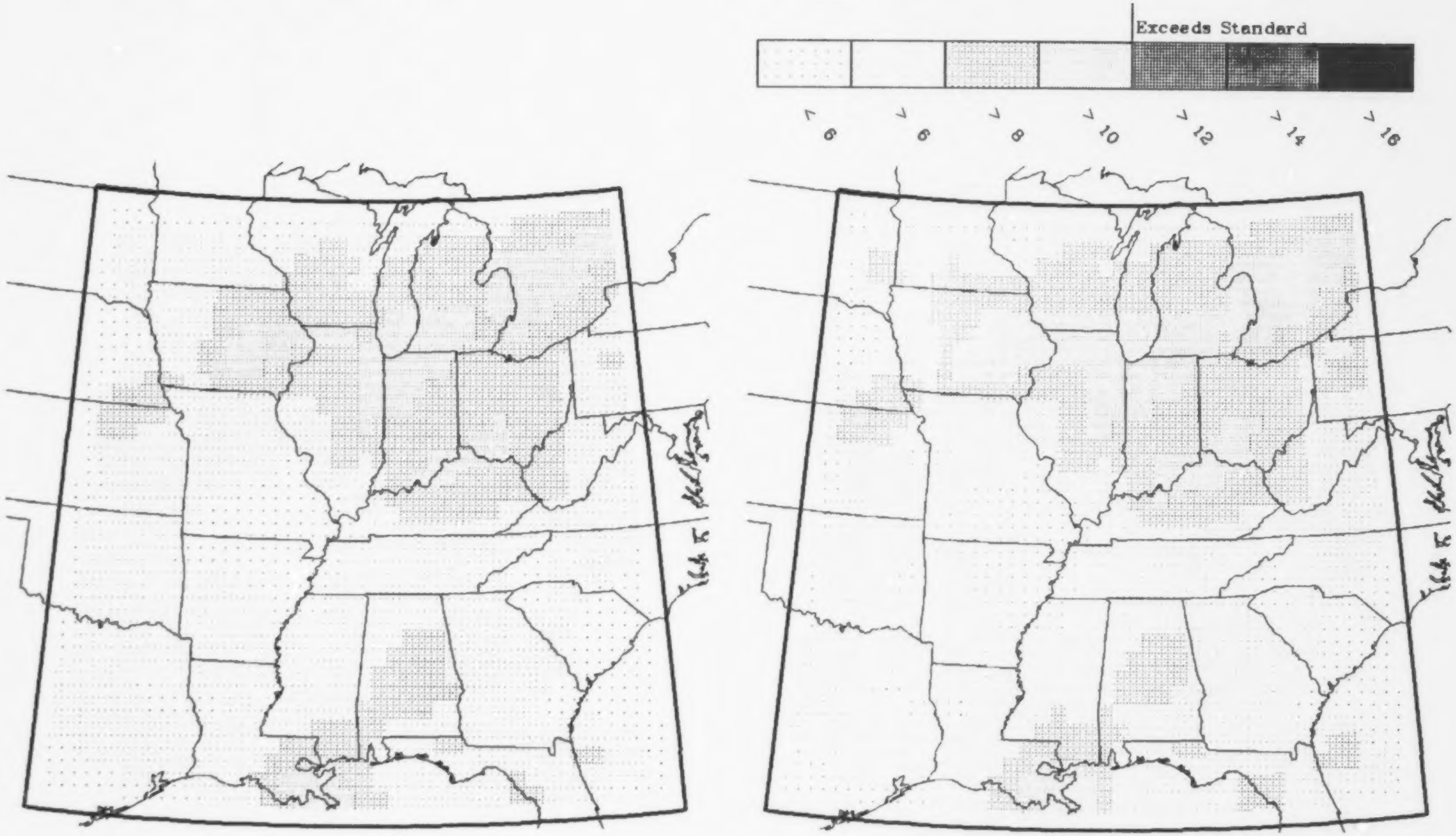
Exceeds Standard
< 6
> 6
> 8
> 10
> 12
> 14
> 16

Base Case

Climate Sensitivity Scenario #1

FIGURE 2-10b. **Comparison of predicted maximum daily ozone concentrations (pphm) for the base case and climate sensitivity scenario #1 (temperature and water increase) for July 15, 1980**

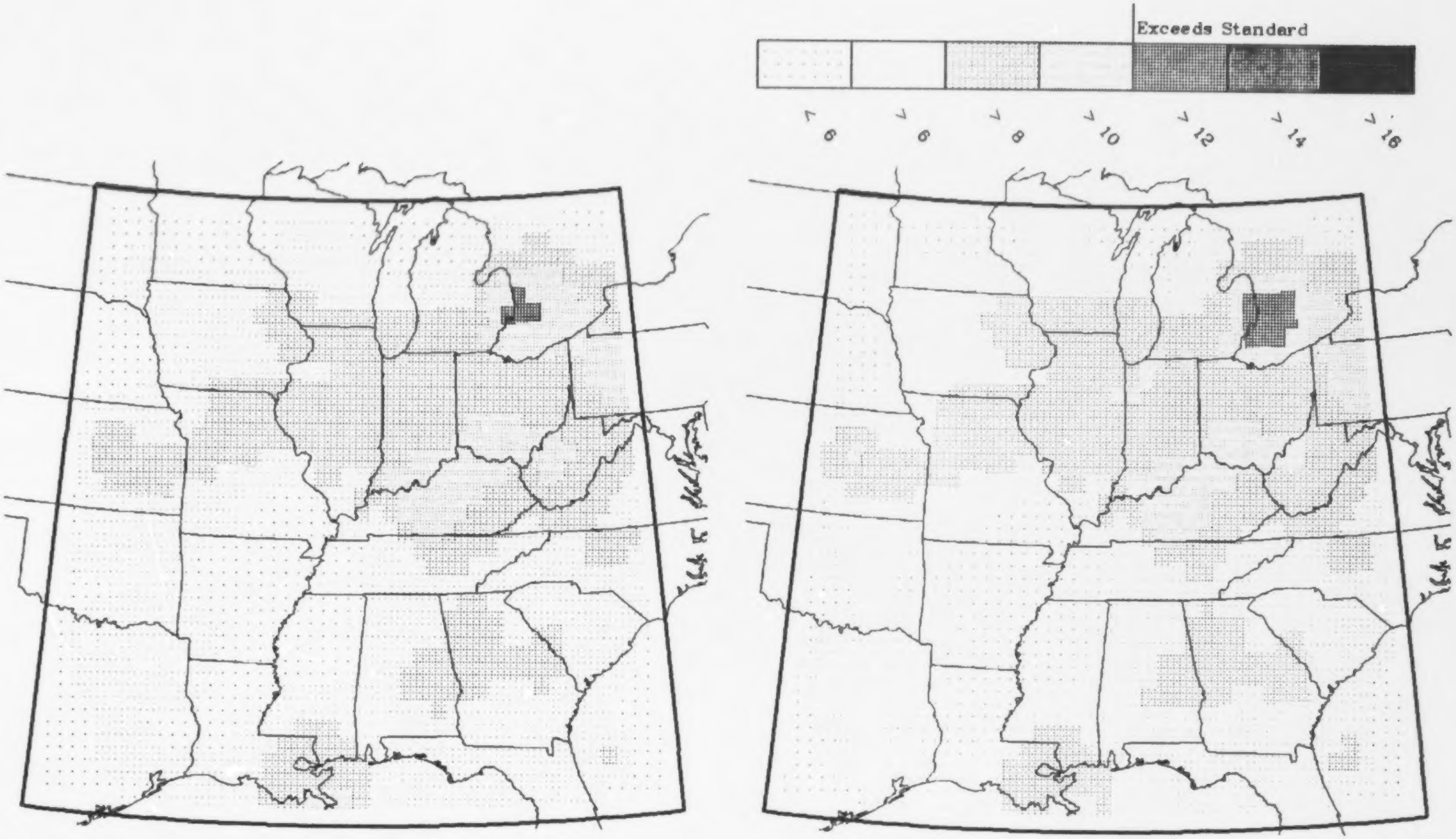
Exceeds Standard
< 6
> 6
> 8
> 10
> 12
> 14
> 16

Base Case

Climate Sensitivity Scenario #1

FIGURE 2-10c. **Comparison of predicted maximum daily ozone concentrations (pphm) for the base case and climate sensitivity scenario #1 (temperature and water increase) for July 16, 1980**

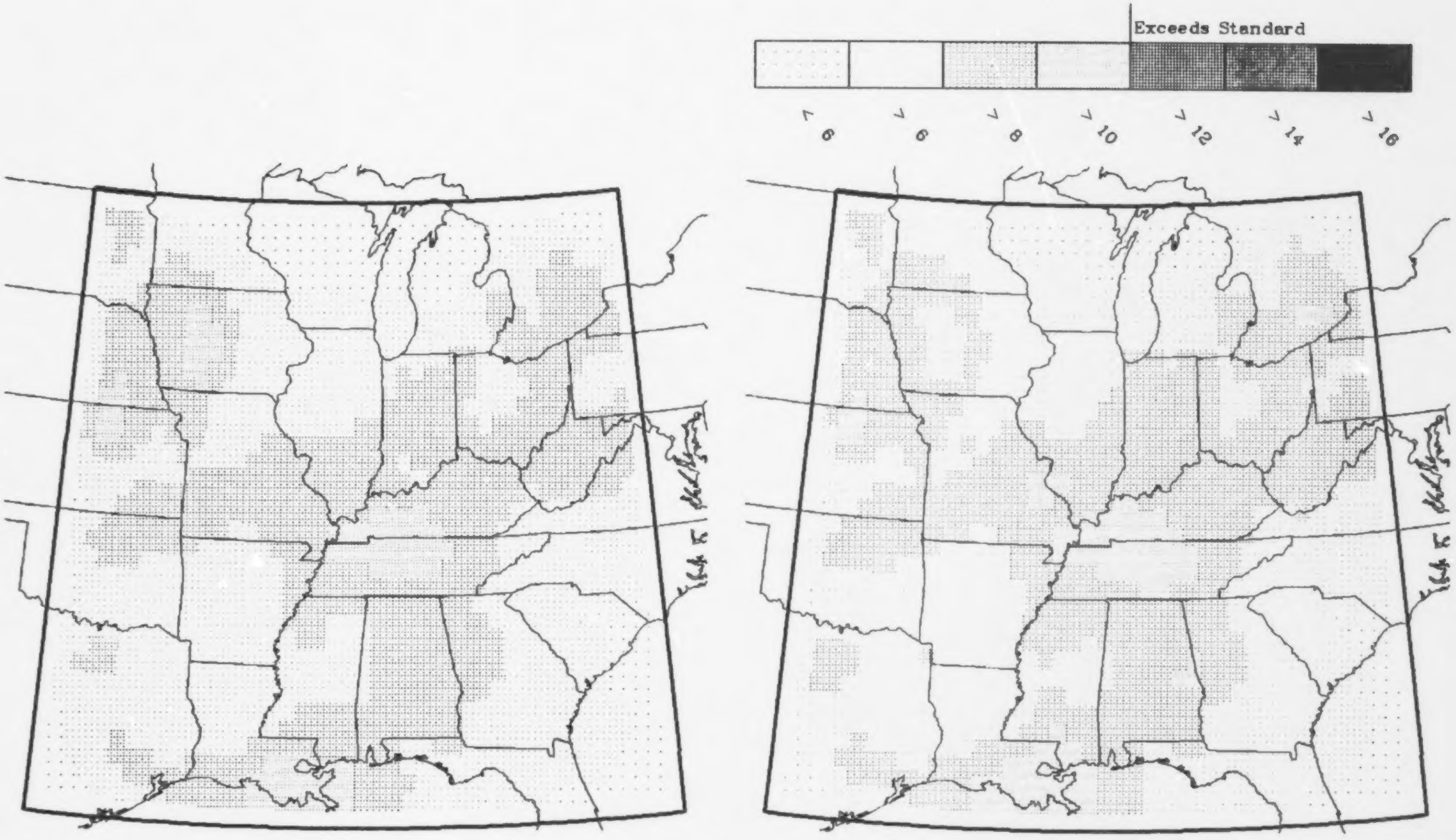
Exceeds Standard
< 6
> 6
> 8
> 10
> 12
> 14
> 16

Base Case

Climate Sensitivity Scenario #1

FIGURE 2-10d. **Comparison of predicted maximum daily ozone concentrations (pphm) for the base case and climate sensitivity scenario #1 (temperature and water increase) for July 17, 1980**

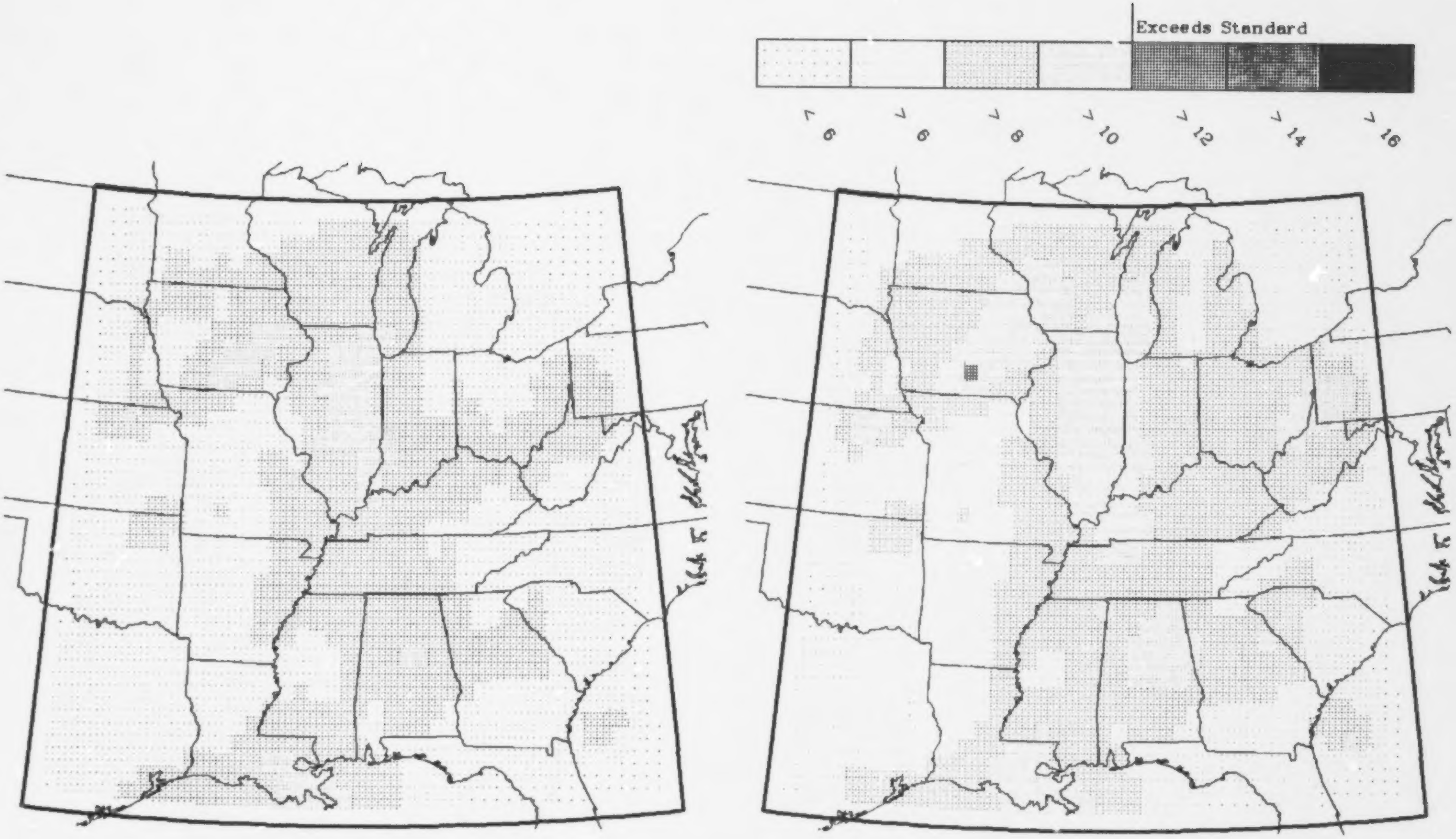
Exceeds Standard
< 6
> 6
> 8
> 10
> 12
> 14
> 16

Base Case

Climate Sensitivity Scenario #1

FIGURE 2-10e. **Comparison of predicted maximum daily ozone concentrations (pphm) for the base case and climate sensitivity scenario #1 (temperature and water increase) for July 18, 1980**

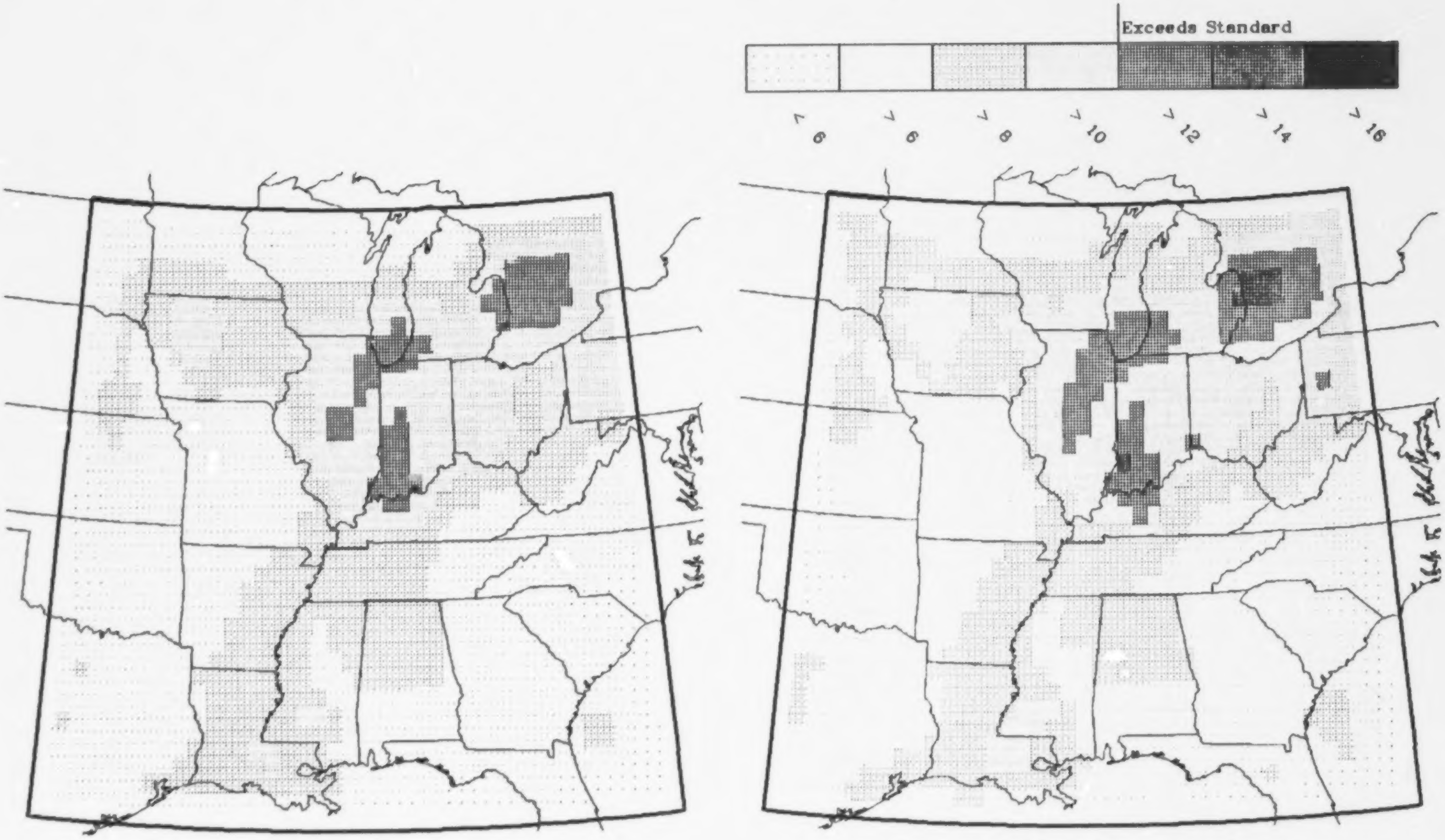
Exceeds Standard
< 6
> 6
> 8
> 10
> 12
> 14
> 16

Base Case

Climate Sensitivity Scenario #1

FIGURE 2-10f. **Comparison of predicted maximum daily ozone concentrations (pphm) for the base case and climate sensitivity scenario #1 (temperature and water increase) for July 19, 1980**

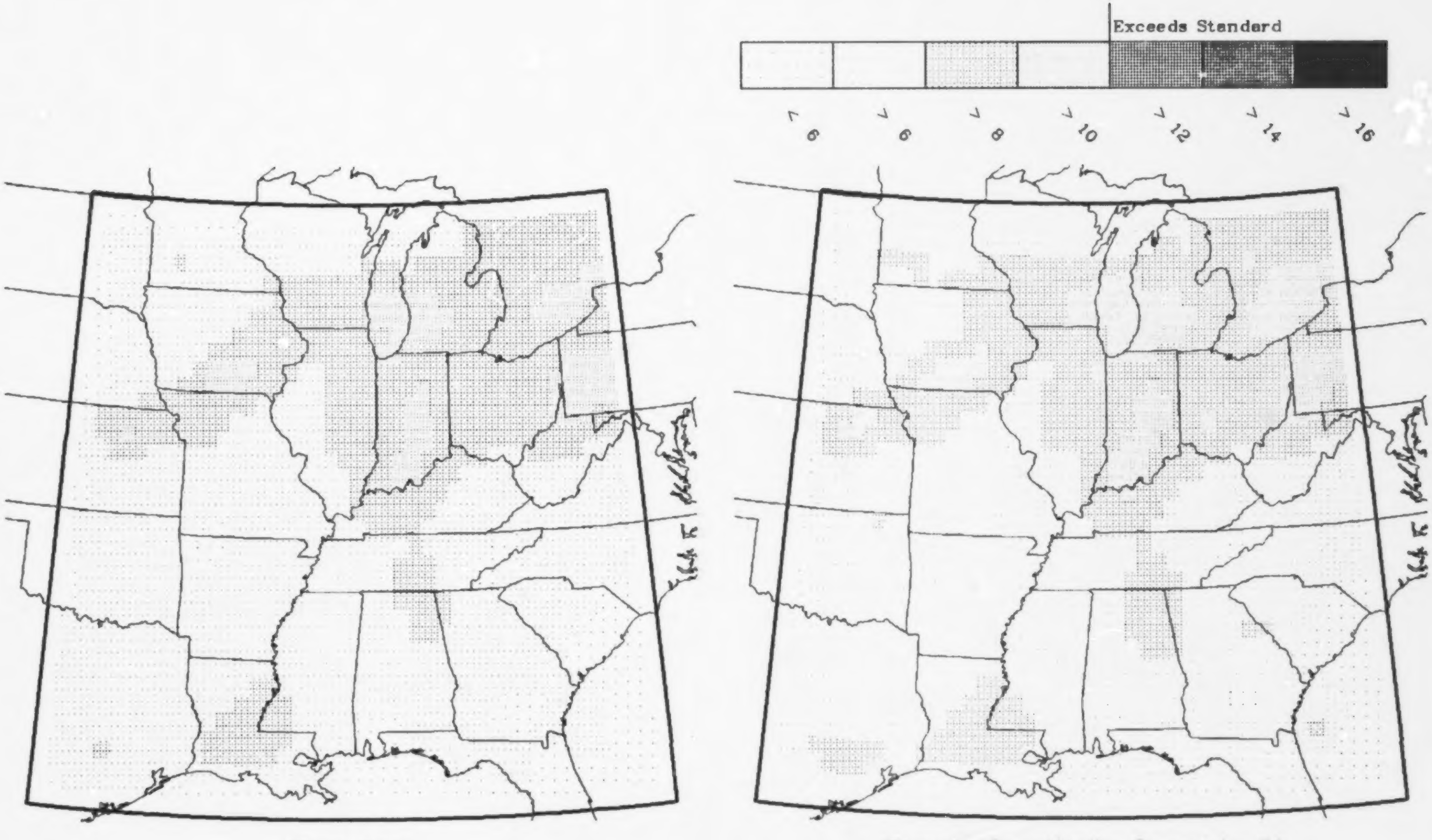
Exceeds Standard
< 6
> 6
> 8
> 10
> 12
> 14
> 16

Base Case

Climate Sensitivity Scenario #1

FIGURE 2-10g. **Comparison of predicted maximum daily ozone concentrations (pphm) for the base case and climate sensitivity scenario #1 (temperature and water increase) for July 20, 1980**

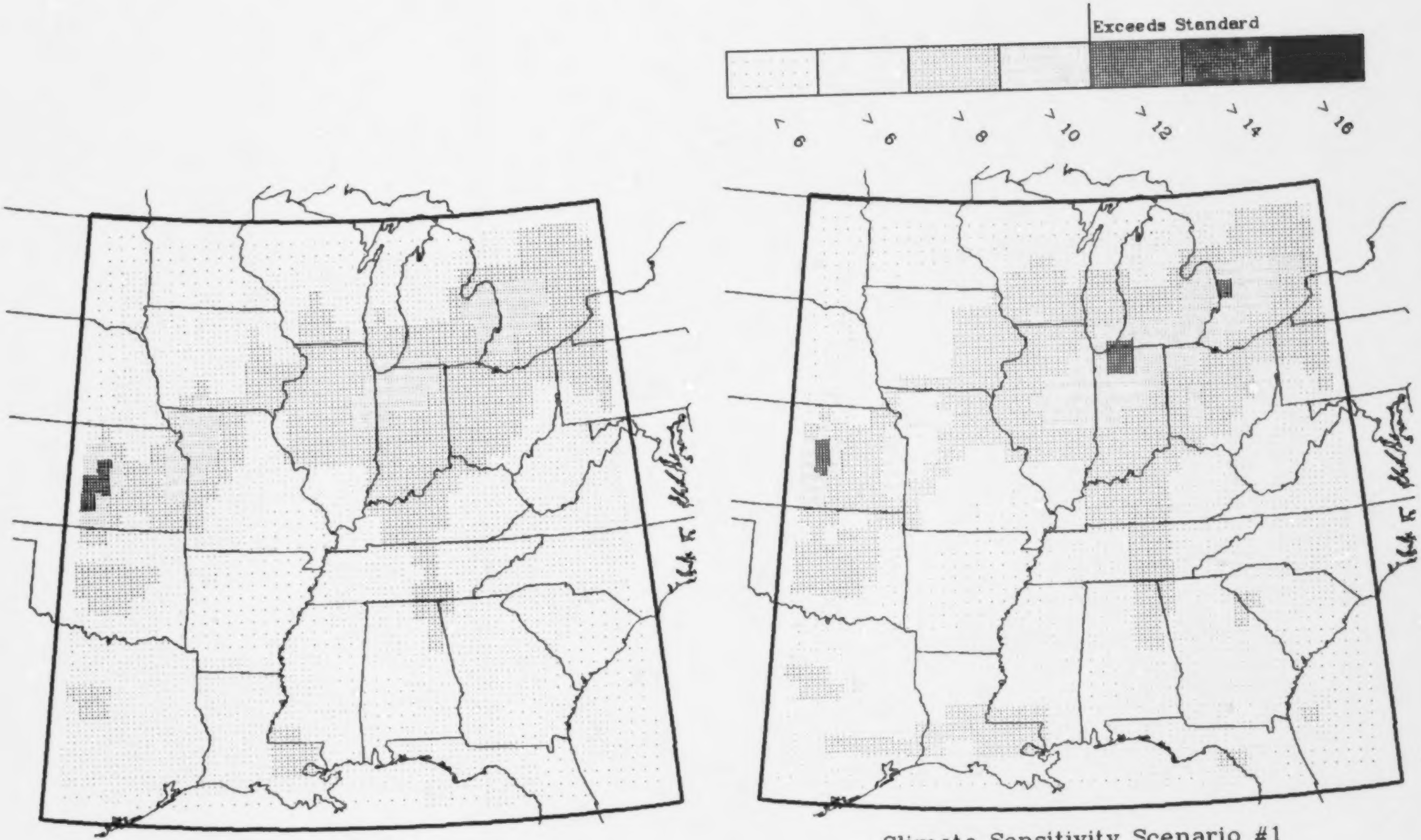
Exceeds Standard
< 6
> 6
> 8
> 10
> 12
> 14
> 16

Base Case

Climate Sensitivity Scenario #1

FIGURE 2-10h. **Comparison of predicted maximum daily ozone concentrations (pphm) for the base case and climate sensitivity scenario #1 (temperature and water increase) for July 21, 1980**

3 THE SENSITIVITY OF OZONE CONCENTRATIONS TO CLIMATE VARIABILITY

Changes in climate that are forecast to occur in the next several decades will probably manifest themselves as changes in the frequency distribution of climatic variables. For example, a global warming might (1) shift the frequency distribution of temperatures toward warmer values, decreasing the chances of cold temperatures occurring, or (2) change the shape of the distribution to include a higher frequency of high temperatures, so that the chances of cold temperatures occurring remain the same. In other words, future frequency distributions of climatic variables will largely be made up of events that have occurred historically, but their chances of occurring will change. Therefore, we are justified in using historical data to examine the impact of future meteorological conditions on ozone concentration. In so doing, we can gain insight into the sensitivity of ozone to potential changes in specific meteorological variables. We can also gain insight into which meteorological variables are associated with particular weather regimes, which is useful for introducing realistic climatic perturbations into an air quality model.

We performed an analysis to:

(1) Assess the sensitivity of ozone concentrations to meteorological variables.

(2) Evaluate methods of grouping the meteorological variables into weather types that are associated with ozone concentrations.

If such groups prove to be useful in characterizing various levels of ozone, additional analyses can be performed in the future to (1) produce realistic estimates of the type and degree of climatic perturbation that might occur according to predictions of global climate models, and (2) determine the sensitivities of ozone concentrations to climatic perturbations.

Because data inputs to air quality models are a convenient source of relatively complete information on meteorological variables that influence ozone concentrations, we examined the data inputs and ozone predictions for three applications of the PHOXA version of the RTM-III. The main difference between this version and the RTM-III used in the study discussed in Section 2 is that the PHOXA version includes an early version of the CBM-IV chemical mechanism (Whitten and Gery, 1985).

METHODOLOGY

The analysis consisted of several steps:

(1) Meterological variables that potentially influence ozone concentrations were selected.

(2) Measures of these variables were developed, through spatial and temporal averaging, that would best relate them to ozone concentrations.

(3) The measures were grouped into climatic types that are associated with ozone concentrations.

(4) The feasibility of using such grouping schemes to predict ozone concentrations was assessed.

Selection of Meteorological Variables

The RTM-III model inputs include all climatic information needed to model ozone formation and transport. These variables, which together constitute the "world" according to the RTM-III model, are the following:

(1) At each of the RTM-III layers, gridded and time-dependent arrays of:
    temperature
    wind speed and direction
    water vapor mixing ratio

(2) Gridded and time-dependent arrays of:
    - mixing height
    - emission rates of ozone precursors
    - exposure class
    - precipitation rates
    - cloud cover

(3) Time-dependent boundary conditions of chemical species at the sides and top of each model layer.

In addition, the RTM-III derives the radiative flux for photochemical reactions (based on the date and time of day, latitude, and cloud cover).

To make the selection of meteorological variables as straightforward as possible, it is necessary to develop simple techniques for reducing the thousands of data points available for each day to a dozen or so which have the greatest predictive power for maximum daily ozone concentrations. The following reduction techniques were used:

(1) Variables were combined into composite indexes based on a knowledge of chemistry, dispersion, and emissions. For example, wind speed and the mixing height can be multiplied into a product which is sometimes known as the 'ventilation'.

(2) Redundant data were eliminated by combining or removing intercorrelated variables and deemphasizing areas where there is no need for representation by a classification variable. For example, water vapor mixing ratios and temperatures are of interest only in the mixed layer, where the bulk of ozone formation takes place.

(3) Data were systematically averaged in time and space.

(4) Variables were extracted from the model. For example, the algorithm for producing estimates of radiative flux for photochemistry was taken out of RTM and used in conjunction with other input variables to make estimates of radiative flux.

One complicating factor is that the maximum daily ozone is usually affected by the meteorology of the preceding hours. In addition, there is occasionally a substantial buildup and carryover of ozone concentrations from one day to the next. Since we have classified each day separately, we have not treated multi-day serial correlation of ozone levels.

Once a dozen or so candidate variables have been selected, an objective method can be applied to simplify the selection. The creation of a correlation matrix for all of the discriminatory variables will reveal redundancy in the form of correlation between variables. Those variables can then be combined into more powerful variables, or simply eliminated if their ability to predict ozone is poor.

Classification of Meteorological Variables

The goal of the analysis is to provide a scheme for classifying each day of RTM-III input data and evaluate the ability of such a scheme to predict ozone concentrations. There are two separate ways to proceed. The first is to divide the days on the basis of ozone levels. For example, one can define three ranges of ozone concentration and then lump the days, first by ozone, and then by meteorology. This method insures a significant discrimination of ozone levels.

The second approach is to classify days only on the basis of meteorological variables, and to treat ozone as a dependent variable. While this approach results in unique meteorological classes, each class can include such a wide range of ozone concentrations that the meteorological variables would not be useful in predicting levels of ozone.

For our purposes it was more efficient to use the former method, i.e., define ranges of ozone, then classify the days falling under each ozone class by meteorology. In this way the usefulness of the meteorological variables in characterizing ozone levels (which is the information we seek) can be evaluated in a straightforward manner. For example, if one meteorological class is associated with more than one ozone class, the meteorological variables included in that class are probably not good indexes of ozone concentration.

THE DATA BASE

RTM-III Simulations

The data base for this analysis was developed from three RTM-III simulations (Table 3-1). The simulations are briefly described below and are discussed in greater detail in Appendix B.

> Eastern US Simulation: This simulation was performed over a domain that encompasses nearly all of the eastern United States and a large portion of the Midwest (Figure 3-1). The modeling period, 15 August to 15 September 1978, included several ozone episodes in various parts of the domain. The highest maximum daily ozone predictions generally occurred in areas in or downwind of major emission areas, such as the mid-Atlantic seaboard and the Ohio River valley. The cell size in this simulation, 80 x 80 km, was the largest of the three simulations.
>
> Midwestern/Southeastern US Simulation: The midwestern domain extends from the Great Plains to just west of the mid-Atlantic seaboard, and from the northern Great Lakes area to central Florida (Figure 3-2). This domain overlaps about two-thirds of the modeling domain for the eastern United States simulation. The simulation includes three separate ozone episodes. The first episode (April 1980) features elevated ozone concentrations in eastern Texas and Louisiana. The second episode (July 1980) features elevated ozone concentrations primarily in the Ohio-Indiana region. In the third episode (August 1980), both of the aforementioned regions experience high ozone concentrations.
>
> Central California Simulation: The central California domain is the smallest of the three, covering an area roughly bounded by the Pacific coast and Sierra Nevada, and the San Francisco Bay Area and Tehachapi Mountains (Figure 3-3). The episode is brief and features elevated ozone concentrations throughout the San Joaquin Valley and San Francisco Bay Area. Features unique to

TABLE 3-1. RTM-III simulations used in the historical data analysis.

Region	Domain	Cell Size	Number of Subregions	Subregion Days	Episode
Northeastern USA	2080 x 1840 km	80 x 80 km	3	93	15 August - 15 September 1978
Midwestern USA	1855 x 1942 km	45 x 55 km	4	32 15 12	17-25 April 1980 7-21 July 1980 18-29 August 1980
Central California	320 x 520 km	10 x 10 km	2	12	5-10 August 1981
				164	

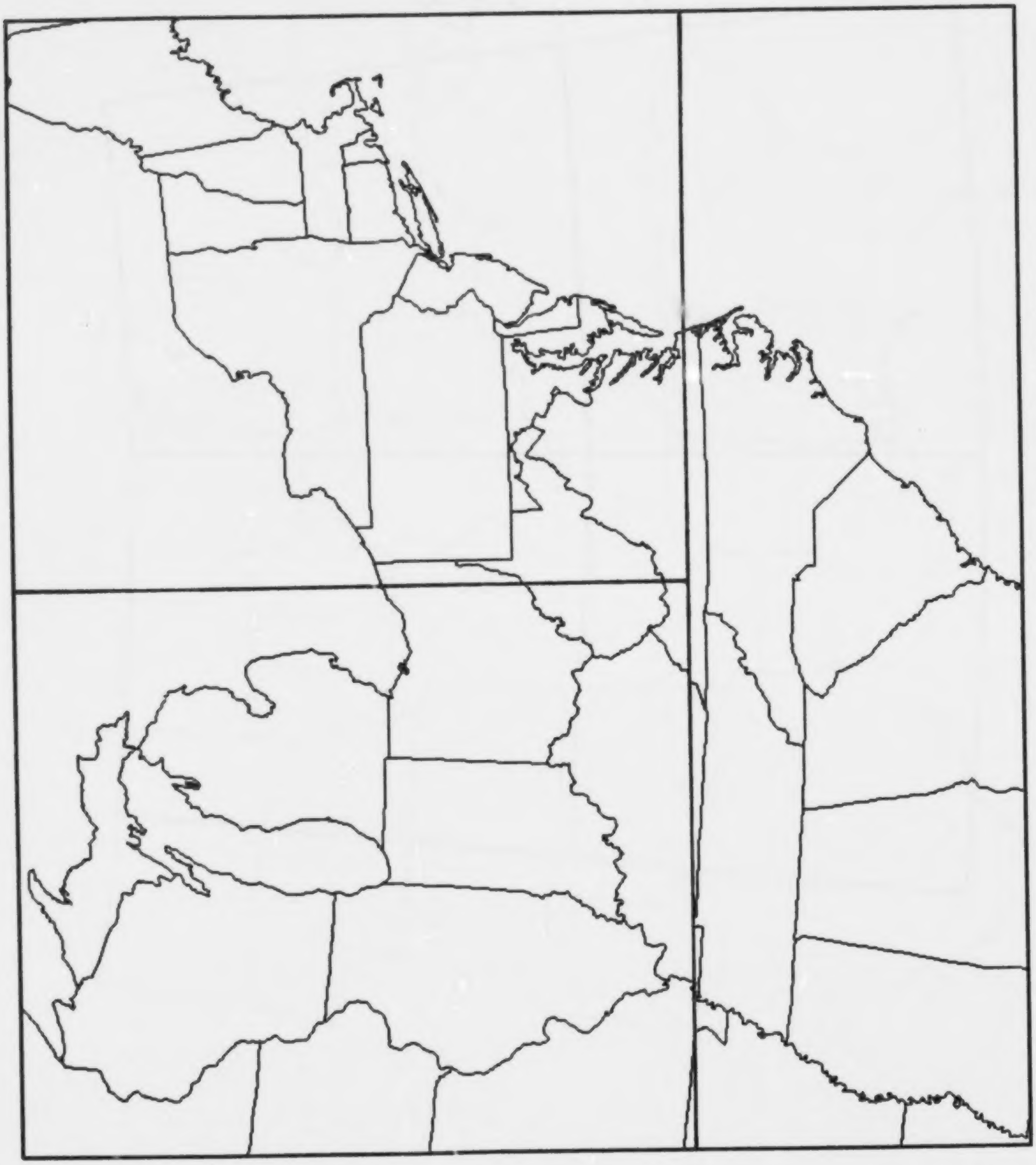

FIGURE 3-1. Northeastern United States modeling region with subregions.

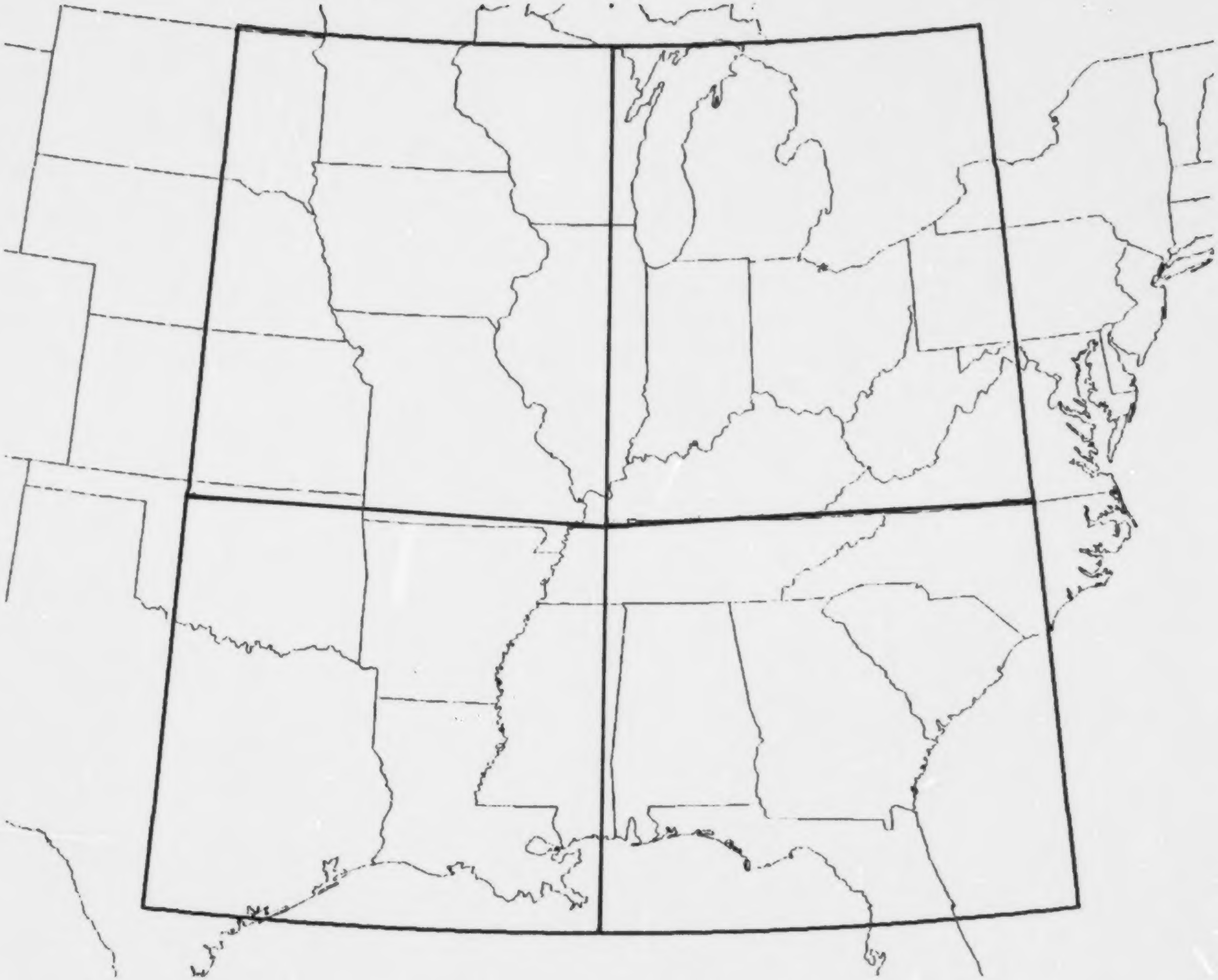

FIGURE 3-2. The midwestern United States modeling region, with subregions.

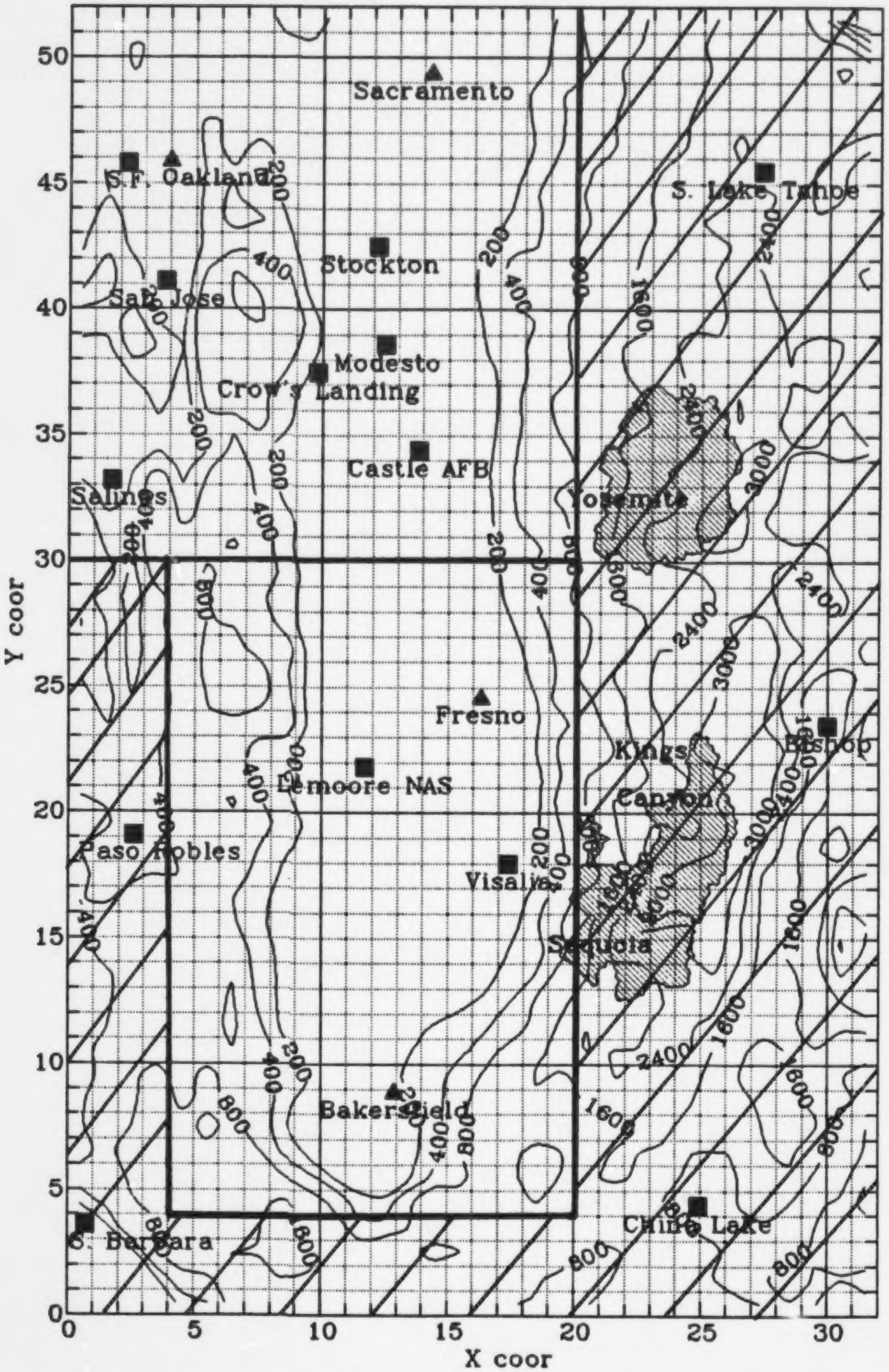
Sacramento
S.F.
Oakland
S. Lake Tahoe
Stockton
San Jose
Modesto
Crow's Landing
Castle AFB
Salinas
Yosemite
Fresno
Kings
Canyon
Bishop
Lemoore NAS
Paso Robles
Visalia
Sequoia
Bakersfield
China Lake
S. Barbara
200
400
800
1600
2400
3000
Y coor
X coor
0
5
10
15
20
25
30
35
40
45
50

FIGURE 3-3. The central California modeling region, with subregions. Hatched portions of the domain were not included in the analysis.

this simulation are the small grid cell size (10 x 10 km), an air flow regime dominated by thermodynamic processes acting on complex terrain, and a lack of cloud cover during the episode. Unlike the other, lengthier simulations, this brief episode does not include periods of relatively low ozone concentrations.

RTM-III Input Variables

Meteorological variables influencing the formation and dispersion of ozone are contained in RTM-III gridded input fields. Of these, five are thought to have a significant influence on ozone concentrations and are relevant to climate change studies. They are: wind speed, mixing height, temperature, water vapor mixing ratio, and solar radiation. Wind speed and mixing height might also be effectively combined into one variable, termed ventilation (wind speed x mixing height), that is a measure of the general capability of the atmosphere to transport and disperse pollutants. Solar radiation is calculated by RTM-III from cloud cover, latitude, time of year and time of day.

A model is, by definition, reality simplified. The way in which the input variables influence the calculations of ozone will not be the exact way in which they influence ozone in reality. For our purposes, it is important to understand the basic differences between the "RTM-III world" and reality, as they apply to our analysis. These differences deal primarily with approximations of vertical structure and processes:

> Vertical Stratification: RTM-III employs a four-layer vertical structure: three prognostic layers (mixed, inversion, and above inversion) and one diagnostic surface layer within the mixed layer. Because the mixed layer is not stratified into more finely divided layers, phenomena that vary with height in the mixed layer in reality are represented by a layer average in RTM-III. Such phenomena include temperature lapse rate, wind speed increase with height, and directional wind shears. When RTM-III is used to study the effects of climatic change, the earth's skin temperature is approximated by the mixed-layer temperature.

Vertical Motion: RTM-III does not address the concept of inversion strength. Gases do not diffuse through the inversion base (defined by the mixing height), but material may pass through this barrier by horizontal transport from areas of higher mixing height to areas of lower mixing height, or through positive vertical velocities produced by convergence in the wind field.

In reality, the inversion strength varies as a function of the amount of subsidence and the temperature lapse rate. Material may pass through the inversion base if it possesses sufficient energy to do so. For example, plumes of warm air or vertical flow produced by cloud pumping can produce updraft venting of material through the inversion base. As previously mentioned, RTM-III has no provision for inhomogeneities in the temperature/energy structure of the mixed layer that might lead to such events. For our purposes, this means that the RTM-III formulation tends to isolate the surface layer from other vertical layers, minimizing the influence of meteorological variables above the mixing height and maximizing the influence of those in the mixed layer. This property of RTM led us to concentrate only on the mixed-layer values of the meteorological variables in this analysis.

SELECTION OF VARIABLES FOR THE ANALYSIS

In an RTM-III simulation meteorological variables are defined at each grid point every hour or three hours; ozone concentrations are predicted each hour at each grid point. To develop indexes that relate the meteorological variables to ozone concentrations, spatial and temporal averaging scales must be determined.

Spatial Grouping of Variables

Since the goal of this study is to investigate relationships between meteorological variables and regional ozone concentrations, the obvious choice is to average variables over each modeling domain. In practice, however, averaging over such large areas smooths over much of the interesting ozone events occurring within the domain; that is, variability in ozone concentrations and the meterological variables, which is necessary for the development of robust statistical relationships, is reduced.

The reason for this problem is that large regional modeling domains encompass several major emission source areas and are often larger than the typical synoptic scale of a particular weather regime (e.g., storm, high-pressure ridge). For example, in the northeastern US simulation, southern New England experienced an ozone episode on 16 August in which predicted ozone concentrations exceeded 10 pphm; meanwhile, the Chicago area experienced much different conditions, with predicted ozone concentrations near background levels (<6 pphm).

To avoid averaging over highly variable ozone patterns and to maximize the strength and coherence in the relationships among variables, each modeling domain was divided into subregions. Each subregion encompasses an area in which the patterns of ozone concentrations vary in a coherent fashion. The divided modeling domains are shown in Figures 3-1 to 3-3. The northeastern US was divided into three subregions: northwestern, covering the Ohio Valley and much of the Great Lakes; northeastern, covering the northeast corridor; and southern, covering the southern one-third of the domain.

The domain for the midwestern US was divided into four equal subregions: northwestern, which includes the Chicago, St. Louis, and Kansas City urban areas; northeastern, which includes the Ohio River valley and Great Lakes region; southeastern, covering the southeastern states; and southwestern, which includes the Dallas, Houston, and New Orleans urban areas.

The central California domain, although relatively small, contains large gradients in many of the meteorological variables because of the presence of large elevational gradients. We found that those areas of large gradients (i.e., the western slope of the Sierra Nevada and the coastal mountains) would have required excessive subdividing to produce subregions that exhibited an appreciable amount of homogeneity. Therefore, the Sierra Nevada and part of the Coast Range were omitted from the analysis. That part of the domain showing relatively little elevational gradient was divided into two subregions, northern and southern. The northern subregion includes the San Francisco Bay Area, Stockton, and Sacramento; the southern subregion covers the southern San Joaquin Valley, including Fresno and Bakersfield.

Temporal Grouping of Variables

The effects of climate change on exceedances of the primary 1-hour ozone standard is the chief interest in this study; therefore, we have chosen the maximum daily one-hour average concentration as the measure of ozone. The maximum daily ozone concentration is influenced by meteorological processes occurring throughout the day, so it is necessary to choose one or more measurement periods for each variable that potentially best relate it to the maximum hourly ozone concentration. The meteorological variables of concern are wind speed, mixing height, temperature, water vapor mixing ratio, solar radiation, and rainfall (Table 3-2).

Wind speed is a measure of the rate of advection and transport, and is often a good indicator of the weather regime affecting an area. Low wind speeds are typically associated with slow-moving high-pressure systems and stagnant air masses, which are often characterized by above average ozone concentrations. High wind speeds are often associated with weather disturbances or the advection of new air masses into an area; both are characterized by relatively low ozone concentrations. Wind speed may affect both the nocturnal buildup and afternoon dispersion of ozone. Therefore, the selected data periods for wind speed are (1) average wind speed over all hours of the day preceding the ozone maximum, and (2) average wind speed during the afternoon, before the ozone peak occurs. The timing of the maximum daily ozone varies depending on location, weather regime, and time of year; however, for the sake of consistency, 1800 hours was chosen as the time of ozone maximum. Maximum ozone values typically occur before this time, so the selected data periods for wind speed will typically include more hours than actually occur before the ozone maximum.

Mixing height is a measure of the depth of the atmosphere over which most emission, transport, transformation, and dispersion processes occur. Generally, small mixing

TABLE 3-2. RTM-III input variables expected to be important in the formation and buildup of ozone concentrations.

Variable	Temporal Resolution	Vertical Specification	Data Selected for Analysis
Wind speed	3 hours*	Mixed layer	0-1800 average; afternoon (1200-1800) average
Mixing height	3 hours*	Mixed layer	0-1800 average; afternoon (1200-1800) average
Temperature	3 hours*	Mixed layer	Daylight (0700-1800) average; maximum 3-hour value
Humidity	3 hours*	Mixed layer	Daylight (0700-1800) average; maximum 3-hour value
Solar radiation	3 hours**	Surface	Daily (0-2400) total; morning (0-1200) total
Ventilation	3 hours*	Mixed layer	0-1800 average; afternoon (1200-1800) average
Rainfall	1 hour**	Surface	Daily total (0-2400)

* One hour in the central California simulation.

** Not available in the central California simulation.

depths are conducive to the buildup of pollutants, resulting in higher ozone concentrations. Elevated mixing heights allow a relatively large amount of vertical dispersion, resulting in lower ozone concentrations. As in the case of wind speed, the mixing height may affect both the nocturnal buildup and afternoon dispersion of ozone. Therefore, the selected data periods for mixing height are the same as for wind speed.

Temperature influences photolysis reaction rates, and so is of greatest importance during daylight hours. Maximum temperatures and peak ozone concentrations often occur at the same time, and temperature can directly influence ozone production and destruction during the buildup of ozone. Therefore, the selected data periods for temperature are (1) average mixed-layer temperature over all daylight hours up to the ozone maximum (1800 hours), and (2) the maximum daily mixed-layer temperature.

Humidity influences the rates and dispositions of many chemical reactions in the atmosphere. It can affect the rate of ozone destruction during the night, but its primary effect is on ozone production during the day. Maximum water vapor mixing ratios often occur near the time of the peak daily ozone concentration, and can affect the rates of ozone formation and destruction at this time. Therefore, the selected data periods for humidity are (1) the average water vapor mixing ratio in the mixed layer during the daylight hours leading up to the ozone maximum (1800 hours), and (2) the daily maximum mixed layer water vapor mixing ratio.

Solar radiation directly dictates photolysis rates and thus is important during all daylight hours, especially the morning hours. A value for solar radiation is calculated by RTM-III by considering cloud cover and sun angle. The selected data periods are: (1) total solar radiation received at the surface during the day, and (2) total solar radiation received at the surface during the morning hours.

Rainfall scavenges ozone and its pecursors from the atmosphere and therefore has a negative relationship with maximum daily ozone concentration. Also, rainfall is usually accompanied by increased wind speeds, mixing heights, and cloudy skies, which also tend to depress ozone concentrations. The accumulated rainfall in an area serves as a measure of the ozone-producing potential of the atmosphere, so the selected data period is total daily rainfall.

Ventilation, defined as the product of the mixed layer wind speed and depth of the mixed layer, is a measure of the overall ability of the atmosphere to transport and disperse pollutants, both vertically and horizontally. It is not a primary meteorological variable, but has a strong influence on the buildup of pollutants during the night; during the day, atmospheric ventilation directly influences the maximum concentrations of ozone in the mixed layer. The selected data periods for ventilation are the same as for wind speed and mixing height.

Ranges of the Meteorological Variables within Episodes

If robust relationships are to be developed between the meteorological variables and ozone concentrations, there must be sufficient variability in both the independent and dependent variables. Table 3-3 shows the mean and range of values for predicted ozone and the meteorological variables for each modeling domain and episode. In the northeastern simulation (Table 3-3a) all meteorological variables exhibit a relatively large range of values. Average rainfall is very low, primarily due to the averaging of spotty rainfall events over relatively large subregions. The temperature range is substantial (about 12 K) and the water vapor mixing ratio varies over a factor of two. Maximum ventilation is over 10 times the minimum, and maximum solar radiation is about three times the minimum. Ranges of mixing height and wind speed reveal that most of the range in ventilation (mixing height x wind speed) is accounted for by variation in the wind speed, which ranges over a factor of 10; mixing height ranges over a factor of two to three. Maximum ozone varies least, ranging over a factor of less than two. However, the minimum of 0.047 ppm is essentially a background ozone concentration, while the maximum of 0.082 ppm indicates that high values are widespread over a subregion. (Predicted maximum ozone concentrations rarely exceed 0.12 ppm for any grid cell in any simulation analyzed.)

Episode 1 in the midwestern region, in April, is characterized by relatively low temperatures and water vapor mixing ratios; both have somewhat larger ranges than in the northeastern episode (Table 3-3b). Temperature ranges over about 15 K, and water vapor mixing ratios vary over a factor of three. Mixing heights are relatively

TABLE 3-3a. Ranges of calculated measures and daily ozone concentrations for the northeastern United States modeling region (all subregions included), 15 August-14 September 1978.

Variable	N	Minimum	Maximum	Mean
Rainfall (inches)	93	0.00002	0.183	0.033
Daylight temperature (°K)	93	285.6	297.4	293.0
Maximum temperature (°K)	93	286.5	298.1	294.0
Average water vapor (ppm)	93	9108	21,826	15,588
Maximum water vapor (ppm)	93	9652	22,690	16,156
Average ventilation (km^2/m)	93	2.65	36.00	13.37
Afternoon ventilation (km^2/m)	93	4.90	57.80	21.33
Daily radiation (w/m^2)	93	858	2548	1928
Morning radiation (w/m^2)	93	337	1079	803
Average mixing height (m)	93	439	924	659
Afternoon mixing height (m)	93	779	1904	1125
Average wind speed (m/s)	93	1.67	11.67	5.27
Afternoon wind speed (m/s)	93	1.67	10.83	5.17
Maximum ozone (ppm)	93	0.047	0.082	0.065

TABLE 3-3b. Ranges of the calculated measures and daily ozone concentrations for the midwestern United States modeling region, episode 1 (all subregions included), 17-25 April 1980.

Variable	N	Minimum	Maximum	Mean
Rainfall (inches)	36	0.00008	0.07677	0.00900
Daylight temperature (°K)	36	276.5	293.4	286.6
Maximum temperature (°K)	36	279.6	295.6	288.0
Average water vapor (ppm)	36	5406	15,207	9036
Maximum water vapor (ppm)	36	5689	15,877	9818
Average ventilation (km^2/m)	36	7.13	29.03	15.02
Afternoon ventilation (km^2/m)	36	9.30	54.28	25.51
Daily radiation (w/m^2)	36	1388	2467	1962
Morning radiation (w/m^2)	36	361	942	654
Average mixing height (m)	36	669	1187	881
Afternoon mixing height (m)	36	1088	2594	1625
Average wind speed (m/s)	36	2.67	8.33	4.86
Afternoon wind speed (m/s)	36	2.33	7.83	4.39
Maximum ozone (ppm)	36	0.053	0.086	0.070

TABLE 3-3c. Ranges of the calculated measures and daily ozone concentrations for the midwestern United States modeling region, episode 2 (all subregions included), 7-21 July 1980.

Variable	N	Minimum	Maximum	Mean
Rainfall (inches)	56	0.00097	0.08065	0.02081
Daylight temperature (°K)	60	292.6	302.20	298.7
Maximum temperature (°K)	60	294.8	305.0	300.7
Average water vapor (ppm)	60	16,522	27,461	22,249
Maximum water vapor (ppm)	60	17,467	28,674	23,284
Average ventilation (km^2/m)	60	5.45	25.49	12.14
Afternoon ventilation (km^2/m)	60	8.50	36.89	17.84
Daily radiation (w/m^2)	60	1630	2688	2255
Morning radiation (w/m^2)	60	468	913	740
Average mixing height (m)	60	505	963	709
Afternoon mixing height (m)	60	761	1727	1117
Average wind speed (m/s)	60	2.17	8.33	4.74
Afternoon wind speed (m/s)	60	2.17	7.67	4.36
Maximum ozone (ppm)	60	0.057	0.091	0.072

TABLE 3-3d. Ranges of the calculated measures and daily ozone concentrations for the midwestern United States modeling region, episode 3 (all subregions included), 18-29 August 1980.

Variable	N	Minimum	Maximum	Mean
Rainfall (inches)	48	0.00174	0.10169	0.02507
Daylight temperature (°K)	44	291.6	301.1	296.2
Maximum temperature (°K)	44	292.2	304.0	297.2
Average water vapor (ppm)	44	16,283	26,964	21,102
Maximum water vapor (ppm)	44	16,485	28,365	22,166
Average ventilation (km^2/m)	48	3.09	21.09	8.54
Afternoon ventilation (km^2/m)	48	6.27	30.91	14.55
Daily radiation (w/m^2)	48	1361	2283	1846
Morning radiation (w/m^2)	48	358	812	599
Average mixing height (m)	48	377	777	543
Afternoon mixing height (m)	48	747	1436	1015
Average wind speed (m/s)	48	2.17	8.33	4.41
Afternoon wind speed (m/s)	48	2.17	8.00	4.05
Maximum ozone (ppm)	48	0.056	0.089	0.073

TABLE 3-3e. Ranges of the calculated measures and daily ozone concentrations for the central California modeling region, 5-10 August 1981.

Variable	N	Minimum	Maximum	Mean
Rainfall[a] (inches)	--	--	--	--
Daylight temperature (°K)	12	298.6	303.5	301.3
Maximum temperature (°K)	12	300.9	307.3	304.5
Average water vapor (ppm)	12	4814	8350	6433
Maximum water vapor (ppm)	12	6887	8959	7690
Average ventilation (km^2/m)	12	1.68	5.24	3.25
Afternoon ventilation (km^2/m)	12	3.51	13.64	7.59
Daily radiation (w/m^2)[b]	--	--	--	--
Morning radiation (w/m^2)[b]	--	--	--	--
Average mixing height (m)[c]	--	--	--	--
Afternoon mixing height (m)[c]	--	--	--	--
Average wind speed (m/s)[c]	--	--	--	--
Afternoon wind speed (m/s)[c]	--	--	--	--
Maximum ozone (ppm)	12	0.074	0.091	0.081

[a] No rainfall in region during episode.
[b] Skies were cloud-free during episode.
[c] Not used in analysis; see text.

high, averaging 30-40 percent higher than in the northeastern episode; in contrast, rainfall is low. The ranges and values of the other variables are roughly similar.

Episode 2 in the midwestern region occurred in July; this is reflected in the highest temperatures and water vapor mixing ratios of any of the simulations (Table 3-3c). In general, the ranges of the descriptive measures are somewhat less than those in the northeastern episode; the range of ozone concentrations is almost identical to the two previously discussed episodes; but the average is higher.

Episode 3 in the midwestern region, in August, exhibits means, maxima, and minima similar to episode 2, except that solar radiation and mixing heights (and hence, ventilation) are slightly lower (Table 3-3d).

The central California episode has fewer meteorological variables (Table 3-3e). There was no rainfall or cloudiness during the episode, which is typical for this region. Mixing height and wind speed are not broken out into separate variables (they are shown combined in the ventilation variable). A visual examination of the variable fields revealed that the mixing height was relatively constant during the episode; therefore, ventilation was a good proxy for wind speed. The ranges of the variables are much smaller than in the other episodes. Temperature ranges over less than 7 K, and water vapor mixing ratios vary over a factor of less than 1.5. Ventilation is generally lower than in the other simulations, and the range of ozone concentrations is much more restricted. The minimum ozone concentration of 0.074 ppm is by far the highest of any simulation.

THE SENSITIVITY OF MAXIMUM DAILY OZONE CONCENTRATION TO THE METEOROLOGICAL VARIABLES

A General Conceptual Model

Based on experience and theory, we developed a conceptual model of the expected relationships between maximum ozone concentration and the relevant meteorological variables. This model, illustrated in Figure 3-4, is used as a reference point in comparing the results of the analyses. The model states that maximum daily ozone concentration is positively correlated with temperature, humidity (though only weakly so), and solar radiation, and negatively correlated with mixing height, wind speed, ventilation (by definition), and rainfall. Temperature, water vapor mixing ratios, and solar radiation all affect the rates of chemical reactions that produce ozone--increases in the values of these variables increase the rates of these reactions. Mixing height, a measure of volume of the mixed layer, often increases ozone concentrations when low; low wind speeds indicate stable conditions, which are associated with high ozone concentrations; ozone and its precursers are scavenged by rainfall events, and such events are usually accompanied by cloudy skies.

Correlational Analysis

A correlational analysis was performed to investigate relationships between (1) ozone concentration and the meteorological variables and (2) the meteorological variables themselves. The strength of relationships of the former type is a measure of the ability of a variable to predict ozone concentration, while that of the latter type is a measure of the degree of redundancy within a set of variables. Relationships significant at the 95% confidence level are shown in Table 3-4.

Results

In the northeastern region the maximum daily ozone concentration is significantly correlated (95% confidence level) to rainfall, maximum temperature, morning and total daily solar radiation, daily average and afternoon ventilation, and daily average and afternoon wind speed (Table 3-4a). Most highly correlated are morning and daily total solar radiation (r = 0.56 and 0.53, respectively) and rainfall (r = -0.51). This is consistent with our conceptual model: higher radiation increases the rates of photolysis reactions that produce ozone, and rainfall scavenges ozone and its precursors from the atmosphere. The cross-correlation coefficients shows that rainfall is highly negatively correlated with radiation (rainfall is accompanied by cloudy skies), and positively correlated with wind speed (storms often produce strong winds). The

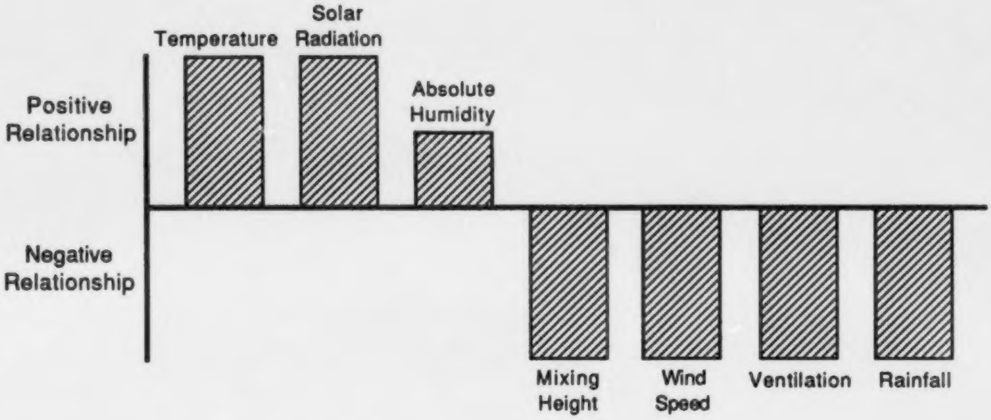

FIGURE 3-4. Conceptual model of the relationships between maximum daily ozone concentration and relevant meteorological variables.

TABLE 3-4a. Correlations (significant at the 95 percent confidence level) between maximum daily ozone concentration and the calculated measures--Northeastern U.S., all subregions (N = 93).

	Rain	Temp. (Day)	Temp. (Max.)	H_2O (Avg.)	H_2O (Max.)	Rad. (A.M.)	Rad. (Total)	Vent. (Avg.)	Vent. (Aft.)	WS (Avg.)	WS (Aft.)	MH (Avg).	MH (Aft.)
Rain	--					-0.81	-0.84	0.35	0.28	-0.38	0.38		
Temp. (Day)		--					0.31						
Temp. (Max.)			--			-0.21	0.38			-0.23	-0.23		
H_2O (Avg.)			0.74	--									
H_2O (Max.)			0.73		--								
Rad (A.M.)	-0.84		0.21			--	0.96	-0.38	-0.31	-0.43	-0.42		
Rad (Total)	-0.81		0.38			0.96	--	-0.41	-0.34	-0.47	-0.47		
Vent. (Avg.)	0.35					-0.38	-0.41	--	0.94	0.96	0.93		
Vent. (Aft.)	0.28					-0.31	-0.34	0.94	--	0.84	0.92		
WS (Avg.)	0.38		-0.23			-0.43	-0.47	0.96	0.84	--	0.94		
WS (Aft.)	0.38		-0.23			-0.42	-0.47	0.93	0.92		--		
MH (Avg.)								0.79	0.82	0.64	0.61	--	
MH (Aft.)								0.29	0.48				--
O_3 (Max.)	-0.51		0.24			0.56	0.53	-0.29	-0.22	-0.35	-0.30		

TABLE 3-4b. Correlations (significant at the 95 percent confidence level) between maximum daily ozone concentration and the calculated measures--Midwestern U.S., episode 1, all subregions (N = 36).

	Rain	Temp. (Day)	Temp. (Max.)	H_2O (Avg.)	H_2O (Max.)	Rad. (A.M.)	Rad. (Total)	Vent. (Avg.)	Vent. (Aft.)	WS (Avg.)	WS (Aft.)	MH (Avg.)	MH (Aft.)
Rain													
Temp. (Day)		--	0.98	0.68	0.70		0.55						
Temp. (Max.)		0.98	--	0.59	0.61		0.62						
H_2O (Avg.)		0.68	0.59	--	0.98								
H_2O (Max.)		0.70	0.61	0.98	--								
Rad (A.M.)						--	0.63						
Rad (Total)		0.55	0.62			0.63	--						
Vent. (Avg.)													
Vent. (Aft.)					0.34								
WS (Avg.)													
WS (Aft.)					0.35								
MH (Avg.)													
MH (Aft.)													
O_3 (Max.)		0.67	0.64	0.42	0.44	0.37	0.54						

TABLE 3-4c. Correlations (significant at the 95 percent confidence level) between maximum daily ozone concentration and the calculated measures--Midwestern U.S., episode 2, all subregions (N = 60).

	Rain	Temp. (Day)	Temp. (Max.)	H_2O (Avg.)	H_2O (Max.)	Rad. (A.M.)	Rad. (Total)	Vent. (Avg.)	Vent. (Aft.)	WS (Avg.)	WS (Aft.)	MH (Avg.)	MH (Aft.)
Rain							-0.40						
Temp. (Day)							0.64						
Temp. (Max.)							0.69						
H_2O (Avg.)									-0.43				
H_2O (Max.)									-0.36				
Rad (A.M.)							0.26						
Rad (Total)							--						
Vent. (Avg.)								--	0.88				0.35
Vent. (Aft.)									--				0.56
WS (Avg.)									0.74	--			
WS (Max.)									0.82		--		
MH (Avg.)									0.63			--	0.86
MH (Aft.)									0.56				--
O_3 (Max.)							0.37		-0.30				-0.29

TABLE 3-4d. Correlations (significant at the 95 percent confidence level) between maximum daily ozone concentration and the calculated measures--Midwestern U.S., episode 3, all subregions (N = 48).

	Rain	Temp. (Day)	Temp. (Max.)	H_2O (Avg.)	H_2O (Max.)	Rad. (A.M.)	Rad. (Total)	Vent. (Avg.)	Vent. (Aft.)	WS (Avg.)	WS (Aft.)	MH (Avg.)	MH (Aft.)
Rain	--			0.32	0.33								
Temp. (Day)		--		0.55	0.65								
Temp. (Max.)			--	0.54	0.64							0.38	
H_2O (Avg.)	0.32			--	0.97							0.44	
H_2O (Max.)	0.33			0.97	--								
Rad (A.M.)						--		-0.49	-0.45				
Rad (Total)							--						
Vent. (Avg.)								--	0.92			0.72	
Vent. (Aft.)								0.92	--			0.59	
WS (Avg.)								0.95	0.92	--		0.53	
WS (Aft.)								0.89	0.92		--	0.37	
MH (Avg.)								0.72	0.59			--	
MH (Aft.)									0.30			0.65	
O_3 (Max.)	-0.30			-0.34				-0.31	-0.34			-0.34	

solar radiation measures are positively correlated with temperature (high temperatures usually occur under sunny skies), and negatively correlated with wind speed (sunny skies often occur under stagnant high pressure systems).

In the midwestern episode 1 (April 17-25 1980) the maximum daily ozone is significantly correlated (95% confidence level) with daily average and maximum temperature, daily average and maximum water vapor mixing ratio, and daily total and morning solar radiation (Table 3-4b). Most highly correlated are daily average temperature (r = 0.67) and daily total solar radiation (r = 0.54). This follows our conceptual model--high temperatures and sunny skies are conducive to ozone formation. As mentioned earlier, temperatures during this episode were much lower than those of other episodes; it appears that this episode was caused by a brief period of summer-like conditions (warm and sunny) in mid-spring. Cross-correlation coefficients show that temperature is positively correlated to solar radiation and water vapor mixing ratio (absolute humidity tends to increase as the water-holding capacity of the atmosphere increases at higher temperatures). As expected, solar radiation is potively correlated with temperature.

In the midwestern episode 2 (7-21 July 1980) the relationships between the meteorological variables and maximum daily ozone concentrations are relatively weak (Table 3-4c). Those significant at the 95% confidence level are daily total solar radiation (r = 0.37), afternoon ventilation (r = -0.30) and afternoon mixing height (r = -0.29). Again, results are in keeping with our conceptual model; ozone concentrations are highest under conditions of sunny skies, low ventilation, and low mixing heights. Cross-correlation coefficients show typical relationships with solar radiation--negative with rainfall and positive with temperature. Ventilation shows a negative relationship with water vapor mixing ratio; it appears that periods of relatively stagnant weather were characterized by humid conditions in this episode.

In the midwestern episode 3 (8-18 August 1980) the maximum daily ozone concentration is significantly correlated (at the 95% confidence level) with rainfall, daily average and maximum water vapor mixing ratio, daily average and maximum ventilation, and daily average mixing height (Table 3-4d). All correlation coefficients were negative and relatively low; none exceeded 0.34 (absolute value). These results are consistent with our conceptual model, except that water vapor mixing ratio is negatively correlated with ozone. Humidity appears to have complex relationships with other variables that can alter its relationship with ozone. For example, increasing humidity increases photochemical reaction rates, thus increasing the rate of ozone production; however, humidity may be high during cloudy, rainy weather, which is not typically associated with high ozone concentrations. Cross-correlation coefficients show humidity to be positively correlated with temperature (higher temperature produces higher water-holding capacity) and ventilation to be negatively correlated with morning radiation (sunny days often occur under stagnant, high-pressure conditions).

In the central California episode no meteorological variables are correlated with maximum daily ozone at the 95% confidence level. This may be due to the small sample size (N = 12). The strongest relationship was that of daily average ventilation and ozone, (r = -0.590). This is typical for the region, where complex terrain can restrict air flow and produce an ozone episode if wind speeds and mixing heights are low.

Interpretation

Overall, solar radiation appears to have the strongest and most consistent relationship with ozone. One or both measures of solar radiation (morning or total daily) were among the top three variables with the strongest relationship with ozone in three out of the five episodes analyzed. However, typically clear skies during the ozone season in California make solar radiation a poor descriptor of ozone. Here the dominant influence on air quality is the interaction of mesoscale air flows with complex terrain; thus, wind speed and ventilation are highly related to ozone in California.

Other variables are occasionally highly related to ozone concentrations; their importance seems to be tied to the magnitude of the variables involved. For example, in the midwestern episode 1 (April 1980) there is a relatively strong positive relationship between temperature and ozone concentration. Temperatures during this episode were much lower than during the other two midwestern episodes, which occurred in summer (see Table 3-3). The northeastern episode had the second lowest average temperature, and was the only other episode in which temperature was significantly correlated with ozone. These results suggest that the lower the temperature, the greater its influence on ozone concentrations.

Rainfall is another example of a variable whose magnitude influences its relationship with ozone. Average and maximum rainfall were highest in the northeastern episode and second highest in the midwestern episode 3 (see Table 3-3); these two episodes also exhibit the strongest and second strongest relationships between rainfall and ozone concentration, respectively. From these results, it appears that if rainfall occurs infrequently and in small amounts, it does little to influence ozone concentrations; conversely, when relatively large amounts of rainfall occfur, it has a strong (negative) influence on ozone concentrations.

Cluster Analysis

We performed a cluster analysis to investigate the possibility of devising a classification scheme for RTM-III meteorological input variables that has the ability to discriminate among low, medium, and high classes of maximum daily ozone concentration. As discussed at the beginning of this section, such an analysis can proceed in two ways: (1) do a cluster analysis based on meteorology only, or (2) stratify the data by ozone class first, then cluster by meteorology. The second method was chosen as the most efficient method of attaining the goal of the analysis. There are many ways to cluster meteorological variables, some of which may or may not describe ozone concentrations well. Stratifying by ozone before clustering isolates those clusters that have some discriminatory power. The strength of the clusters serves as a measure of the usefulness of the clusters to discriminate among ozone levels.

A cluster analysis was performed for the northeastern episode because it was the longest episode modeled (31 days in summer 1980). The list of meteorological variables was reduced, based on results from the correlational analysis and preliminary cluster analyses. Those variables that exhibited consistently low correlations with ozone and did not cluster well were removed. A list of the reduced variable set is shown in Table 3-5.

TABLE 3-5. Mean (χ) and standard deviation (σ) for the meteorological variables in each of three ozone classes.

Meteorological Variable	Low Ozone		Medium Ozone		High Ozone	
	χ	σ	χ	σ	χ	σ
Maximum ozone (ppm)	0.056	0.0037	0.066	0.0029	0.074	0.0032
Rainfall (inches)	0.053	0.046	0.028	0.026	0.017	0.022
Average temperature (°K)	292.7	3.12	293.1	2.29	293.2	2.29
Average water vapor (ppm)	16,243.0	3729.0	15,455.9	2851.0	15,063.0	2005.0
Average ventilation (km^2/h)	14.4	7.87	15.0	7.68	10.7	5.37
Daily radiation (w/m^2)	1726.0	383.4	1968.0	303.0	2089.8	238.2
Average mixing height (m)	657.0	123.0	676.3	93.2	643.4	85.4
Maximum wind speed (m/s)	5.58	2.25	5.50	2.13	4.38	2.10

The reduced data set was stratified by maximum daily ozone concentration. Three groups were formed by ranking the 93 ozone values (31 days for each of three subregions) and selecting the lower third (low ozone), the middle third (medium ozone), and the upper third (high ozone). The data were then standardized to produce a mean of zero and standard deviation of one for all variables.

Results

Descriptive statistics for the meteorological variables in each of the three ozone classes for the northeastern episode are shown in Table 3-5. Maximum daily ozone concentrations range from 0.056 ppm in the low ozone class to 0.074 in the high ozone class. While this appears to be a relatively small range, it must be recognized that the concentrations are averages over subregions that are hundreds of square kilometers in size; hence, the standard deviation is very small (usually about 0.003 ppm). Rainfall is quite variable within each ozone class, but exhibits a consistent downward trend from low to high classes. Average temperature increases slightly from the low to high ozone classes, while daily solar radiation increases markedly. Water vapor mixing ratio and maximum wind speed decrease slightly from low to high ozone classes. Average ventilation and average mixing height reach maxima in the medium ozone class, and therefore do not show consistent trends across the ozone classes.

The cluster analysis produced several meteorological clusters and outlying cases in each ozone class. Two clusters in each class accounted for most of the days in that class. In the low ozone class, 24 out of 31 days were grouped into two clusters; in the medium ozone class, 16 out of 31 were grouped into two clusters; two clusters accounted for 22 of 31 days in the high ozone class.

The major meteorological clusters are illustrated in Figure 3-5. The 0.25 standard deviation threshold was applied to the values of the standardized measures in each cluster to determine if it was significantly above or below the mean. In the top tier of clusters only rainfall and solar radiation show significant, consistent trends from the low ozone class to the high ozone class. For example, rainfall is above average during low ozone days, about average for medium ozone days, and below average for

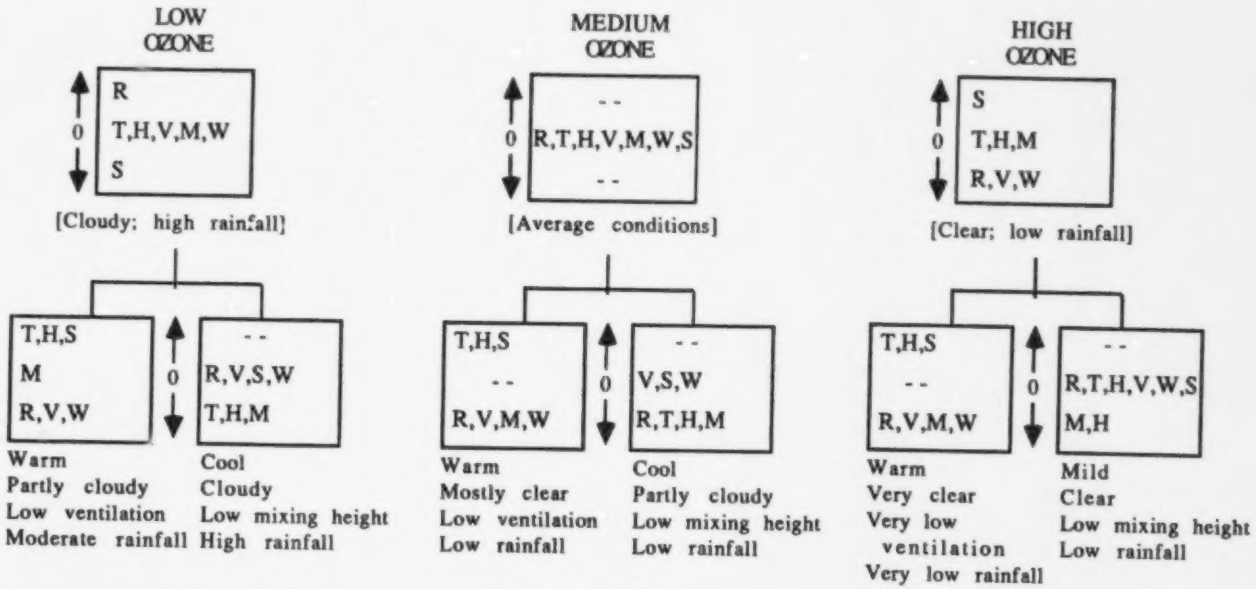
LOW OZONE
R
0
T,H,V,M,W
S
[Cloudy; high rainfall]
T,H,S
M
R,V,W
0
- -
R,V,S,W
T,H,M
Warm
Partly cloudy
Low ventilation
Moderate rainfall
Cool
Cloudy
Low mixing height
High rainfall
MEDIUM OZONE
- -
0
R,T,H,V,M,W,S
- -
[Average conditions]
T,H,S
- -
R,V,M,W
0
- -
V,S,W
R,T,H,M
Warm
Mostly clear
Low ventilation
Low rainfall
Cool
Partly cloudy
Low mixing height
Low rainfall
HIGH OZONE
S
0
T,H,M
R,V,W
[Clear; low rainfall]
T,H,S
- -
R,V,M,W
0
- -
R,T,H,V,W,S
M,H
Warm
Very clear
Very low ventilation
Very low rainfall
Mild
Clear
Low mixing height
Low rainfall

FIGURE 3-5. Meteorological clusters for three classes of maximum daily ozone concentration for the northeastern episode. Symbols in boxes are as follows: R = rainfall; T = temperature; H = humidity; V = ventilation; M = mixing height; W = wind speed; S = solar radiation (see Table 3-5 for description of variable used). In the upper tier of boxes the variables are ranked relative to the mean for the unstratified data. In the lower tier the ranking is relative to the mean of the data for the one ozone class only. An up-arrow (↑) indicates a variable is at least 0.25 standard deviation below average; a down-arrow (↓) indicates a variable is at least 0.25 standard deviation below average; a "0" indicates a variable is within 0.25 standard deviation of the mean.

high ozone days. Solar radiation exhibits the opposite trend. Ventilation and wind speed fall significantly below average during high ozone days, and are about average for the other two classes. All other measures remain about average across all three classes. Meteorological conditions characteristic of each class are: cloudy and rainy in the low ozone class, average conditions in the medium class, and clear with low rainfall in the high ozone class. This follows our conceptual model of ozone behavior, but the influences of certain variables, such as temperature, are notably absent. The analysis suggests that warm temperatures may not necessarily be a factor in an ozone episode.

When the second tier of clusters is compared to the first tier, we find that each cluster has at least one unique attribute (Figure 3-5). Interestingly, only the clusters in the high ozone class show significant differences in ozone concentration; the "warm" cluster exhibits higher ozone than the "mild" cluster. The warm cluster, characterized by very clear skies, very low ventilation, and very little rainfall, is the classic ozone-producing situation. We now see that although temperature is not a factor in the three-class ozone stratification, warm temperatures are required for a severe ozone episode to occur.

Interpretation

In the northeastern episode only daily solar radiation and daily rainfall exhibit systematic trends across the three ozone classes. Ozone concentrations increase with increasing solar radiation and decreasing rainfall. These two variables are generally associated; for example, cloudy weather (low solar radiation) is required for rainfall, which reduces ozone further through washout processes. This finding is in agreement with the correlational analysis concerning solar radiation; however, the correlational analysis shows rainfall to be important only in the northeastern episode and unimportant in the midwestern and California episodes.

The clusters of meteorological variables within each ozone class do little to discriminate between ozone levels within individual classes, except within the high ozone class. This would suggest that clustering by meteorology within each ozone class is not a useful excercise. However, it is the high ozone cases we are interested in, and for these we are able to produce clusters that have discriminatory power.

THE FEASIBILITY OF USING METEOROLOGICAL CLASSIFICATION SCHEMES FOR PREDICTING OZONE CONCENTRATIONS

From this exploratory analysis, we found that solar radiation is the best overall descriptive measure for maximum daily ozone concentrations. Other measures, such as temperature and rainfall, may be important under certain conditions. Meteorological variables associated with ozone levels in central California are much different than those in the Midwest or Northeast. Since cloudless and rainless skies are the rule during the ozone season in California, measures such as solar radiation and rainfall are not relevant to that area; measures dealing with the dispersive character of the atmosphere, such as ventilation, are attractive descriptors for ozone in California.

The formulation of solar radiation in RTM-III is not a fully accurate reflection of what occurs in reality. RTM-III only uses time of day, latitude, and cloud cover to calculate solar radiation. Attenuation by ambient aerosols and gases and fugitive dust are not treated. Therefore, in a given region for a given day, only changes in cloudiness would affect radiation levels in RTM-III. It follows that RTM-III will be very sensitive to future climatic scenarios that involve changes in cloudiness.

The high incidence of cross-correlation among the meteorological variables illustrates the complexity involved in grouping meteorological variables by ozone level. In the RTM-III application to central California described in Section 2, temperature was increased to 4°C. To be consistent, the absolute humidity also had to be increased, since the two are highly correlated. Likewise, if RTM-III were to be applied to the northeastern episode with increased solar radiation, associated changes would also be necessary in wind speed, ventilation, temperature and rainfall to accurately depict the change (see Table 3-4a).

The analysis of RTM-III simulations to estimate the sensitivity of calculations of ozone to climatic variability has been instructive and encouraging. It has provided: (1) an indication of the sensitivity of ozone concentrations to changes in meteorology; and (2) a better understanding (for the northeastern United States, at least) of those variables that are likely to vary together as a group. We now know what degree of change in meteorological variables is necessary to change, for example, a medium ozone day to a high ozone day. In addition, we also know what degree of change in meteorological variables is necessary to change a high ozone day to a very high ozone day. Recommendations for further work are provided in Section 4.

4 RECOMMENDATIONS

This study explored the sensitivity of a regional oxidant model, RTM-III, to variations in atmospheric parameters in an effort to establish the usefulness of using a photochemical model to analyze the impact on air quality of global climate changes. The results of the study indicate that the ozone concentrations predicted by a complex model using current atmospheric chemistry are sensitive to the climate change scenarios studied. Within the uncertainties present, the modeling results suggest there could be potentially significant increases in photochemical pollutants due to future climate changes.

Given the preliminary nature of this study, and its limitations, it is recommended that in future studies the potential air quality impacts of global climate change be examined in more detail. While such details are impossible to completely define because of the exploratory nature of such a study, it is possible to provide an outline of possible recommended approaches.

1. Include more complex climate change scenarios. In the preliminary study reported here only two meteorological parameters were changed: UV intensity at the surface and atmospheric temperature. A third parameter, atmospheric water vapor, was calculated as function of temperature, assuming that the specific humidity was held constant. Future studies should examine an expanded set of linked meteorological parameters (wind, relative humidity, cloud type and cover, precipitation, etc.) in addition to those used in this preliminary examination.

2. Consider climatic feedback and consistency in meteorological parameters. If linked parameters are to be considered, it is imperative that climatic feedback be treated in the simulations. Feedback is included, to a limited degree, in the scenarios produced by the General Circulation Models (GCMs). However, the GCMs do not at present report results at

sufficient spatial and temporal resolution to be of use in applying regional air quality models. Present-generation GCMs do not calculate regional-scale cloud distributions, winds, stabilities, etc. However, several meso-scale and one-dimensional boundary layer structure models are available that may be able to link the large-scale GCM output to the smaller scales required by regional models. These models may be able to use the GCM outputs to generate sets of temporally and spatially varying meteorological parameters that are consistent with each other.

3. Broaden the range of climate perturbations. While we attempted to use the climate scenarios predicted by the GCMs in the calculations of regional air quality, it was clearly not possible at this time to include all variations in climate conditions contained in the GCM scenarios. Only the effects of varying temperature and surface UV intensity were examined. Moreover, it was not possible to consider more than a few values of these two parameters. UV intensity at the surface was calculated assuming either 300 Dobson or 270 Dobson; atmospheric temperature was assumed to be either baseline or 4° C above baseline. Given the uncertainties inherent in the construction of future climate scenarios, and the fact that GCM-predicted climate variations represent gross spatial and temporal averages, we recommend that future studies include a broader range of meteorological parameters that are varied.

4. Analyze the Impact of global change on the effectiveness of current air quality strategies. The study reported here examined future air quality conditions assuming no change in precursor emissions from today. Current regulatory efforts to reduce ozone concentrations involve reducing emissions of VOCs and NO_x, which could dramatically alter the chemical mix of the atmosphere and possibly the chemical response to potential changes in climate. Future studies should examine the impacts of global climate change on an environment that more closely resembles the one that is likely to result from the implementation of possible control strategies. Such an examination will not only provide a more realistic picture of the impacts that could occur in the near future, but will also provide

insight into the possible success of alternative emission control strategies. This preliminary study has suggested that the greatest impact of climate change on photochemical pollutants is likely to be in the urban environment or immediately downwind.

5. Increase the number of regions and meteorological conditions. This preliminary study was severely restricted, by time and resources, to an examination of the climatic sensitivity of a model for two specific ozone episodes in two regions of the U.S. Future studies should increase the number of regions and meteorological scenarios analyzed, thereby permitting somewhat more general conclusions about the impact of global climate change on air quality.

With respect to the analysis described in Section 3, we recommend the following.

1. Extend the analysis of input data. The analysis of the input data for past RTM-III applications described in Section 3 was both preliminary and incomplete. Although past applications of RTM-III to four regions of the U.S. were examined to relate climate variation to elevated ozone concentrations, only the application to the Northeast was subjected to cluster analysis. The input data from the other applications (Midwest, Southeast, and West) should also be analyzed using cluster analysis.

   The analyses should be extended in several ways. The formation of groups of days by meteorology and ozone conditions can be simplified and made more robust. For example, a principal-components analysis could determine the one or two components that describe most of the variability in the input data and predicted ozone concentrations. (The analysis of the northeastern data reported here indicates that as much as 90 percent of the variability can be described using the first two components alone). The cluster or group analyses can then be peformed on the principal components rather than on several original variables with substantial intercorrelation.

2. Extend the analyses to observed data. The analyses reported here was based on RTM-III predictions rather than observations of ozone. Model predictions are calculated from input data sets that represent a limited and imperfect description of the meteorology during days when high regionwide ozone concentrations occur. A better approach would be to apply the same statistical analysis described in this report to observed ozone and meteorological data. Such an analysis would have the following advantages:

   Meteorological parameters that are not included in the input data for RTM-III but which are important to ozone formation--such as inversion strength, pressure and temperature gradients, and boundary-layer variables (convective and friction velocities)--could be estimated from meteorological observations, possibly providing more robust meteorological variables to relate to elevated ozone concentrations.

   Observations provide a longer and more complete data set, giving an opportunity to analyze high as well as low ozone conditions and their frequency of occurrence.

3. Changes in the frequency of ozone exceedances. The data analysis reported in Section 3 does not address how a change in climate may result in an increase in the number of exceedances of the ozone air quality standard. Obviously this is an important component of analyzing the potential effects of climate change on air quality. A methodology should be developed that will relate changes in meteorological parameters to changes in the observed frequency of ozone exceedences with some estimate of the uncertainty included.

References

Builtjes, P.J.H. 1987. "Calculation and Evaluation of the Photochemical Episode of July 22-26, 1980." TNO, Apeldoorn, The Netherlands (87-278).

Builtjes, P.J.H., and E. Luken. 1987. "Sensitivity Calculations of the Photochemical Episode of May 29 - June 3, 1982." TNO, Apeldoorn, The Netherlands (87-277).

Cicerone, R. J., S. Walters, and S. C. Liu. 1983. Nonlinear response of stratospheric ozone column to chlorine injections. J Geophys. Res., 88:3647-3661.

Craig, H., and C. C. Chou. 1982. Methane--the record in polar ice cores. Geophys. Res. Lett., 9:1221-1224.

Dickinson, R. E., and R. J. Cicerone. 1986. Future global warming from atmospheric trace gases. Nature, 319:109.

Fawcett, E. B. 1977. Current capabilities in prediction at the National Weather Service's National Meteorological Center. Bull. Am. Meteorol. Soc., 58:143-149.

Gery, M. W., R. D. Edmond, G. Z. Whitten. 1987. "Tropospheric Ultraviolet Radiation: Assessment of Existing Data and Effect on Ozone Formation." Systems Applications, Inc., San Rafael, California (SYSAPP-87/191).

Gery, M. W., G. Z. Whitten, and J. P. Killus. 1988. "Development and Testing of the CBM-IV for Urban and Regional Modeling." Systems Applications, Inc., San Rafael, California (SYSAPP-88/002).

Kessler, R. C., and S. G. Douglas. 1988. "Analysis of Wind Fields for the SCCCAMP 1985 Intensive Measurement Periods." Systems Applications, Inc., San Rafael, California (SYSAPP-88/055).

Liu, M. K., R. E. Morris, and J. P. Killus. 1984. Development of a regional oxidant model and application to the northeastern United States. Atmos. Environ., 18(6):1145-1161.

Moore, G. E., R. E. Morris, and C. Daly. 1987. "Application of a Regional Air Quality Model to the California San Joaquin Valley." Systems Applications, Inc., San Rafael, California (SYSAPP-87/155).

Moore, G. E., R. E. Morris, and S. G. Douglas. 1988. "Application of a Regional Oxidant Model to Central California. Volume I." Systems Applications, Inc., San Rafael, California (SYSAPP-88/045a).

Morris, R. E. 1987. "Preparation of Meteorological and Air Quality Inputs for the RTM-III for the TSDF and Rural Ozone Projects." Systems Applications, Inc., San Rafael, California (SYSAPP-87/077).

Morris, R. E., R. C. Kessler, S. G. Douglas, and K. R. Styles. 1987. Rocky Mountain Acid Deposition Model Assessment Project: Evaluation of Mesoscale Acid Deposition Models for Use in Complex Terrain. U.S. Environmental Protection Agency (EPA-600/3-88/008; NTIS BP88-167481-AS).

Morris, R. E., S. D. Reynolds, and M. K. Liu. 1987. "The Systems Applications, Inc. Regional Transport Model--Current Status and Future Needs." APCA Conference on the Scientific and Technical Issues Facing the Post 1987 Ozone Control Strategies, Hartford, Connecticut, November 16-19, 1987.

Morris, R. E., and D. A. Stewart. 1987. "Refinement of a Regional Oxidant Model and Application to National Parks in the Eastern United States. Part I: Incorporation of a Nested Lagrangian Reactive Plume Model and Application to the Eastern U.S." Systems Applications, Inc., San Rafael, California (SYSAPP-87/142).

Paumier, J., D. Stinson, T. Kelly, and C. Bollinger. 1986. MPDA-1: A Meteorological Processor for Diffusion Analysis. User's Guide. U.S. Environmental Protection Agency (EPA-600/8-86-011).

Pielke, R. A. 1974. A three-dimensional numerical model of the sea breezes over southern Florida. Mon. Weather Rev., 102:115-139.

Pielke, R. A. 1984. Mesoscale Meteorological Modeling. Academic Press.

Prather, M. J., M. B. McElroy, and S. C. Wofsy. 1984. Reductions in ozone at high concentrations of stratospheric halogens. Nature, 312:227-231.

Ramanathan, V. 1988. The greenhouse theory of climate change: A test by an inadvertent global experiment. Science, 240:293ff.

Shuman, F. G. 1978. Numerical weather prediction. Bull. Am. Meteorol. Soc., 59:5-17.

Stewart, D. A., R. E. Morris, and S. D. Reynolds. 1987. "Application of the Regional Transport Model (RTM-III) to Western Europe." Systems Applications, Inc., San Rafael, California (SYSAPP-87/030).

Turner, D. B. 1970. "Workbook of Atmospheric Dispersion Estimates." U.S. Environmental Protection Agency, Research Triangle Park, North Carolina.

Weiss, R. F. 1981. Temporal and spatial distribution of tropospheric nitrous oxide. J. Geophys. Res., 86:7185-7195.

Wuebbles, D. J., and J. E. Penner. 1988. "Sensitivity of Urban/Regional Chemistry to Climate Change: Report of the Workshop." Lawrence Livermore National Laboratory, Livermore, California (UCRL 99436).

Yu, T. 1978. Determining the height of the nocturnal boundary layer. J. Appl. Met., 17:28-33.